

SURFACE ANALYSIS OF POLYMER MICROARRAYS

Michael Taylor

Thesis submitted to the University of Nottingham for the
degree of Doctor of Philosophy

October 2008

Publications

Taylor M., Urquhart A.J., Zelzer M., Davies M.C., Alexander M.R. Picoliter Water Contact Angle Measurement on Polymers. *Langmuir* 2007;23(13):6875-6878.

Urquhart A.J., Anderson D.G., Taylor M., Alexander M.R., Langer R., Davies M.C. High throughput surface characterisation of a combinatorial material library. *Advanced Materials* 2007 Sep;19(18):2486-2490.

Urquhart A.J., Taylor M., Anderson D.G., Langer R., Davies M.C., Alexander M.R. TOF-SIMS analysis of a 576 micropatterned copolymer array to reveal surface moieties that control wettability. *Analytical Chemistry* 2008 Jan;80(1):135-142.

Taylor M., Urquhart A.J., Anderson D.G., Williams P.M., Langer R., Alexander M.R., Davies M.C. A Methodology for Investigating Protein Adhesion and Adsorption to Microarrayed Combinatorial Polymers. *Macromolecular Rapid Communications* 2008;29(15):1298-1302.

Taylor M., Urquhart A.J., Anderson D.G., Langer R., Davies M.C., Alexander M.R. Partial Least Squares Regression as a Powerful Tool for Investigating Large Combinatorial Polymer Libraries. *Surface and Interface Analysis (In Press)* 2008.

This thesis is dedicated to my Dad, who died shortly after it was completed.

Allegretto.

The musical score consists of four staves. The top two staves are in treble clef, and the bottom two are in bass clef. The key signature is one flat (B-flat) and the time signature is 4/4. The tempo is marked 'Allegretto.' The score includes dynamics such as *pp*, *sf*, *p*, and *pizz.* (pizzicato). The music features various rhythmic patterns, including eighth and sixteenth notes, and rests.

Contents

Abstract	i
List of Abbreviations	iv
List of Figures	vi
List of Tables	xi

Chapter 1. Introduction

1.1 Polymers as biomaterials	2
1.2 High throughput and combinatorial methods for the discovery of new polymers.....	6
1.2.1 Large scale discrete libraries.....	7
1.2.2 Gradient material libraries	10
1.2.3 Micro-patterned material arrays.....	15
1.2.4 Three-dimensional polymer libraries.....	19
1.4. Research involving high-throughput surface characterisation of polymeric materials.....	20
1.5 Aims and objectives of thesis	24

Chapter 2. Experimental Methods

2.1 Time of Flight Secondary Ion Mass Spectrometry (ToF-SIMS).....	26
2.2 X-ray Photoelectron Spectroscopy (XPS)	28
2.3 Atomic Force Microscopy (AFM)	31

Chapter 3. Surface Chemical Analysis of Polymer Microarrays using ToF-SIMS and XPS

3.1 Introduction.....	36
3.2 Methods and Materials.....	40
3.2.1 Microarray Synthesis	40
3.2.2 Time-of-Flight Secondary Ion Mass Spectrometry	40

3.2.3 X-ray Photoelectron Spectroscopy	41
3.2.4 Principal Component Analysis	41
3.3 Results	44
3.3.1 Time-of-Flight Secondary Ion Mass Spectroscopy	44
3.3.2 X-ray Photoelectron Spectroscopy	47
3.4 Discussion	50
3.5 Conclusions	59

Chapter 4. Picolitre Contact Angle Measurements on Polymers

4.1 Introduction	61
4.2 Methods and Materials	62
4.2.1 Preparation of polymer films.	62
4.2.2 Preparation of radial plasma polymer gradient.	62
4.2.3 CA measurements.	63
4.3 Results and Discussion	63
4.4 Conclusion	71

Chapter 5. Surface Energy Analysis of Polymer Microarrays to Investigate the Chemical Basis of Surface Energy

5.1 Introduction	73
5.2 Methodology	75
5.2.1 Polymer Microarray Synthesis.	75
5.2.2 Contact angle Measurements.	75
5.2.3 X-ray Photoelectron Spectroscopy.	77
5.2.4 Time-of-Flight Secondary Ion Mass Spectroscopy.	77
5.2.5 Atomic Force Microscopy Imaging of Polymer Spots.	78
5.3 Results	78
5.3.1 Surface energy measurements.	78
5.3.2 X-ray Photoelectron Spectroscopy.	80
5.3.3 Time-of-Flight Secondary Ion Mass Spectroscopy analysis.	82
5.4 Discussion	84
5.5 Conclusions	94

Chapter 6. Partial Least Squares Regression as a Powerful Tool for Investigating Large Combinatorial Polymer Libraries

6.1 Introduction.....	97
6.2 Methodology	99
6.2.1 Polymer Microarray Synthesis.....	99
6.2.2 Preparation of Polymer Films	100
6.2.3 Time-of-Flight Secondary Ion Mass Spectrometry	100
6.2.4 Partial Least Squares Regression	101
6.2.4 Surface Energy Measurements	102
6.3 Results and Discussion	102
6.3.1 The influence of sample number on ions identified in regression vector	104
6.3.2 Investigating the predictive ability of the PLS model outside of the training set.....	109
6.3.2.1 Acrylate copolymers synthesised using monomers included in the training set.....	111
6.3.2.2 Acrylate copolymers containing minor monomers not included in the training set.....	112
6.3.2.3 Polymers which are chemically unrelated to the training set	113
6.4 Conclusions.....	115

Chapter 7. A Methodology for Investigating Protein Adhesion and Adsorption to Micro-arrayed Polymers

7.1 Introduction.....	118
7.2 Methods and Materials.....	120
7.2.1 Array synthesis.....	120
7.2.2 AFM imaging and force measurements.....	120
7.2.3 Contact angle measurements.....	121
7.2.4 Fluorescently labelled protein adsorption.....	121
7.3 Results and Discussion	122
7.4 Conclusions.....	131

Chapter 8. Conclusions

8.1 General Conclusions133
8.2 Final Comments136

Abstract

Polymers have been used as biomaterials for nearly a century and have recently become the material of choice for use in tissue engineering. However, the classes of biodegradable and biocompatible polymers available for use in biomedical devices and as tissue engineering scaffolds are limited. This lack of available polymers with suitable properties could inhibit the development of biomedical devices with improved biocompatibility and hinder the growth of the fledgling tissue engineering field. Researchers in the polymer and biomaterials fields have tried to remedy this problem by applying combinatorial and high throughput methods developed in drug discovery to the search for new polymers. A recent advance has been the development of combinatorial polymer libraries printed as microarrays. This format allows the polymers to be readily screened for their cell adhesion and differentiation properties, allowing 'hit' materials with ideal properties to be identified. However, without knowledge of the surface properties of these novel polymers it is impossible to rationalise their biological properties. The surface characterisation of such microarrays presents numerous practical problems including small sample size, sample number and even analysis of such large amounts of data. It is the aim of this thesis to develop methods for the characterisation of the surface chemistry, wettability and protein adsorption properties of polymers *in situ* in microarray format and within realistic timeframes. The thesis will explore multivariate statistics in the form of PCA and PLS as methods of analysing the large amount of data acquired.

The first part of this thesis describes the surface chemical analysis of a polymer microarray using ToF-SIMS and XPS. A comparison of the polymers' surface to bulk chemistries by XPS indicated that 64 % of the polymers had a surface chemistry which differed from the bulk. This reinforces the need for characterisation of the polymers' surface chemistries, as it is obvious that this can not be inferred from their bulk chemistries. ToF-SIMS imaging was shown to be an ideal method of studying the distribution of specific ion species across the array and to confirm that the microarray was printed in the intended layout.

Principal component analysis is shown to be an ideal technique to analyse both ToF-SIMS and XPS spectral data from the arrays, allowing similarities and differences in the surface chemistry of the polymers to be easily visualised.

To estimate the surface energies of the arrayed polymers it is necessary to use picolitre volume droplets to make contact angle measurements. In Chapter 4 it is shown that contact angle measurements taken from picolitre volume water droplets are equivalent to those measured from more conventional microlitre droplets. In Chapter 5 picolitre contact angle measurements are used to estimate the polar and dispersive surface energies of a polymer microarray, which has been specifically designed to exhibit a maximum range of surface energy values. The analysis shows that there is indeed great variation in the WCA and polar surface energies of the polymers, demonstrating the power of intelligently designed combinatorial libraries. To understand the chemical basis of this large range of surface energies the results are compared to surface chemical data from ToF-SIMS and XPS. Surface atomic and functional data from XPS is unable to provide any definitive explanations for the range of surface energies observed. However, information about the molecular structure of the surface from ToF-SIMS gives an insight into what surface functionalities are responsible for high and low surface energies.

In Chapter 6 PLS regression is investigated further as a method for investigating surface structure-property relationships in large polymer libraries. Specifically two issues are investigated: the influence of sample number on the results obtained and the ability of PLS to make quantitative predictions. The ToF-SIMS and surface energy dataset discussed in Chapter 5 is used for this task. It is demonstrated that the results obtained from PLS models of large polymer libraries are equivalent to those obtained from much smaller datasets, in terms of the ions identified in the regression vector. Using various test sets of polymers it is shown that there is a limit to the predictive ability of PLS: specifically, as the difference between the training and test sets increases, the quality of the predictions decreases. Potential problems with data pre-processing and re-scaling are also identified.

In the final experimental chapter two methods are described for investigating protein adhesion and adsorption to micro-arrayed polymers using AFM and fluorescently labelled proteins. Both methods indicate a wide range of protein adsorption properties within the group of polymers analysed. A good correlation between the two sets of data was observed which appears to validate both methods.

In summary the work described in this thesis has demonstrated the feasibility of the characterisation of the surface chemistry, energetics and protein adsorption properties of a micro-arrayed polymer library within realistic time-frames. PCA and PLS have been shown to be useful tools for analysing the data obtained. It is hoped that the methods described in this thesis will allow the biological data from polymer microarrays to be rationalised using the surface properties of the polymers, allowing the design of new biomaterials.

Abbreviations

AFM	Atomic Force Microscopy
ATR	Attenuated Total Reflectance
DiCA	Diiodomethane Contact Angle
DMF	Dimethyl formamide
EDC	1-ethyl-3 (3-dimethylaminopropyl) carbodiimide hydrochloride
ESCA	Electron Spectroscopy for Chemical Analysis
FDA	Food and Drug Administration
FTIR	Fourier Transform Infrared Spectroscopy
hESC	Human embryonic stem cell
hMSC	Human mesenchymal stem cell
LOO	Leave-one-out (cross-validation)
MLR	Multiple Linear Regression
M_w	Molecular weight
NHS	N-hydroxysulfosuccinimide
NIH	National Institute of Health
PBS	Phosphate Buffered Saline
PC1	1 st Principal Component
PC2	2 nd Principal Component
PC3	3 rd Principal Component
PCA	Principal Component Analysis
PCR	Principal Component Regression
PEO	Polyethylene oxide
PDMS	Poly(dimethyl siloxane)
PHEMA	Poly(hydroxyethyl methacrylate)
PMMA	Poly(methyl methacrylate)
PPAA	Plasma poly(acrylic acid)
PPHex	Plasma poly(hexane)
PLA	Poly(lactic acid)
PLS	Partial Least Squares
PS	Poly(styrene)

PTFE	Poly(tetrafluoroethylene)
SAM	Self-Assembled Monolayer
SEM	Scanning Electron Microscopy
SFM	Scanning Force Microscopy
STM	Scanning Tunnelling Microscopy
T _g	Glass transition temperature
ToF-SIMS	Time-of-Flight Secondary Ion Mass Spectroscopy
UHV	Ultra high vacuum
WCA	Water Contact Angle
XPS	X-ray Photoelectron Spectroscopy

List of Figures

Figure 1. Possible arrangements of monomers in polymeric materials.	4
Figure 2. Water contact angles of the poly(arylate) library.	8
Figure 3. The influence of polymer water contact angle on fibroblast proliferation.....	9
Figure 4. Synthesis of poly(β -amino ester) by reaction of diacrylate with amine monomer.	10
Figure 5. Schematic of the continuous composition gradient deposition process.	11
Figure 6. Plot of average measured RMS roughness as a function of library position.....	12
Figure 7. Plot of average cell number versus library position after culturing for 1(\square), 3(\bullet) and 5(\blacktriangle) days.....	13
Figure 8. Graph showing the composition of the polymer blend library at different positions.	14
Figure 9. Graph showing the roughness (nm) of the surface of the polymer library.....	14
Figure 10. A polymer array containing hMSC stained green with actin.	18
Figure 11. Three dimensional a) gradient b) discrete polymer scaffold libraries.	20
Figure 12. A composition map of a polymer gradient library prepared using FTIR.	22
Figure 13. Relationship between contact angle and spreading area.	23
Figure 14. Diagram illustrating the production of secondary ions from a surface.	27
Figure 15. Example of a broad XPS spectrum.....	29
Figure 16. Example of a high resolution C1s XPS spectrum with component peaks fitted.	30
Figure 17. Diagram describing the typical construction of an AFM.	32
Figure 18. Example force-distance curve.....	33
Figure 19. One principal component in the case of two variables. a) PC1 describes the greatest variance in the 6 sample data set b) Loadings are the cosine	

of the angle between each axis and PC1 c) Scores are the projections of the sample points onto the PC1.....	37
Figure 20. Monomers used to synthesise the polymer microarray.	42
Figure 21. ToF-SIMS imaging of the polymer microarray. Images for 12 example ions are shown: 6 positives on the left and 6 negatives on the right.....	43
Figure 22. Principal component analysis of positive ion intensities from microarray. a) Scores biplot of PC1 and PC2. Polymers are group by their major monomer constituents. b) Loadings versus m/z on PC1. c) Loadings versus m/z on PC2.....	45
Figure 23. Principal component analysis of negative ion intensities from microarray. a) Scores biplot of PC1 and PC2. Polymers are group by their major monomer constituents. b) Loadings versus m/z on PC1. c) Loadings versus m/z on PC2.....	46
Figure 24. Comparison between polymer surface and bulk chemistries. The ratio of polymer surface O:C ratio is plotted versus bulk O:C ratio. Bulk is calculated from theoretical ratios based upon knowledge of the ratio of monomers used to synthesise each polymer (the radical initiator has been included in calculations).	48
Figure 25. XPS analysis of the polymer microarray. a) Example survey spectrum of a representative polymer b) Example high resolution C1s spectrum of a representative polymer c) Example survey spectrum of a fluorinated polymer d) Example high resolution C1s spectrum of a fluorinated polymer e) Atomic percentage of Fluorine for all polymers on microarray.	49
Figure 26. PCA of XPS data from the microarray. a) Scores biplot of PC1 and PC2. Polymers are grouped by their major monomer constituents. b) Scores biplot of PC1 and PC2. Polymers are grouped by their minor monomer constituent c) Loadings biplot of PC1 and PC2.	51
Figure 27. Influences of the addition of minor monomers on the PC1 score values of polymers containing major monomers a) 5 b) 7 and c) 15.....	55
Figure 28. Water Contact Angle versus a) droplet volume and b) droplet Bond number on PMMA. Each water droplet was fitted using both circle and Young-Laplace function functions to model droplet shape. Linear regression fits have been provided to guide the eye.	64

- Figure 29.** Images of the profile of a) 2 μL and b) 100 pL water droplets on PMMA to demonstrate difference in scale. Graphs of WCA versus time for c) 2 μL and b) 100 pL water droplets on five polymers.66
- Figure 30.** Tapping mode AFM height images of P_LLA a) 5 x 5 μm b) 30 x 30 μm and P_{DL}LA c) 5 x 5 μm d) 30 x 30 μm . The RMS roughness values for P_LLA and P_{DL}LA were 29 and 7 nm respectively.....69
- Figure 31.** Three-dimensional wettability map of a radial plasma polymer gradient.70
- Figure 32.** a) Side profile of a 100 pL water droplet sitting on a polymer spot which has been fitted with a circle function b) Birds eye view of a 100 pL water droplet sitting in the centre of a polymer spot.76
- Figure 33.** a) Water contact angle versus the polar component of surface energy b) Water contact angle versus dispersive component of surface energy for 496 polymers on array c) Diiodomethane contact angle versus the polar component of surface energy d) Diiodomethane contact angle versus dispersive component of surface energy. Polymers containing major monomers 7, 10 and 13 have been highlighted to illustrate differences between polymer composition. The array contained 6 repeats of each of the 16 100% major monomers. The error bars represent the standard deviations for these 16 polymers to give an indication of the error of the technique.79
- Figure 34.** a) Polar versus dispersive component for all 496 polymers, and Water Contact Angle versus polar component of surface energy for b) polymers containing monomer 10 as their major constituent c) polymers containing monomer 13 as their major constituent d) polymers containing monomer 7 as their major monomer. For figures b) to d) the black star represents the polymer containing 100% of the major monomer, i.e. no minor monomer additions.80
- Figure 35.** a) O:C ratio versus polar component of surface energy b) O:C ratio versus disperse component of surface energy for 496 polymers.81
- Figure 36.** a) C-O % versus polar component b) C-O % versus disperse component c) C=O % versus polar component d) C=O % versus disperse component of surface energy for 496 components.81
- Figure 37.** RMSECV versus latent variable for a) Total surface energy b) Polar surface energy.82

Figure 38. Calculated $\log P$ versus water contact angle for the 16 major monomer polymers.....	85
Figure 39. PLS model for γ^p (4 latent variables). a) Measured versus predicted γ^p (Linear fit shown, $R^2 = 0.82$) b) Regression vector plotted as regression coefficient versus peak m/z for the concatenated data set.	90
Figure 40. PLS model for γ (5 latent variables). a) Measured versus predicted γ (Linear fit shown, $R^2 = 0.87$) b) Regression vector plotted as regression coefficient versus peak m/z for the concatenated data set.	91
Figure 41. ToF-SIMS positive ion spectra of a) polymer containing 100 % monomer 10 and b) polymer containing 100 % monomer 13.	93
Figure 42. PLS models constructed using a) & b) 496 polymers, c) & d) 248 polymers (Major monomers 1 to 8), e) & f) 248 polymers (Major monomers 9 to 16) and g) & h) 124 polymers (Major monomers 1 to 4). Measured versus Predicted surface energy and Regression coefficient versus m/z is shown for each PLS model. X = Y lines are provided to guide the eye.....	106
Figure 43. PLS models constructed using a) & b) 31 polymers (Major monomer 1), c) & d) 336 polymers (Minor monomers A to D. Measured versus Predicted surface energy and Regression coefficient versus m/z is shown for each PLS model. X = Y lines are provided to guide the eye.	108
Figure 44. Measured versus predicted surface energy values for a) 12 acrylate copolymers synthesised from monomers common to training set b) 160 acrylate copolymers synthesised from monomers not used in training set c) 6 commercially available linear polymers, using data mean-centered using means from the training set. X = Y lines are provided to guide the eye.....	110
Figure 45. Actual surface energy of a polymer versus the error in the predicted surface energy using PLS model.....	111
Figure 46. Measured versus predicted surface energy values for a) 12 acrylate copolymers synthesised from monomers common to training set b) 160 acrylate copolymers synthesised from monomers not used in training set c) 6 commercially available linear polymers, using data mean-centered using means from the test set. X = Y lines are provided to guide the eye.....	114
Figure 47. The 24 monomers used to synthesis the polymer library. Monomer 17 was substituted for * as a minor monomer to increase hydrophilicity.	119

Figure 48. Formation of an amide bond between carboxylic groups on ppAA and amine functionalities on fibronectin (Figure adapted from Tsapikouni <i>et al</i> [145]).	122
Figure 49. Typical force-distance curves measured between a fibronectin coated AFM probe and three control surfaces: glass, PTFE and fibronectin adsorbed to silicon.....	123
Figure 50. Example force-distance curve for the polymer containing 70 % monomer 21 and 30 % 1.	124
Figure 51. Graph displaying the maximum adhesion force between a fibronectin coated probe and 48 polymers.	125
Figure 52. Histograms displaying adhesive forces (nN) between a fibronectin coated AFM probe and polymers synthesised from a) 70 % monomer 21 & 30 % monomer 2 b) 70 % monomer 21 & 30 % monomer 7.	126
Figure 53. Graph displaying the normalised fluorescent intensities of 48 polymers after adsorption of fluorescent labelled fibronectin.	127
Figure 54. RMS roughness versus normalised fluorescent intensity for 24 polymers containing monomer 1 as their major constituent.	128
Figure 55. Adhesion force versus normalised fluorescent intensity for 48 polymers ($R^2 = 0.89$).....	129
Figure 56. Relationship between protein adhesion force and water contact angle for 48 polymers.	130

List of Tables

Table 1. Water contact angles of six polymers measured from picolitre and microlitre volume droplets (\pm standard deviation).....	68
Table 2. Surface tension values (including dispersive and polar values) for test liquids.[107, 108].....	76
Table 3. Ion assignment for the ions with the largest regression coefficients for γ^p PLS model.....	83
Table 4. Structural assignments for the ions with the largest regression coefficients for γ PLS model.....	84
Table 5. Comparison of PLS models with different numbers of samples.....	107

Chapter 1

Introduction

1.1 Polymers as biomaterials

The term biomaterial is commonly defined in either of two ways: a material derived from a biological source or a material used in the treatment of a medical condition within the human body.[1] This thesis is concerned with the latter of the two definitions, i.e. materials used within the human body for the purpose of treating disease. Although the term biomaterial has only been defined relatively recently, the use of materials in medicine has been common practice for most of recorded history. Examples include the use of gold fillings in dentistry over two thousand years ago and the manufacture of replacement eyes out of glass in the middle ages.[2] However, modern biomaterials science really started at the beginning of the 20th century with the use of modern, synthetic polymers. In the 1940's nylon sutures were used for the first time during surgical procedures.[3] The use of polymers such as poly(methyl methacrylate) (PMMA), polyesters and poly(vinyl chloride) (PVC) in surgery was reported not long after.[4] Many of these materials' utility as biomaterials were discovered by accident. For example, after the Second World War a British ophthalmologist called Harold Ridley discovered that fragments of PMMA from the shattered windows of fighter planes did not cause any long term inflammation when embedded in the eyes of pilots. These polymers (along with poly(tetrafluoroethylene) (PTFE) and poly(urethanes)) are still in common usage as hip implants, artificial lenses, catheters, sutures, stents and many other medical devices.[5]

The aforementioned biomaterials have served their purpose well, however they are far from perfect. Problems include chronic inflammatory responses by the body towards implanted biomaterials which can lead to a poorly vascularised fibrous layer being formed around the implant.[1] This response can be desirable as it helps to anchor the implant to the host tissue; however related clinical complications such as infection and tissue contraction are major problems. Although research has found ways to improve the functionality of these polymers in their myriad of uses, the amount of time they have been in use is perhaps indicative of the lack of progress in the development of new, specifically designed biomaterials.

Tissue engineering is a relatively new field which is concerned with the application of biology and engineering to the development of substitutes to replace tissue which has been damaged through disease or old age.[6] Two main approaches have been taken in the quest to create new tissue. The first approach involves isolating cells of interest and culturing them *in vitro* until they are ready to inject directly into the patient at the site of need. The second approach involves growing the isolated cells on or within matrices which are then implanted into the patient. These matrices are intended to replicate the natural cell environment and to give the implant the desired physical properties of the tissue until the implanted cells can establish themselves with the patient.[7]

Developing biomaterials to use in the manufacture of these cell supports is a major challenge as there are many properties which are required, many of which are specific to the tissue being engineered. For simplicity these requirements can be divided into two types: bulk and surface properties. Bulk properties include mechanical strength and chemical reactivity, both of which greatly influence the utility of a material. For example, if a biomaterial is going to be used to make a replacement hip the mechanical properties are very important as the material will be load bearing. However, the main interaction between the material and the body will be at the material surface. In the words of Ratner *et al* “the body will ‘read’ this surface structure” and will then decide how it will react.[2] Historically it is this reaction which has caused the failure of biomedical devices, as the body ‘sees’ the implant surface as foreign and therefore directs the body's immune system to react. Therefore it has been common to try to modify the surface of biomaterials to make them as inert as possible once implanted into the body, using methods such as plasma treatment. Recently it has been the goal of researchers working in the field to design biomaterials with biologically active surfaces, i.e. instead of initiating a negative response, they will actively encourage the body to accept the material. It has been demonstrated that both the surface chemical, topographical and mechanical properties can all influence biocompatibility. Hence it is important that a potential biomaterial's surface is well characterised.

This thesis is concerned with the development and screening of new polymeric biomaterials; therefore it is necessary to begin by defining what

constitutes a polymer. In simple terms a polymer can be defined as a substance composed of molecules made up of long sequences of one or more species (atoms or groups of atoms), usually linked by covalent bonds.[8] It is important to note that there are many different classes of polymer, the simplest of which is called a homopolymer. A homopolymer is composed of only one type of monomer, an example of which is poly(ethylene) which is composed solely of the monomer ethylene.[9] Copolymers are polymers which contain more than one type of monomer, for example poly(lactic-co-glycolic acid) which contains the two monomers lactic and glycolic acid. The monomers that are used to synthesise copolymers can be in varying proportions and can polymerise to form different types of copolymer (Figure 1). For example, a random co-polymer is one where its constituent monomers are in no discernable order, whereas the constituent monomers in a block copolymer form long sequences or “blocks” of the same type. The way copolymers monomers order themselves can greatly influence the morphology and therefore physical properties of the resulting polymer.[9] Polymeric biomaterials can be divided into those which are natural in origin and those which are artificial, i.e. have been synthesised by man.

Homopolymer	AAAAAAAAAAAA
Block Copolymer	AAABBBAAABBB
Random Copolymer	AABABABBABBA
Alternating Copolymer	ABABABABABAB

Figure 1. Possible arrangements of monomers in polymeric materials.

The most commonly used natural polymeric biomaterials are collagens, which are a family of fibrous proteins that are found in nearly all mammalian tissues.[10] Natural polymers such as collagen are useful as they commonly have a greater intrinsic biocompatibility than polymers of synthetic origin. However, one major disadvantage is the natural batch-to-batch variation in these materials which can cause major problems in the regulatory process.

Polymers are not the only materials used in medicine. Metallic biomaterials are commonly used in orthopaedics to replace worn-out joints such as knees, hips or ankles.[2] They are also used to manufacture dental implants, craniofacial plates, screws and devices such as pacemakers. Metal alloys are generally used rather than the metals themselves, due to their superior properties. It is common for these alloys to undergo some form of surface treatment before use, either to facilitate fixation of implants into the bone or to improve biocompatibility.[2] The most commonly used are stainless steels, cobalt-based alloys and titanium alloys. Ceramics and glasses are essential materials for the manufacture of diagnostic instruments, tissue culture flasks and fibre optics for endoscopy. They are also used extensively in dentistry to make dentures and cements. Ceramics are particularly useful biomaterials due to their physical and mechanical properties, i.e. they can replace hard skeletal and connective tissues.[2] However, their success relies greatly on them being able to adhere sufficiently to the surrounding connective tissue, hence it is commonly their surface properties which are lacking.

A review of the relevant literature reveals that the vast majority of polymers used in tissue engineering research are still simple copolymers of lactic and glycolic acid.[11] The situation is better in the more established field of biomedical devices, however there are still only a small number of classes of synthetic biodegradable polymers that are approved by the FDA for use. Indeed an NIH report on the subject concluded that attempts to tailor polymers' properties to specific applications were based almost entirely on "trial and error" with existing classes of polymers.[12] The lack of potential polymers available for use in the biomedical and tissue engineering fields could potentially retard the rapid growth that has been seen in these areas over the past decade.[11, 13]

In summary, there is a need for new biomaterials (particularly polymers) for use in both biomedical devices and tissue engineering. These materials require both the correct bulk and surface properties to suit their desired application.

1.2 High throughput and combinatorial methods for the discovery of new polymers

High-throughput screening in the biological sciences has caused a revolution in the way research is done. Traditionally, new compounds or materials were developed and investigated individually or in small groups using information on their probable action; a very time consuming and labour intensive exercise which has been likened to finding a needle in a haystack! Combinatorial methods allow the synthesis and screening of hundreds, or even thousands, of samples in a relatively short period of time. Theoretically this should increase the chance of finding a compound with the desired properties; however some critics have suggested that these methods only serve to increase the size of the haystack! Hence, it has been argued that a more evidence based, traditional approach using structure-activity relationships is superior. However, the two methodologies are not mutually incompatible as it is highly beneficial to use existing knowledge of compound properties to design a combinatorial library. The success of high-throughput techniques in areas such as genomics, proteomics and drug discovery has prompted interest by researchers in other areas such as materials science. High throughput research in the materials field has mainly centred on polymeric materials, particularly for use as biomaterials. Indeed, the years 1998 to 2006 have seen a considerable body of research into combinatorial and high-throughput methods in polymer research.[14] Various methods have been trialled to build combinatorial libraries of novel polymers with varied success. These libraries have been presented for analysis as discrete samples, gradients and micro patterned arrays; all of which present challenges for characterisation. A review of this research and a discussion of the merits of each approach are presented below.

The first step in high-throughput material discovery is the synthesis of a large library of new materials to be screened. Polymers are well suited to this task as large libraries can be prepared by simply mixing a small number of monomers in a pair wise fashion or blending polymers in different ratios. Blending different polymers commonly results in a material with intermediate properties to the constituent polymers. Different surface features can be produced by processes

such as annealing or mixing.[14] These new materials can either be analysed individually or fixed to a chip in an organised fashion to allow high speed screening. There are two approaches to this task: discrete and continuous libraries. The relative merits of the two approaches are discussed later. Finally, methods must be developed to determine whether the new materials on the chip have the properties desired.

1.2.1 Large scale discrete libraries

The first large scale work using a combinatorial method to synthesise a library of novel polymers was reported by Brocchini *et al.*[15] A library of 112 degradable polyacrylates was prepared by reacting various tyrosine based monomers together in different combinations in parallel. Fourteen different diphenol monomers were each reacted with eight diacid monomers to create the 112 polymers. Each pair of monomers was reacted in an individual vial to ensure the purity of the resulting polymer. The glass transition temperature (T_g), molecular weight, water contact angle and tensile properties of each polymer were then determined. The T_g values were determined using DSC and the molecular weight using gel-permeation chromatography. The tensile properties of the polymers were investigated by taking stress-strain curves of solvent cast films of the samples. It is perhaps disappointing that the authors did not carry out a more detailed surface characterisation, rather than simply measuring the polymers' wettability.

In a follow-up study, glass cover slips were spin coated with the polymers and fetal rat fibroblasts were cultured on their surfaces to determine the ability of the polymers to support cell growth.[16] The T_g and contact angle values varied incrementally across the polymer library (Figure 2). It was noted that the T_g of the polymers decreased with increasing numbers of methylene groups in the pendent chain and backbone. Conversely, the water contact angles of the polymers increased with increasing numbers of methylene groups.

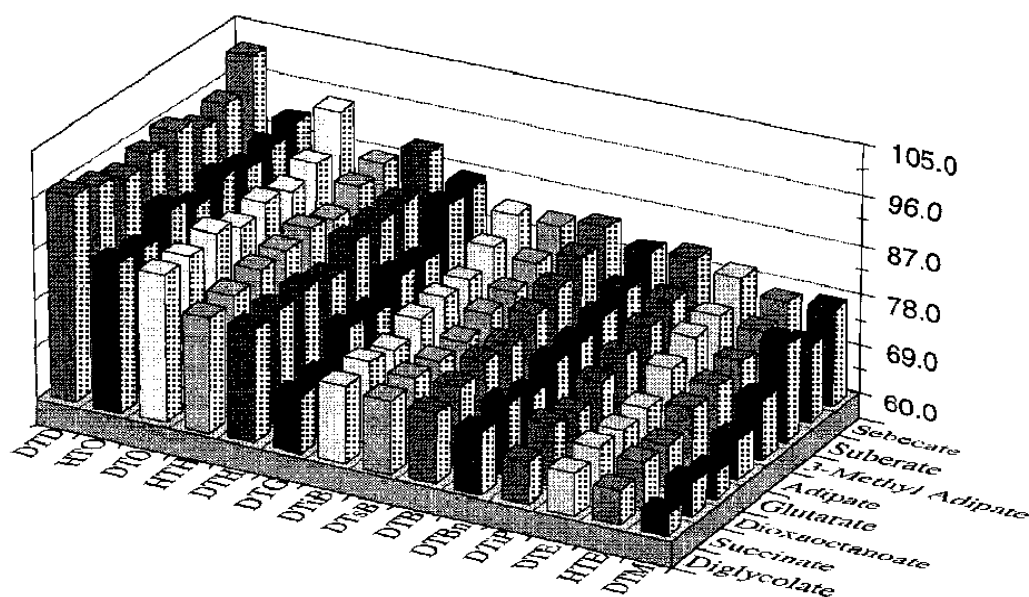


Figure 2. Water contact angles of the poly(arylate) library.[16]

When the authors used the same polymer library to investigate the relationships between polymer structure and cell response,[16] the extent of fibroblast proliferation on the polymers ranged from total coverage of the polymer film to complete absence of growth. There were significant correlations between cell proliferation and the contact angle of the polymers (Figure 3), where it was noted that fibroblast proliferation decreased as the contact angle of the polymers increased. This effect of surface hydrophobicity on fibroblast cells has been observed in other studies.[17-19] However, there was an exception to this trend: those polymers whose backbone contained oxygen supported cell growth even with contact angles exceeding 95° . This study was one of the first to demonstrate the benefits of producing combinatorial libraries of polymers for biomaterials research. In fact one of the polymers in the library developed has since been approved by the FDA for use in a new hernia repair device which is marketed in the United States.[20] The work showed the speed at which new polymers with a range of desired physical and biological properties can be prepared. However, the way in which the polymers were synthesised and investigated was not new: only the scale of synthesis. In fact the way in which the polymer library was prepared was relatively time-consuming and hinders rapid analysis. Before analysis each polymer had to be individually spin-coated into a large scale film and then analysed with traditional low throughput methods. It is for these reasons that the

next step in combinatorial biomaterials research was towards miniaturisation using gradients and micro patterned arrays. However, very recently Brocchini *et al*'s approach (large scale preparation of polymer libraries prior to screening) has been praised as it allows thorough characterisation of the polymers' bulk properties, such as glass transition temperature and molecular weights.[21] However, this criticism neglects to mention the importance of the polymers' surface properties and may be left redundant by some of the developments in polymer library characterisation presented in this thesis.[22]

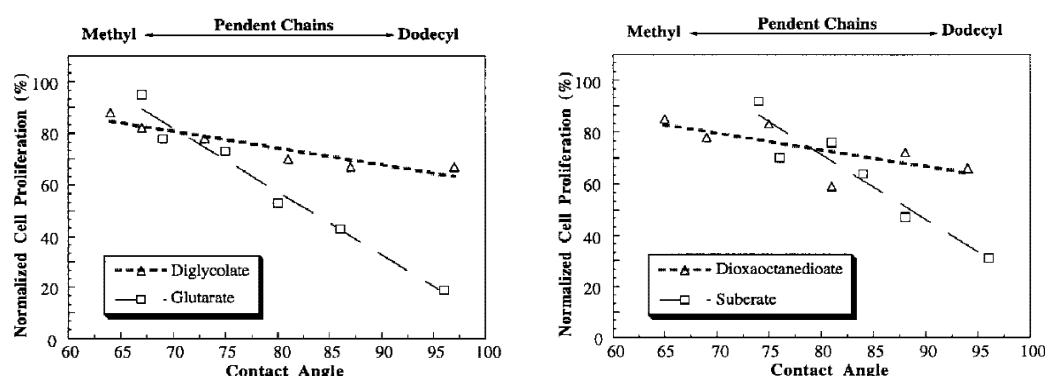


Figure 3. The influence of polymer water contact angle on fibroblast proliferation.[16]

A similar approach to that taken by Brocchini *et al*, albeit with different monomers was used by Lynn *et al* in the development of a polymer library to be screened for use as possible DNA transfection vectors.[23] Seven diacrylate monomers were mixed pairwise in all possible combinations with twenty amine monomers to produce 140 structurally unique polymers. The amine monomers are able to insert into the diacrylate backbone to produce biodegradable cationic polymers with the ability to condense DNA at physiological pH (Figure 4). Half of the polymers synthesised were not sufficiently water soluble to undergo a DNA-binding assay. However, those polymers which were water soluble were analysed using an electrophoresis assay to identify those with greater DNA-binding ability than the commercially produced Lipofectamine 2000, which is a leading lipid-based transfection vector. Seven polymers from the library were identified as having high DNA-binding ability, validating this combinatorial approach as a viable method for discovering new polymers for gene delivery. The method was taken further by the same authors by vastly increasing the number of

monomers used.[24] This enabled them to create a combinatorial library of 2350 novel poly(β -amino esters) which they again screened for DNA-binding ability. This time 46 new polymers were identified as potential gene delivery systems, demonstrating that increasing the size of the combinatorial library analysed can increase the chances of finding a polymer with the desired properties.

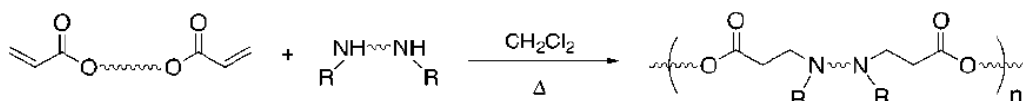


Figure 4. Synthesis of poly(β -amino ester) by reaction of diacrylate with amine monomer.

1.2.2 Gradient material libraries

A gradient surface is one in which a property of the surface (chemical, physical or morphological) gradually changes.[25] Gradient surfaces have become an important tool for the high throughput investigation of interfacial phenomena in areas as diverse as physics, biology and materials sciences. A large amount of this research has concerned polymeric gradients, with various methods proposed for creating surface chemical and morphological differences.

The combinatorial approach taken by Brocchini *et al* was developed by Meredith *et al* using polymer film gradients.[26] They prepared polymer libraries containing a continuum of distinct surface chemical and topographical properties using composition spread and temperature gradient techniques. This involved pumping one polymer into a vial which already contains another polymer, while a syringe is used to withdraw the resulting blend.[17] This blend was then spread using an automated knife onto a 25 x 30mm silicon wafer producing a film with a thickness that varied from 345-510 nm (Figure 5).

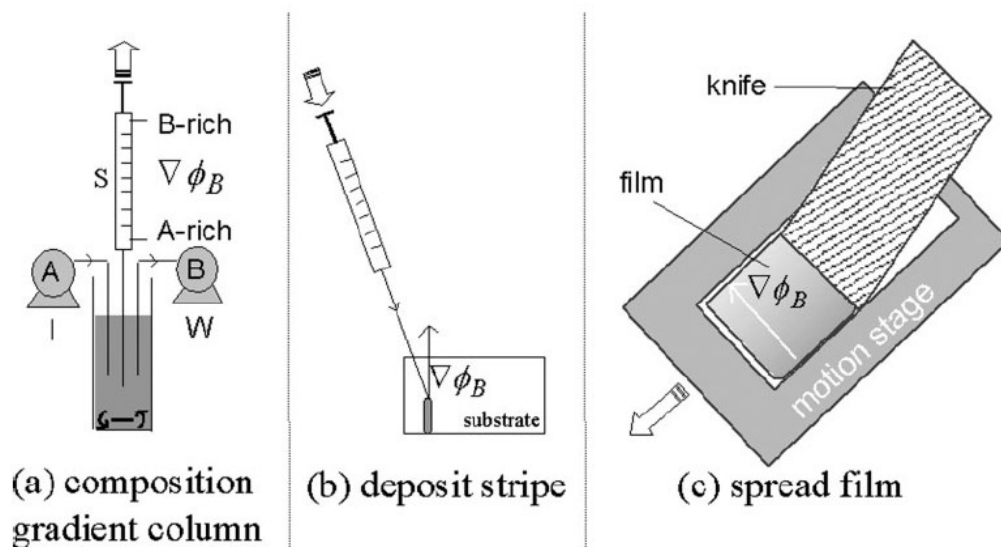


Figure 5. Schematic of the continuous composition gradient deposition process.[17]

The two polymers used were poly(D,L-lactide) (P_DLA) and poly(ϵ -caprolactone); both chosen because they are FDA approved for use in certain medical devices. The polymer films were annealed at different temperatures to produce varied morphological features on the polymer surfaces.

The polymer films were analysed with Atomic Force Microscopy and Fourier Transform Infrared Spectroscopy (FTIR). Osteoblasts were then cultured on the wafers to test cell response to the polymer blends. Cell density and morphology were assayed with light and fluorescence microscopy. The analysis showed that cell adhesion and function were strongly influenced by microstructures on the polymer surface. Many of these microstructures were produced by polymer phase separation induced by the annealing process. The cells appeared to attach preferentially to surfaces rich in P_DLA which is hydrophilic. Most importantly it was observed that when the osteoblasts were cultured on one polymer blend there was upregulation of alkaline phosphatase expression within the cells. This blend was 45 % PCL and 55 % P_DLA, annealed at 100 °C. It is likely that the surface chemistry and morphology of this blend induce cell shape changes and mechanical stresses with the cells that lead to upregulation of alkaline phosphatase expression. This research demonstrated the value of high throughput methods in characterising cell-surface interactions. However, the way they prepared the polymers (as gradient libraries on slides)

does not necessarily allow “statistically relevant combinatorially designed” selections of polymer composition.[14] In contrast a discrete library allows intelligently selected polymer compositions, gradient libraries such as this leave it almost to chance.

A similar investigation to the one described above was carried out by Washburn *et al* who used high-throughput methods to investigate osteoblast response to nanometre-scale roughness on polymer surfaces.[18] Gradients of roughness on films of poly(L-lactic acid) (PLLA) were produced by annealing different parts of the film at different temperatures. The root-mean-square (RMS) roughness of sections of the sample was determined using tapping mode Atomic Force Microscopy. This showed that the annealing process had produced a roughness gradient along the slide (Figure 6), although the actual variation was minimal.

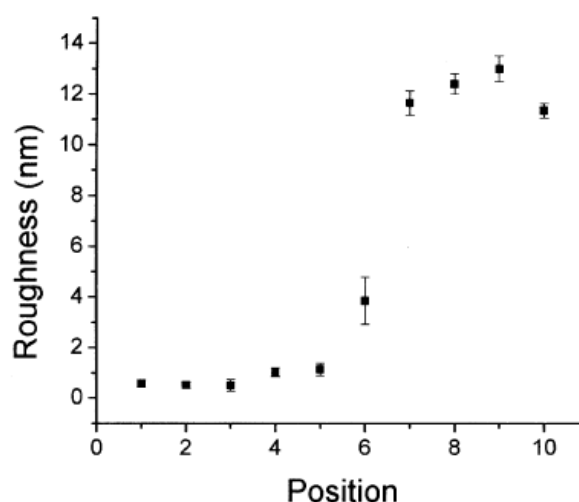


Figure 6. Plot of average measured RMS roughness as a function of library position.[18]

Osteoblasts were then cultured on the polymer films for between one and five days to test cell response. Automated fluorescence microscopy was used to determine the number of cells on different parts of the polymer film. Figure 7 shows the average cell numbers observed on different positions on the gradient, demonstrating that the rate of proliferation of the osteoblasts was greatest on the smoother, amorphous surface. The rate of proliferation decreased as the surface got rougher.

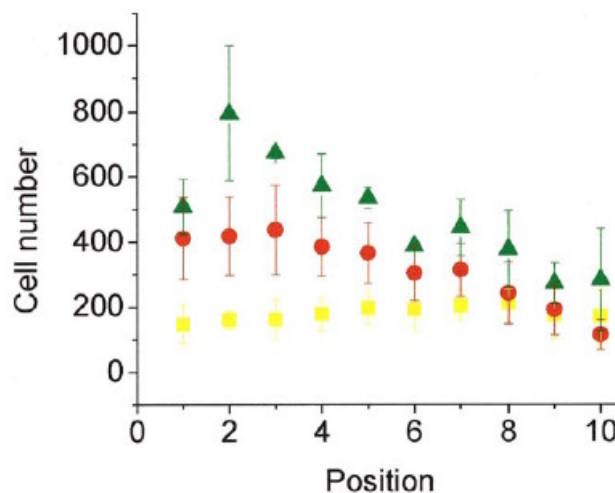


Figure 7. Plot of average cell number versus library position after culturing for 1(○), 3(●) and 5(▲) days.[18]

Another example of using polymer gradient libraries to investigate cell response to polymeric materials is the research carried out by Simon *et al.*[27] They prepared gradient libraries containing blends of poly(L-lactic acid) (PLLA) and poly(D,L-lactic acid) PDLLA, then determined the composition of the blends using FTIR. The roughness of the libraries was measured from images acquired using AFM. After characterisation murine osteoblasts were cultured on the polymer blend libraries; then cell adhesion and proliferation were analysed using automated fluorescence microscopy. Figure 8 shows the percentage bulk composition at different points along the library as determined by FTIR and Figure 9 shows the roughness of the surface of the library.

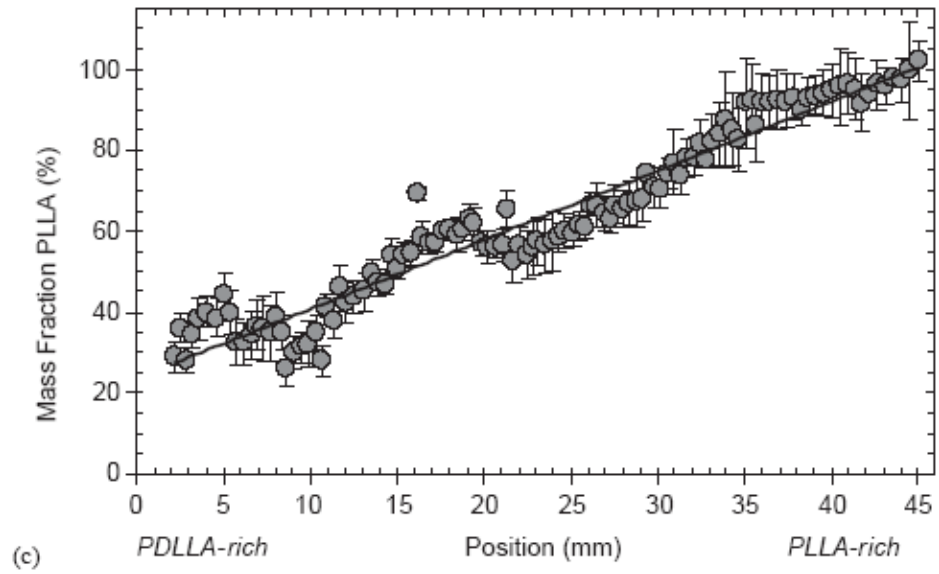


Figure 8. Graph showing the composition of the polymer blend library at different positions.[27]

Generally the osteoblasts adhered well to all areas of the library including both P_{DLA} and P_{LLA} rich areas. However, cell proliferation was greatest at the P_{DLA} -rich end of the library. It is possible that this could be due to the surface of the P_{DLA} -rich end being smoother than other areas of the library.

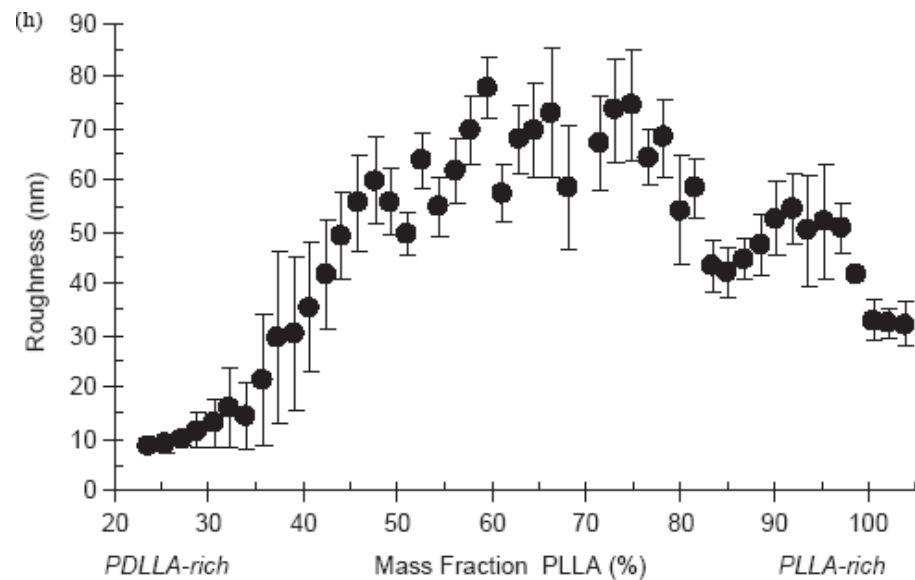


Figure 9. Graph showing the roughness (nm) of the surface of the polymer library.[27]

1.2.3 Micro-patterned material arrays

So far the research discussed has been that involving the preparation of polymer libraries as either gradients or as large scale samples, with their associated disadvantages. Recently, there has been great interest in the application of array technology to materials development.[28, 29] Previously it was only water soluble molecules such as DNA and RNA that were printed and screened using array systems.[28] The use of arrays for investigation of materials in the solid state, for example polymers, has been a more recent development and has presented a number of challenges due to their difference to established methods used in drug discovery.[30] These challenges include the differing rheological properties of polymer solutions compared to the aqueous solutions printed in biological array manufacture. Hence, the added viscosity of polymer solutions can complicate the printing process if necessary measures are not taken. Two principal methods have been reported for the manufacture of polymer microarrays: inkjet printing and contact printing. Schubert *et al* have investigated the use of inkjet printers to print polymers in some detail,[31, 32] however it has only been within the past year that the first full inkjet printed microarray has been reported. Zhang *et al* prepared a hydrogel microarray by sequential inkjet printing of acrylate monomers and initiator, allowing *in situ* polymerisation.[33] However, with the above exception, the remaining literature has described polymer microarray fabrication using contact printing and it will be this that is described below.

A major advance in high throughput polymer research came in 2004 with the development of a method of preparing miniaturised micro-patterned polymer arrays using a contact printing methodology. Since this development the polymer microarray field has taken two different approaches. Firstly the contact printing of existing polymer libraries and secondly the contact printing of monomer mixtures which are polymerised *in situ* in array format. Anderson *et al* reported a method of rapidly producing large discreet libraries of different polymers and screening them for their effects on stem cell adhesion and differentiation.[34] They selected 25 different acrylate, diacrylate, dimethacrylate and triacrylate monomers and

mixed them in 576 different combinations. These mixtures were deposited in 576 individual spots on a glass slide where they were polymerised using UV radiation. Three arrays of 576 polymer spots were printed onto each glass slide to allow the reproducibility of the method to be assessed. The glass slide was coated with poly(hydroxyethyl methacrylate) prior to the addition of the polymer spots, as this polymer has been proven to inhibit cell growth.[35] Manufacturing polymer libraries as microarrays allows the advantages of using both large discrete samples (i.e. each sample is assessed individually), but also all printed on one support to aid a rapid analysis.

To test the newly synthesized polymer spots for their effects on human embryonic stem cell growth and differentiation, each spot on the arrays was seeded with embryoid bodies. The cells were then incubated with retinoic acid for six days, after which the arrays were fixed and stained for cytokeratin 7 (an intermediate filament protein found in most epithelial cells) and vimentin (an intermediate filament protein found in cells with mesenchymal origin). It was found that nearly all the new materials allowed cell attachment and growth, however polymers containing monomers 6, 18 and 21 inhibited cell growth or attachment to varying degrees. It was also observed that cells on a majority of the polymers were cytokeratin-positive, i.e. showing differentiation into epithelial-type cells. The researchers also grew cells from an embryonic muscle line on the arrays to examine the polymers effects on non-human embryonic stem cells. These muscle cells grew on all polymer spots except those containing monomer 18, demonstrating that human embryonic stem cells are strongly influenced by the surface they are cultured on in different ways to normal cells.

The research was taken further by identifying those polymers on the array that supported cell growth particularly well and retesting them on different arrays. These arrays contained only 24 different polymers repeated 72 times. The polymer spots on these arrays were then seeded with hESC and cultured with and without retinoic acid. In the absence of retinoic acid there was lower expression of cytokeratin, but the number of cells per spot was higher and they were more closely packed together. However, some polymer spots could only support hESC growth with retinoic acid (e.g. 100% monomer 6). This type of investigation

demonstrates that cell experiments on microarrays do not have to be just simple cell adhesion assays; more sophisticated differentiation studies and alike are possible.

Another difference between the research described in the above paper and that which had been done before is scale. The methods described enable hundreds of polymers to be synthesised and tested for the ability to support cell growth in a relatively short period of time. The research also reinforced the fact that materials can have a large influence on hESC growth and differentiation. The same research group published a second research article shortly afterwards further demonstrating the potential of the arrays they have developed.[36] However, this differed from their previous research because the polymers were not synthesised *in situ* on the array, but were commercially available and already well-characterized. The polymer library was created by blending 24 commercially available polymers pairwise at ratios of 70:30 and 90:10 to produce 1152 different combinations in total, i.e. double the size of their previous library. The 24 polymers used were all biodegradable polyesters except for one which was an anhydride. Several different cell types were cultured on these arrays. These cell types were human mesenchymal stem cells (hMSC), bovine articular chondrocytes and murine neural stem cells.

The hMSC attached and spread on most of the polymer spots, however there were polymer blends that did not allow cell attachment. For example, the polymer blends containing poly(ethylene glycol) inhibited cellular attachment. It is well known that this polymer does not support cell attachment.[37] Figure 10 shows the polymer array in question containing hMSC which have been stained green with actin. It is obvious on the image which spots have not allowed cell attachment as these spots are only partially stained or not stained at all.

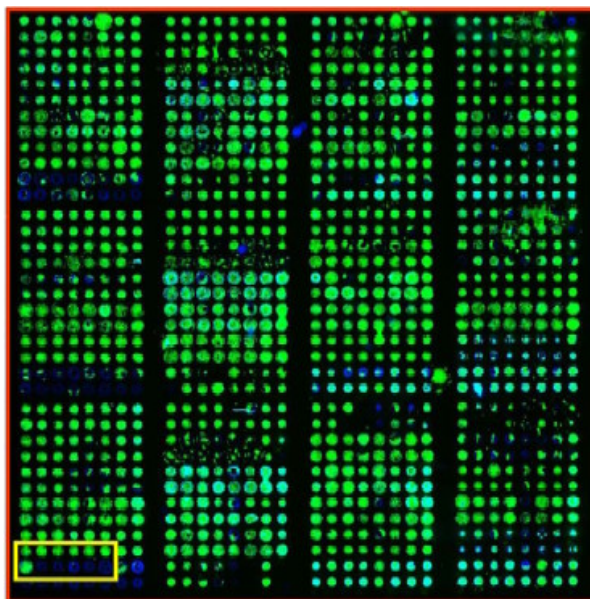


Figure 10. A polymer array containing hMSC stained green with actin.[36]

The bovine articular chondrocytes attached well to the polymer spots and multiplied to produce larger numbers of cells than the hMSC. Finally, neural stem cells were grown on the array then stained for glial fibrillary acidic protein (expression of which suggests differentiation towards astrocytes). The neural stem cells formed monolayers on all the polymer spots and stained brightly for glial fibrillary acidic protein. The authors of the research noted that heterogeneous phase separation of the polymer blends, which changes the polymer microstructure, could influence cell behaviour.[36] It would have been preferable if this had been confirmed using an imaging technique such as atomic force microscopy. This research further demonstrates the potential of microarrays in the study of cell-material interaction, whilst suggesting the feasibility of using multiple cell types on the arrays.

Since the pioneering work in this area by Anderson *et al* there have been a number of papers published by different groups replicating the research, albeit with different cell types. However, Bradley *et al* have taken a rather different approach, after criticising the *in situ*, nanolitre scale polymerisation approach used by Anderson *et al*. The specific criticisms were related to the fact that the arrayed polymers had not undergone the classical bulk characterisation common in the polymer sciences for novel polymers.[21] They also took issue with the perceived problems that may be encountered due to rapid evaporation of the printed

monomer solutions before polymerisation (i.e. the exact composition of the final polymers is unknown).[21] It could be argued that the first issue is irrelevant as bulk characterisation of ‘hit’ polymers could be undertaken once the polymers were scaled up in the later stages of investigation. Similarly, the second issue could be minimised by printing the arrays under the correct environmental conditions. However, it was these issues that prompted Bradley *et al* to manufacture microarrays by contact printing a library poly(urethane)s. Prior to printing this library had already been well-characterised by gel permeation chromatography, differential scanning calorimetry and water contact angle measurement. These microarrays were then used in renal epithelial cell adhesion assays to identify the most cell-adhesive polymers in the library.[21] The same group has since published studies using the same library to screen for dendritic cell adhesion and to screen for polymers that direct drug crystal growth.[38, 39]

One major issue with polymer libraries printed and analysed in a miniaturised array format, is the relevance of the data gained from them to the macro world. In other words, if the polymers on a microarray are scaled up into large scale samples and retested, will they yield identical biological, physical and chemical properties to those observed when they are printed as 300 μm spots?

1.2.4 Three-dimensional polymer libraries

The methods described above all focus on the two dimensional interaction of cells with a flat surface. Cells *in vivo* do not exist in such an environment, rather in a three dimensional matrix allowing interaction with surrounding cells and ECM proteins.[7] Cells behave in a more natural way in a three dimensional environment, hence the development of three dimensional scaffolds for use in tissue engineering. Simon *et al* have proposed a method for preparing discrete and gradient three dimensional polymer scaffold libraries.[40] This involves blending two polymers in different compositions with sodium chloride, then leaching the salt out of the polymer blends once they have set using water to form a porous scaffold (Figure 11).

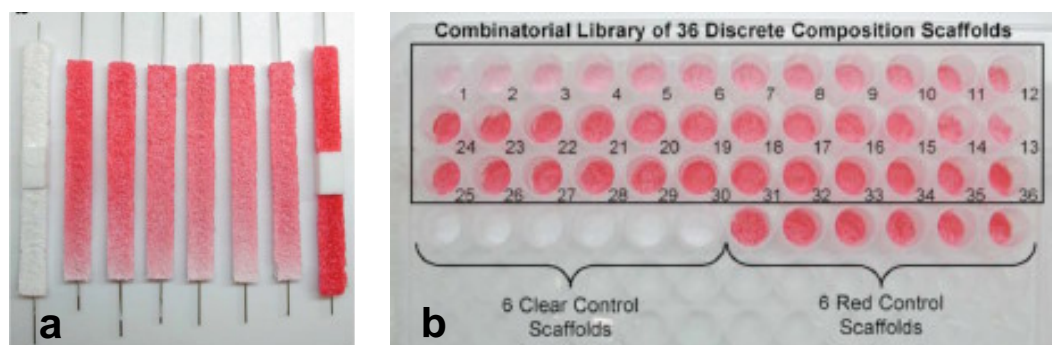


Figure 11. Three dimensional a) gradient b) discrete polymer scaffold libraries.[40]

The authors used this technique to form a 48 member library of discrete 3D polymer scaffolds from two commercially available tyrosine-derived poly(carbonates).[41] Osteoblast cells were cultured on these scaffolds to investigate which polymer blends supported cell attachment.

1.4. Research involving high-throughput surface characterisation of polymeric materials

It is interesting to note that the surface chemical and physical characterisation of the polymer libraries discussed above has been minimal. This may be due to the investigators being more interested in the polymers' biological properties or perhaps because of the difficulties associated with analysing large numbers of samples in unfamiliar formats. The small number of studies involving such characterisation will be discussed below. In this context FTIR spectroscopy (in its attenuated total reflectance mode) will be treated as a surface sensitive technique due to its common usage in the field, although technically it is defined as only a near-surface technique (1 to 4 μm).[42]

Thissen *et al* have investigated the viability of XPS as a method for analysing polymers printed as microarrays.[43] Poly(ethylene glycol) methacrylate (PEGMA) was printed onto a poly(styrene) coated substrate to produce polymer spots with a diameter of approximately 375 μm . During analysis the aperture on the XPS was adjusted to collect electrons from only a small area of approximately 120 μm diameter. XPS survey and high resolution C1s spectra

were then acquired from both the poly(styrene) substrate and a printed PEGMA spot. The two sets of spectra were distinct and were identical to the spectra of pure poly(styrene) and PEGMA respectively, thus confirming the feasibility of analysing arrayed polymers with XPS.

Nanoindentation involves applying a rigid indenter onto a surface while continuously measuring the load applied and the displacement of the indenter into the surface. It can provide information on a sample's near surface mechanical properties including elastic modulus E and hardness H , and has been shown to be well-suited to characterisation of discrete or gradient material libraries.[44] This technique was applied to a large array of 1728 polymer spots by Tweedie *et al* to investigate the possibility of characterising the mechanical properties of a large number of polymer samples.[45] The polymer arrays used were produced using the same method as described by Anderson *et al* which are discussed above.[34] The nanoindentation measurements were carried out using an automated nanoindenter produced by Micromaterials Ltd and characterisation of the entire array took less than 24 hours. The results of the experiment demonstrated that the elastic modulus of any particular polymer depended almost entirely on the major monomer constituent; i.e. the minor monomer constituent had very little influence on elastic modulus of the polymer spot. However, two monomers did have a considerable influence on elastic modulus when they were a minor component. The most important result of this research is the demonstration of the feasibility of characterising the mechanical properties of large numbers of polymer samples on microarrays using nanoindentation.

Similar work to the research discussed above has been carried out by Kossuth *et al*, but not on the same scale. They used a Symyx Parallel Dynamic Mechanical Analyzer to take modulus measurements of discrete polymer samples mounted on arrays. The modulus measurements were taken by measuring the force needed to deform a thin polyimide substrate by a set amount with and without the sample present. The modulus of the sample was calculated relative to that of the polyimide using a well-known mathematical model. Plateau modulus and glass transition temperatures can also be measured using this technique.

An attempt to develop high-throughput methods for determining structure/mechanical property relationships for polymers has been made by Sormana *et al.*[46] Temperature gradient libraries of segmented polyurethaneurea (SPUU) elastomers were prepared on silicon wafers. SPUU elastomers are block co-polymers with a micro-phase separated morphology. The gradient libraries were analysed using FT-IR spectroscopy and non-contact atomic force microscopy. Then stress/strain curves were measured at various points across the libraries using a high-throughput impact and strain apparatus developed for characterisation of polymer gradient libraries. The FT-IR was used to measure the degree of hydrogen bonding between the segments of the polymer by observing three peaks in the carbonyl region of the infra red spectra.

Fourier transform infrared microspectroscopy was also used by Eidelman *et al* to characterise combinatorially prepared gradient polymer blend libraries. The libraries tested were blends of PLLA and PDLLA, both polymers which are commonly used in tissue engineering. The gradient libraries were thin films on low emission reflective slides. The FTIR spectrophotometer was used in reflectance mode to analyze the gradient libraries and the results used to produce images that showed the chemical composition of all areas of the library. Figure 12 is an example of the composition maps produced from the arrays showing the ratio of PLLA to PDLLA in different areas.

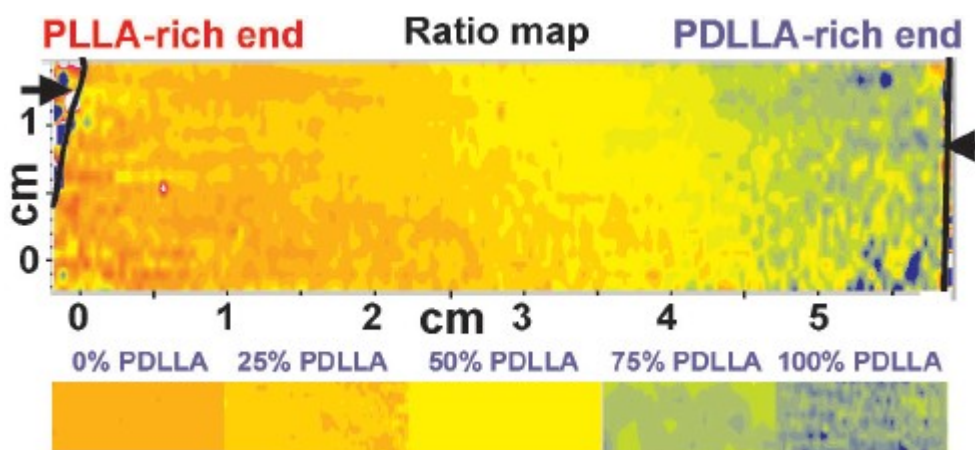


Figure 12. A composition map of a polymer gradient library prepared using FTIR.

FTIR imaging is a useful technique for visualizing the near-surface of a polymer blend - showing where on a sample different polymers dominate. This technique

could be applied to a discrete polymer library also, depending upon what substrate it was prepared on.

Thaburet *et al* have developed a high throughput methodology to determine the wettability of a large library of polyurethanes.[47] A robotic liquid handler was used to dispense microlitre water droplets onto spin coated films of the polymers, and then a camera fixed to the handler was used to take top-down images of the droplets. A calibration curve was then use to determine the polymers' contact angles from the spreading area of the droplets (Figure 13). Although this work was a nice demonstration of how wettability measurements can be automated, there was not much new about how the library was prepared for analysis. Each polymer still had to be individually spin-coated onto a substrate prior to analysis; a very time consuming exercise for 280 polymers!

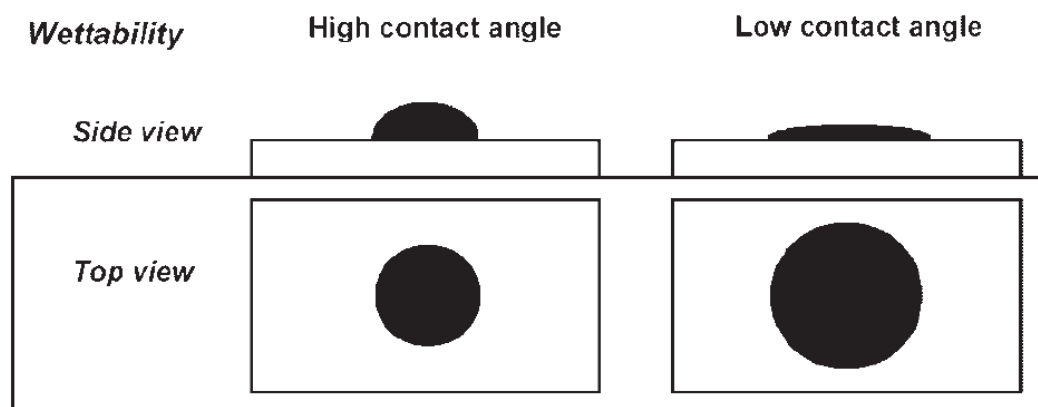


Figure 13. Relationship between contact angle and spreading area.[47]

1.5 Aims and objectives of thesis

Thus far the reader has been introduced to the different approaches that have been trialled to speed the discovery of new polymeric biomaterials. It is hoped that this has emphasised the fact that the general characterisation, and particularly the surface characterisation, of these combinatorial polymer libraries arrays has been neglected. Indeed if any surface characterisation is undertaken it is often in the form of simple wettability measurements or near-surface spectroscopy e.g. FTIR. With the advent of polymer microarrays there is a real opportunity to use large libraries of polymers to study the fundamental science behind the biological response to polymeric materials. However, without knowledge of the polymers' surface properties it will be impossible to rationalise the biological data from these polymers, nor study surface structure-property relationships.

It is the aim of this thesis to develop methods for the characterisation of the surface chemistry of polymers *in situ* in microarray format and within realistic timeframes. Multivariate statistics in the form of principal component analysis will be investigated as a method of dealing with the massive amounts data obtained from such arrays. Methods will also be described for the estimation of the surface energy of microarrayed polymers and the characterisation of their protein adsorption properties: both are properties which have previously been used to rationalise cell response to materials. Finally the data obtained will be used to demonstrate how surface chemical data from polymer microarrays can be related to other surface properties using partial least squares regression.

Chapter 2

Experimental Methods

2.1 Time of Flight Secondary Ion Mass Spectrometry (ToF-SIMS)

ToF-SIMS is a very surface sensitive technique which allows a mass spectrum of a material's surface to be obtained to a depth of approximately 1 to 2 nm.[48] This spectrum can give a great detail of information about the molecular structure of the material's surface. To obtain a mass spectrum the surface is bombarded with primary ions, which results in the emission of positive and negative secondary ions (plus a large amount of neutral fragments) (Figure 14). Although SIMS appears to be a destructive technique, in static SIMS the primary ion dose is kept very low (always less than 10^{13} ions cm^{-2}), meaning that within the time-frame of the experiment less than 1 % of the top layer of a material's surface receives an ion impact.[49] Hence the spectral information gained should always be from undamaged areas of the sample surface. The relatively high energy impact of the primary ions into the surface results in a large amount of bond breakage and fragmentation at the collision site, causing the emission of atomic species. The kinetic energy of the primary ions is transferred to the atoms of the sample by a cascade of collisions. As the distance from the collision site increases the collisions are less energetic and hence result in fewer bonds breaking and therefore the emission of molecular and quasi-molecular species. Primary ion sources which are in common use include Caesium, Gallium and Bismuth.[48]

The primary ion beam is pulsed over very short periods of time which produces discrete 'packets' of secondary ions from the surface. The 'packets' of ionised species emitted are accelerated over a very short distance resulting in all the ions having virtually identical kinetic energies, which is vital to the working of the Time-of-Flight spectrometer. The 'packet' of ionised species then travels through a drift tube on their way to the analyser. The ions separate by mass as the heavier ions have a lower velocity than the ions of lower mass.[49] This effect is described in the following equation:

$$E_k = \frac{1}{2}mV^2 \quad (1)$$

where E_k is the kinetic energy, m is the mass and V is the velocity of the ion. The differing velocities of the ions will result in them arriving at the analyser at different times. The following equation can then be used to calculate each ion's mass from the time it takes for them to travel the length of the drift tube:

$$t - t_0 = L \left(\frac{m}{2E_k} \right)^{1/2} \quad (2)$$

where L is the length of the flight path, t_0 is the start time and t is the arrival time at the detector. A Time-of-Flight instrument allows much greater mass resolution to be obtained than older systems which employ Quadrupole detectors, particularly when a reflectron is used.[49] Although all secondary ions are accelerated to have approximately the same kinetic energies, there is still a small spread of energies for ions with the same mass. This can result in a lower mass resolution. To compensate for this spread many Time-of-Flight instruments employ a reflectron, which is essentially a retarding electric field that allows ions with a higher kinetic energy to penetrate further into the reflectron. This results in higher energy ions travelling further and hence compensating for the spread in kinetic energies. A major advantage of Time-of-Flight systems is that they allow the whole mass spectrum to be collected in parallel, thereby greatly reducing the primary ion dose needed.

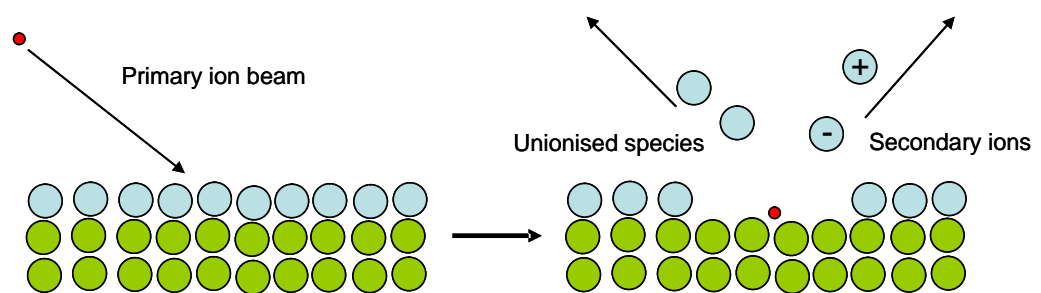


Figure 14. Diagram illustrating the production of secondary ions from a surface.

When using ToF-SIMS to analyse insulating materials such as polymers, it is necessary to employ a charge compensation device. This is because the sample gains a net positive charge due to dosing with positive primary ions and emission

of secondary electrons.[49] This compensation device is normally in the form of an electron gun which floods the sample surface with electrons which stabilises the surface potential.

ToF-SIMS can also be used to image surfaces thereby showing the distribution of selected atomic or molecular species on a sample surface. Using a modern instrument it is possible to image areas ranging in size from a few micrometres to tens of millimetres, by rastering the primary ion beam over the surface of the sample by means of a motorised stage.[49] Time-of-Flight detectors are ideally suited to imaging due to their high transmission and most importantly their simultaneous collection of all masses. This results in ToF-SIMS images having a full mass spectrum per pixel allowing retrospective visualisation of any ion in the spectrum. ToF-SIMS image interpretation can be challenging due to topographic and matrix effects on the intensity of ions from different parts of the sample.[48] Therefore care must be taken to separate intensity variation which is due to changes in surface chemistry from those that are simply due to topography.

2.2 X-ray Photoelectron Spectroscopy (XPS)

XPS or ESCA (electron spectroscopy for chemical analysis) is a highly surface-sensitive technique (top 1 to 10 nm), which provides quantitative information about all elements except Hydrogen and Helium.[50] The defining event in its history was the discovery of the photoelectric effect by Heinrich Rudolph Hertz in 1887, which describes the emission of electrons from a material after absorption of energy in the form of electromagnetic radiation such as X-rays.[49] The X-rays used for analysis are generated by bombarding an anode with high energy electrons from a heated filament. The anode is commonly made out of Aluminium or Magnesium. The X-rays produced are generally monochromated to provide a smaller range of energies, thereby improving the resolution of the technique.

The technique involves directing a beam of X-rays onto a sample, which penetrates to a distance of a few micrometres. This causes the ejection of electrons from core energy levels in atoms on or near the surface, but only if the energy of the X-rays is great enough to overcome the energy holding the electrons to the nucleus (known as the binding energy). Only a small amount of these electrons emerge from the sample surface without suffering any energy loss through collisions on the path through the sample bulk. The chance of an electron reaching the surface without any energy loss decreases greatly as the distance from the surface increases. The binding energy of an electron can then be calculated if the kinetic energy of the electrons is known.[51] The following equation is used to describe the relationship between the binding energy of an electron and its kinetic energy when ejected from its orbital:

$$E_{kin} = h\nu - E_{bind} - \Phi \quad (3)$$

where E_{kin} is the electrons kinetic energy, E_{bind} is its binding energy, $h\nu$ is the energy of the X-rays used and Φ is the work function of the spectrometer.

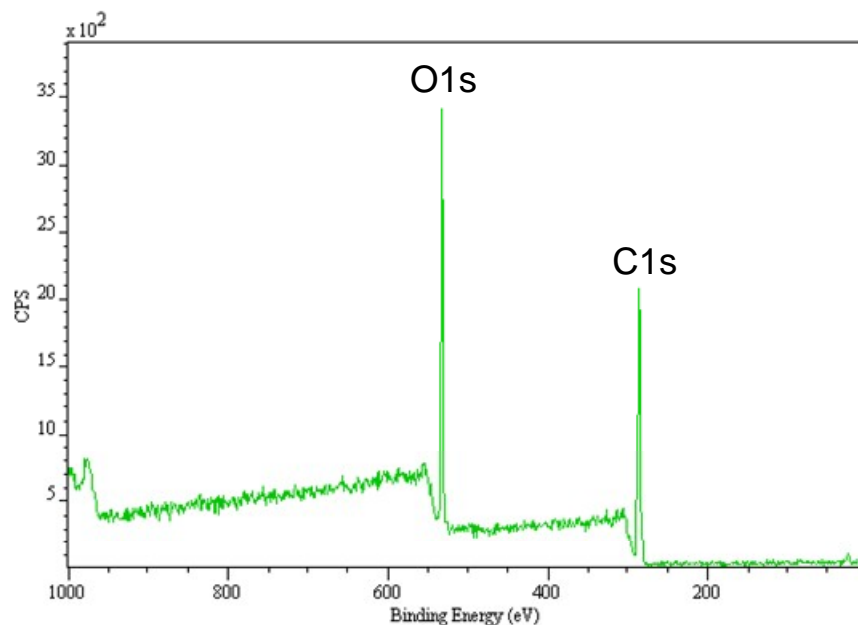


Figure 15. Example of a broad XPS spectrum.

The binding energies of core electrons from different atoms are unique, therefore an XPS spectrum can show what atoms are present on the surface of a

sample. A survey XPS scan of a surface is commonly carried out first which covers the entire binding energy range (generally 0 to 1000 eV). Integrating the area under each of the peaks on this spectrum can give the relative quantity of each of the atoms on the surface. This survey scan is a useful way of identifying what elements are present on a surface and their relative quantities (Figure 15).

The XPS spectrum of a hydrocarbon polymer containing no impurities is very simple, as only the Carbon 1s peak is visible. Surface contaminants such as adventitious hydrocarbons, surface oxidation products or PDMS are often visible on XPS survey spectra. Therefore it is very important that care is taken during the preparation, handling and analysis of samples to minimise surface contamination.

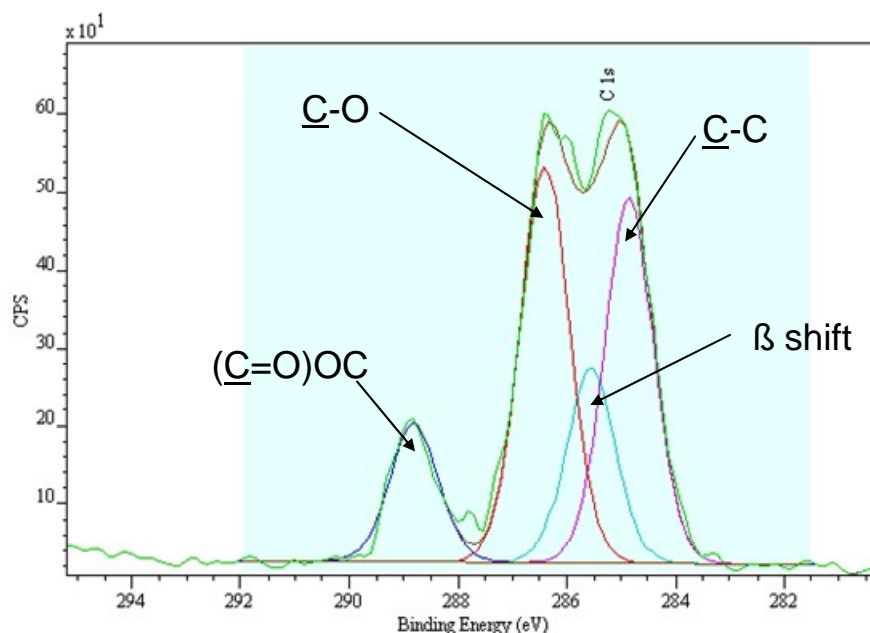


Figure 16. Example of a high resolution C 1s XPS spectrum with component peaks fitted.

XPS spectra can be obtained at high resolution, focusing on specific binding energies. This is useful as the binding energies of detected photoelectrons are also dependent on their local chemical environment. Therefore small shifts in binding energy can be observed when an atom is bound to different atoms. Hence XPS can provide information not only on what atoms are present at a surface, but also the chemical environment that these atoms are in. When analysing the surfaces of polymers a large amount of information can be gained from close study of the C 1s peak in particular (Figure 16). The C 1s peak is generally the sum

of a number of component peaks which are each caused by carbon atoms in different chemical states. For example, Carbon bonded to another carbon atom or hydrogen gives a peak at 285 eV, whereas carbon single bonded to oxygen (for example in an ether functionality) gives a peak at ~ 286.5 eV. Hence a shift in bonding energy of ~ 1.5 eV due to the different chemical environments of the carbon atoms. These component peaks of the high resolution C1s peak can also be integrated to give a quantitative assessment of the relative quantities of different functional groups on a surface.

Sample charging can also be a problem in XPS analysis of insulating materials such as polymers, due to the removal of electrons from the surface region, resulting in a net positive charge. Sample charging can cause shifts in the binding energies of peaks on an XPS spectra. As with ToF-SIMS analysis an electron flood gun is generally used to minimise this charge. The spectra can also be charge corrected prior to analysis.

2.3 Atomic Force Microscopy (AFM)

The Atomic Force Microscopy (AFM) was developed by Binnig *et al* in 1986 following on from the invention of Scanning Tunnelling Microscope (STM) in 1981.[52] AFM is now the most commonly used type of scanning probe microscope principally because, unlike STM, it can be used to image insulating samples such as biologics. AFM can also be operated in ambient and aqueous environments. An AFM consists of a very sharp tip at the end of a cantilever which is generally either moved along a surface (contact AFM) or tapped onto a surface (tapping mode AFM) (Figure 17). A laser focused on the cantilever is used to detect the vertical movement of the tip and the information used to create an image of the surface, i.e. these microscopes image a sample by ‘feeling rather than looking’. These images can provide useful information on surface topography and roughness down to the nanoscale, far surpassing the resolution of optical and electron microscopes.

In tapping mode AFM further information can be gained by observing the phase lag of the cantilever as it oscillates on the surface. This lag is caused by interactions between the surface and tip which cause the cantilever to oscillate out of sync with the driving mechanism.[53] Therefore phase images can provide useful information about the morphology of the surface being studied, for example whether a polymer blend is phase separated, or the mechanical properties of the surface. The information in the height images can be used to get quantitative information on a samples roughness allowing the roughness of more than one sample to be compared statistically. The root mean square roughness is commonly used to describe the roughness of surfaces. This is calculated by taking the centre line of a surface profile and calculating the route mean square deviation of a number of points on the profile from the centre line. Further information on the theory and uses of both contact and tapping mode AFM can be found elsewhere.[54, 55]

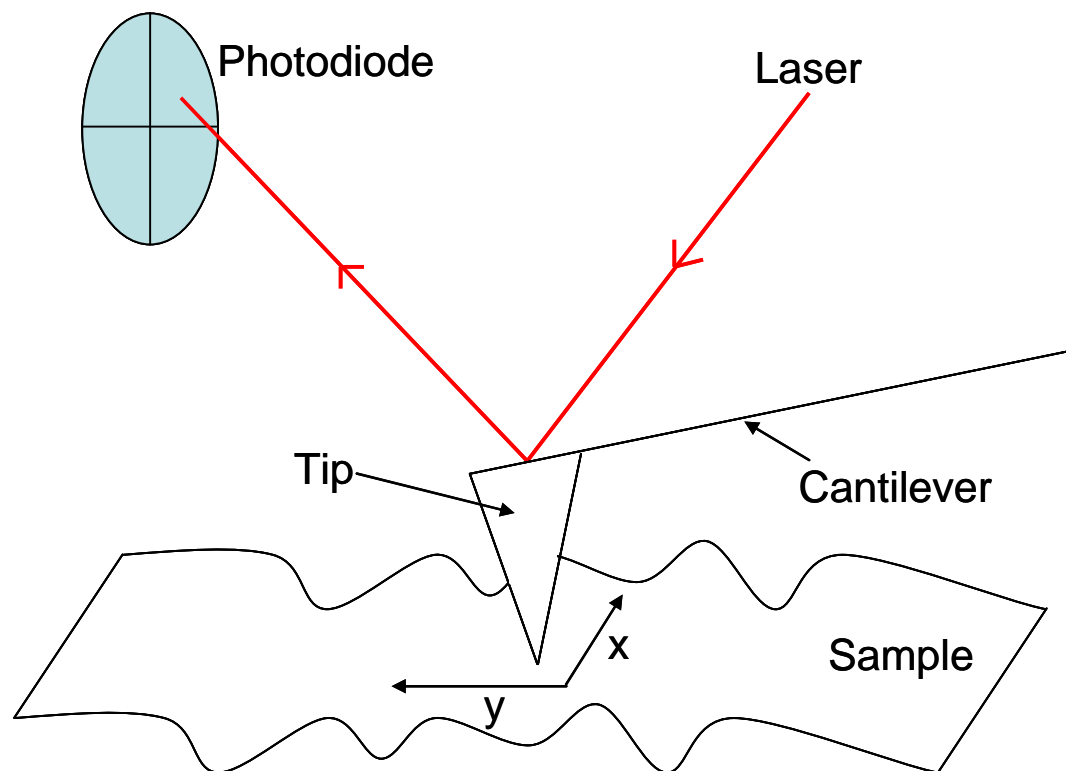


Figure 17. Diagram describing the typical construction of an AFM.

As well as imaging a sample by rastering the tip across the surface, an AFM may also be used to study the adhesive force between the AFM tip and a

sample. It is also possible to attach molecules to the AFM tip to measure the interaction force between the molecules and a surface. An example of this is the attachment of proteins to the AFM tip to measure the adhesion force between the protein molecule and a surface.[56] The tip is driven towards the sample while the cantilever deflection is monitored. A plot of the vertical position of the tip relative to the sample versus cantilever deflection is called a force-distance curve (or simply a force curve) (Figure 18).

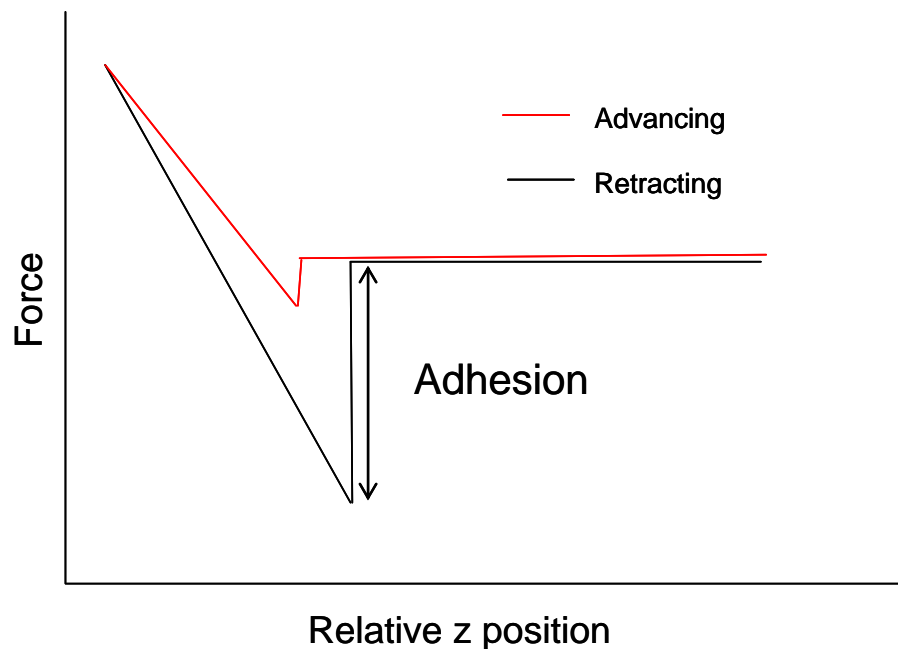


Figure 18. Example force-distance curve.

As the tip is driven towards the surface there is initially no deflection of the cantilever as the tip is not close enough to interact with surface forces. When the tip comes into range of the surface forces it is pulled towards the surface causing the cantilever to bend (known as ‘snap-to-surface’). As the tip is driven further towards the surface the cantilever straightens again until repulsive forces on the surface cause the cantilever to deflect again. When the cantilever is withdrawn from the surface the tip is held to the surface again by adhesive forces causing the cantilever to deflect (the magnitude of the deflection depends on the strength of the adhesive force). As the cantilever is drawn further away from the surface the tip eventually detaches from the surface and the cantilever straightens again. The magnitude of the deflection of the cantilever is converted to force by the following equation (known as Hooke’s law):

$$F = -kd \quad (4)$$

where F is Force, k is the force constant of the cantilever and d is the cantilever deflection. Measuring the deflection of the cantilever as the tip is drawn away from the surface and converting this into force with the above equation gives the adhesive force. Information about the mechanical properties of a material may also be extracted from a force curve, by analysing the portion of the curve where the tip has been driven into the same. There are various mathematical formulae which allow the calculation of properties such the Young Modulus from the information available in a force curve.[57]

Chapter 3

Surface Chemical Analysis of Polymer Microarrays using ToF-SIMS and XPS

3.1 Introduction

Polymer microarrays have shown promise as a method for screening for new polymers with properties of interest.[29] These include properties such as the ability to support cell growth,[21, 34, 36, 38] mechanical properties[45] and to direct drug crystal growth.[39] Two approaches can be taken with this type of study: screen for hit polymers with properties of interest or to study the relationship between the chemistry of the polymers and the property of interest. Simplistic comparisons may be made between a polymer's bulk chemistry and its various properties. However, this method is redundant if the property that is being studied depends on the chemistry of the polymers' surfaces, rather than their bulk. This is the case in applications as diverse as biomaterials[58] and semiconductors.[59, 60] The surface chemistry of a polymer cannot necessarily be assumed from its bulk chemistry, as issues such as surface contamination and segregation of mobile components can result in the surface being considerably different to the bulk.[42] Hence a detailed characterisation is necessary using surface sensitive techniques. Once this information is acquired it is then possible to study surface structure/property relationships.

The two surface analytical techniques used in this chapter are Time-of-Flight Secondary Ion Mass Spectrometry and X-ray Photoelectron Spectroscopy, both of which are commonly used for the characterisation of polymer surfaces. The theory behind the two techniques is discussed in some detail in Chapter 2. There are a number of challenges to be surmounted to enable a high throughput surface characterisation of a polymer microarray. These includes issues such as the number of samples on the array, the size of the samples (e.g. only 300 μm diameter spots) and importantly methods of analysing such large amounts of data. The two techniques used in this chapter both have the capability of operation with a high spatial resolution, giving reassurance that the data collected is only from the polymer spot analysed and not from the substrate.[61] Automated acquisition software (including a fully automated stage) enable rapid and unattended analysis of large amounts of samples in microarray format.

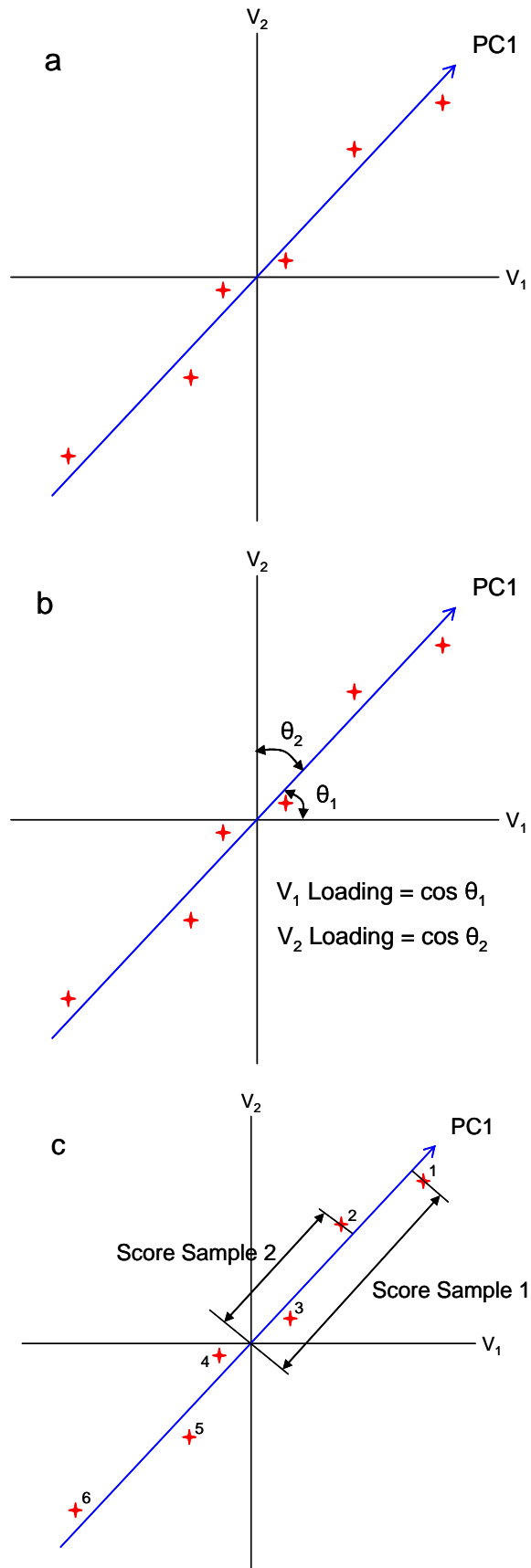


Figure 19. One principal component in the case of two variables. a) PC1 describes the greatest variance in the 6 sample data set b) Loadings are the cosine of the angle between each axis and PC1 c) Scores are the projections of the sample points onto the PC1.

Simple computer programs allow automated calibration and sorting of the large amount of data acquired from a microarray. Finally multivariate statistics can be applied to analyse the large amount of data acquired.

Due to the method of ion generation involved, a ToF-SIMS spectrum can contain hundreds of different ion peaks. It can be a relatively difficult task to interpret the positive and negative spectra of one polymeric sample, but if there are hundreds of samples (e.g. a microarrayed library) the task of manually analysing the spectra becomes lengthy and laborious. This aspect of ToF-SIMS data that makes it difficult to compare multiple samples is due to the fact that it is multivariate in nature, i.e. each measurement (spectrum) is made up of multiple variables. Multivariate statistics in the form of principal component analysis (PCA) is a useful tool for simplifying the analysis of large volumes of data. PCA reduces the dimensionality of ToF-SIMS data to a small number of abstract factors that describe the variation in the data, enabling similarities and differences in the samples to become apparent.[62] To describe how PCA works it is easiest to imagine that each sample is plotted in n dimensional space (n corresponds to how many ion peaks are used), where each axis corresponds to an ion peak and the samples position depends upon the intensity of each peak in its spectrum (Figure 19a). A vector can then be plotted (through the origin) that describes the greatest amount of variation in the group of samples (Figure 19a). This is called the first principal component (PC1). If each sample point is then projected onto this principal component and the distance of this project measured to the origin, we get the score value for this sample on PC1 (Figure 19c). Therefore instead of describing this sample using hundreds of ion peaks, we can describe it using this single score value. PCA assigns each variable (ion peak) with a loadings value which indicates the extent to which this variable is responsible for the variance within the data set. The loadings value is calculated by taking the cosine of the angle between the principal component vector and the axis of each variable (Figure 19b). Therefore it can be reasoned that axis that have a large angle between themselves and the principal component (e.g. $\sim 90^\circ$) do not explain the variance described in the principal component and will have a loadings values close to zero. If an axis has a very small angle between itself and principal component (e.g. $\sim 0^\circ$), it is likely to help explain the variance and will have a

loadings value close to 1. More principal components may be fitted to the data, providing they are orthogonal to the previous components. Each new principal component will describe progressively less variance, until it gets to a point when each new component is simply describing noise within the dataset.

PCA has been widely used in the surface analytical field. There has been much interest recently in the use of PCA for processing ToF-SIMS images,[63, 64] however it is still predominantly used for looking for similarities and differences in the ToF-SIMS spectra of groups of samples. PCA has previously been used to study the composition of adsorbed protein layers[65, 66], the chemistry of self-assembled monolayers[67] and study the influence of surface chemistry on water contact angle.[68]

The published literature concerning the surface chemical analysis of microarrays (DNA, protein or otherwise) is limited. Belu *et al* used ToF-SIMS to image the micropatterned protein streptavidin on a self assembled monolayer (SAM) surface.[69] To distinguish the proteins from the substrate the streptavidin was labelled with the stable isotope ^{15}N , allowing images to be formed by following the intensity of the C^{15}N^- ion. Similar work was reported by Hashimoto *et al* who used ToF-SIMS to image a DNA microarray, using the PO_2^- and PO_3^- ions formed from the DNA backbone.[70] This type of work is aimed more at the confirmation of a particular pattern or layout on a surface, rather than a detailed surface chemical analysis of the arrayed materials. The area was explored further by Lee *et al* who used ToF-SIMS, XPS and fluorescence imaging to analyse a DNA microarray.[71] One interesting observation was that the XPS P 2p atomic percentage of each DNA spot was highly correlated with fluorescence measurements of the amount of printed DNA. PCA was utilised to improve the contrast between the DNA spots and substrate in the images. The work discussed in this chapter will go much further than the work discussed above. Instead of imaging single or small numbers of microarray spots, images of an entire 576 spot microarray were acquired. The feasibility of a detailed surface chemical analysis of an entire microarray using both ToF-SIMS and XPS will be demonstrated.

This chapter describes the application of ToF-SIMS and XPS to the surface chemical analysis of a polymer microarray. ToF-SIMS imaging is utilised to confirm the layout of the entire microarray. Multivariate statistics in the form of principal component analysis (PCA) is used to analysis the large amount of spectral data acquired.

3.2 Methods and Materials

3.2.1 Microarray Synthesis

Epoxy-coated glass slides were dip-coated into 4 % (w/v) PHEMA solution in ethanol and dried for three days. Stock solutions of acrylate monomers were prepared at a ratio of 75 % (v/v) monomer, 25 % (v/v) DMF and 1 % (w/v) 2,2-dimethoxy-2-phenylacetophenone. The monomers were divided into major and minor monomers (Figure 20) and mixed in the following ratios: (major:minor) 70:30, 75:25, 80:20, 85:15 and 90:10 in all possible combinations. Mixing was carried out in 384-well black polypropylene plates. Monomer solutions were then printed using the larger format CMP9B pins with a Pixsys 5500 robot (Cartesian), in an atmosphere of humid argon. The slides were polymerised by exposure to long-wave UV light for approximately 10 seconds, after which they were dried for one week at < 50 mTorr.

3.2.2 Time-of-Flight Secondary Ion Mass Spectrometry

ToF-SIMS analysis was performed using an ION-TOF IV (GmbH, Münster, Germany) instrument. ToF-SIMS images of the microarray were obtained by rastering a primary ion beam over an 18.2 x 18.2 mm area (256 x 256 pixel raster) with 512 ion pulses taken per pixel. To obtain spectra from each polymer spot secondary ions were sampled from a 100 x 100 μm area on each spot. Images and spectra were obtained using a Ga^+ primary ion beam, operated at

25 kV energy. The sampling depth of ToF-SIMS is approximately 2 nm.[72] The acquisition and calibration of all spectra was fully automated via the design of specific macros using instrument software, allowing completely unattended operation.

3.2.3 X-ray Photoelectron Spectroscopy

All XPS analysis was carried out using a Kratos Axis Ultra spectrometer using a mono-chromated Aluminium X-ray gun, with a charge-compensating electron flood. To allow automatic acquisition of spectra from all polymers on the microarray, the coordinates of each polymer spot on the microarray was loaded into the instrument software. Photoelectrons were sampled from a 110 μm diameter area for each polymer to ensure that there was no contribution from the PHEMA substrate. The sampling depth for XPS is approximately 10 nm.[51] To enable the whole microarray to be analysed in a reasonable amount of time, the data acquisition time for each polymer was limited to 9 minutes (6 minutes for survey scan and 3 minutes for C1s high resolution scan). Pass energies of 80 eV and 20 eV were used for survey and C1s scans respectively.

Elemental and functional quantification was achieved using CASA software. A linear background was applied to the C1s high resolution peaks and synthetic Gaussian/Lorentzian peak shapes used to fit the peak components. Bulk O:C ratio was calculated from knowledge of the theoretical monomer composition used to synthesise the polymers (the photo-initiator was also included).

3.2.4 Principal Component Analysis

The positive and negative ion spectra for all 496 polymers were automatically mass calibrated using ION-TOF ToF-Bat software.[73] This automatic calibration was relatively accurate, with mean deviations of < 40 ppm from true mass for m/z 0-100. One peak list each was then created for both positive (344 peaks) and negative (92 peaks) ion spectra using mass spectra taken

from a group of polymers from the array containing monomers with widely varying chemistries. This group included polymers synthesised using all of the monomers in Figure 20. This peak list was then applied to all 496 polymers. The peaks were then integrated using ION-SPEC software and peak intensities exported to Origin Pro 7.5. The positive and negative ion intensities for each polymer were normalised to the total ion count separately, to account for normal variation in secondary ion yield between polymers. PCA analysis was carried out on the positive and negative ion data matrices separately using Eigenvector PLS_Toolbox 3.5 for Matlab. The ToF-SIMS data were mean-centered before analysis.

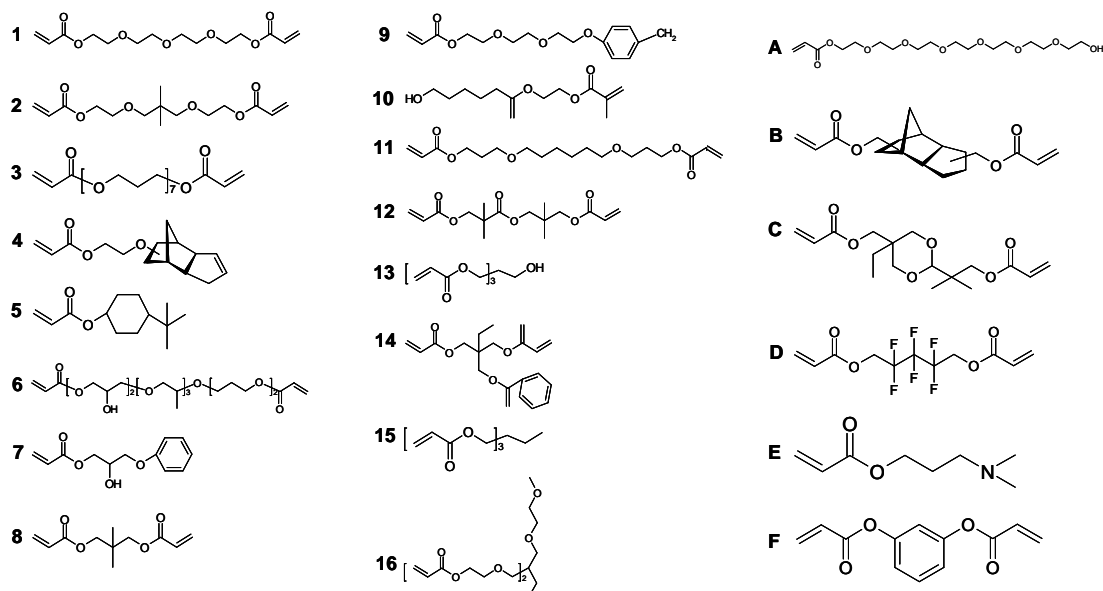


Figure 20. Monomers used to synthesise the polymer microarray.

The atomic and functional group composition data obtained using XPS for all polymers on the microarray was arranged into one data matrix in Origin Pro 7.5, where the each column was a polymer and the rows the XPS data (496 x 8). The data were mean-centered and auto-scaled prior to PCA analysis using PLS Toolbox 3.5.

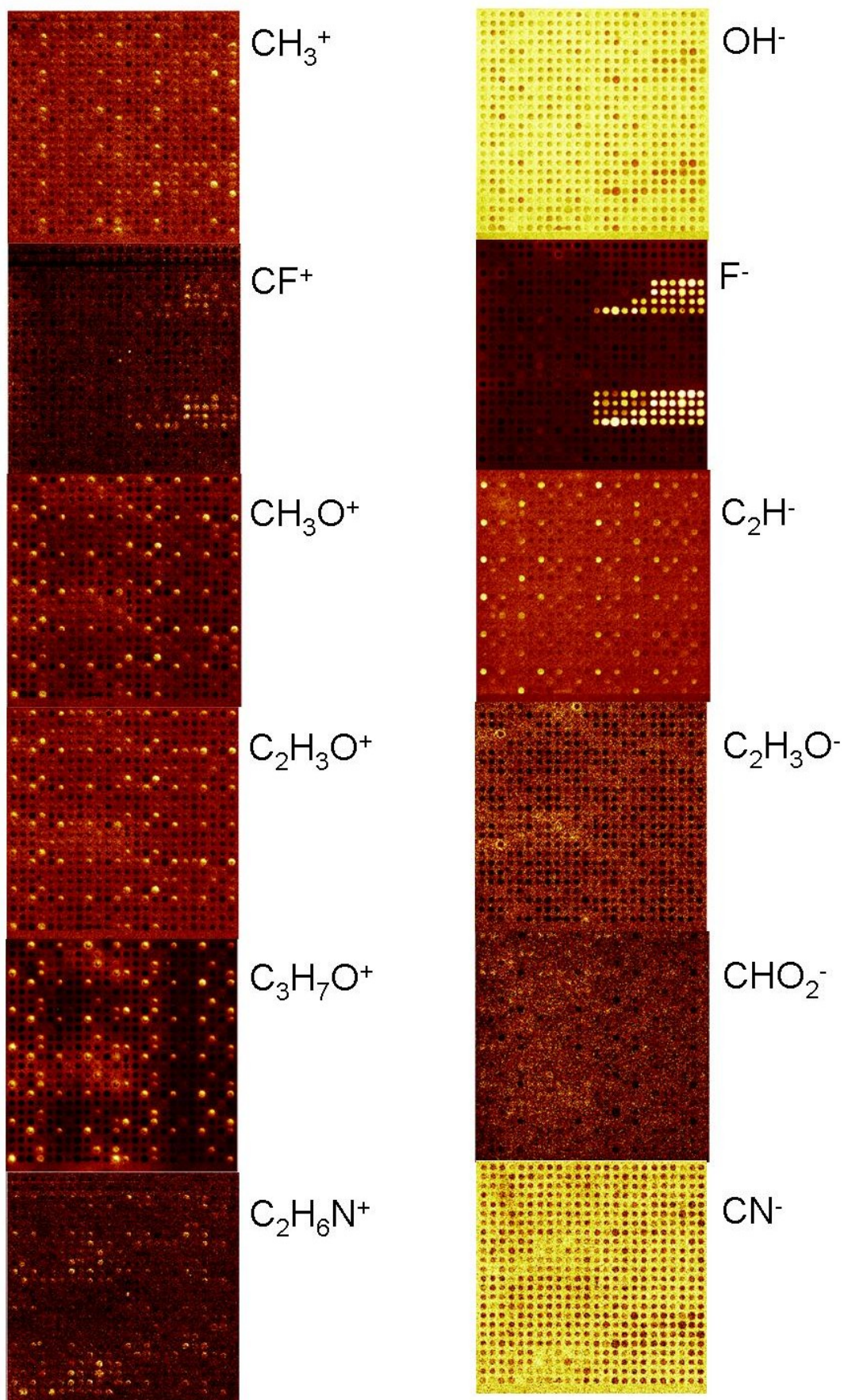


Figure 21. ToF-SIMS imaging of the polymer microarray. Images for 12 example ions are shown: 6 positives on the left and 6 negatives on the right.

3.3 Results

3.3.1 Time-of-Flight Secondary Ion Mass Spectroscopy

ToF-SIMS images were acquired to show the distribution of 12 key ions across the microarray (Figure 21). The individual polymer spots are easily visible on all of the images, with the exception of the CHO_2^- image. The distribution of the different ions varies across the microarray array. The contrast is greatest for the two fluorine containing ions CF^+ and F^- , and least for CHO_2^- .

The positive and negative ToF-SIMS spectra of the micro-arrayed polymers contain previously reported features that are characteristic of acrylic polymers,[74] with trace sodium and silicone contamination. PCA was carried out separately on the positive and negative ToF-SIMS spectra of the polymers from the microarray. The initial positive ion PCA model was dominated by the secondary ions at m/z 73.053 and 147.076, which are characteristic of PDMS contamination. Therefore secondary ions characteristic of PDMS were removed from the positive dataset and PCA analysis repeated. The first two principal components accounted for 61 % of the variance within the data. Figure 22a shows the score values of each of the polymers on the first two principal components. There is some grouping of polymers due to their major monomer component, for example for polymers containing major monomers 1 and 12, however for the majority of the major monomer groups do not. Examination of the loadings for PC1 show that the ions with the greatest positive loadings are m/z 57.074, 41.039 and 29.039, and those with the greatest negative loadings are m/z 59.050 and 45.035 (Figure 22b). Examination of the loadings for PC2 show that the ions with the greatest positive loadings are m/z 59.050, 57.074 and 45.035, and those with the greatest negative loadings are m/z 55.022, 27.024 and 105.036 (Figure 22c).

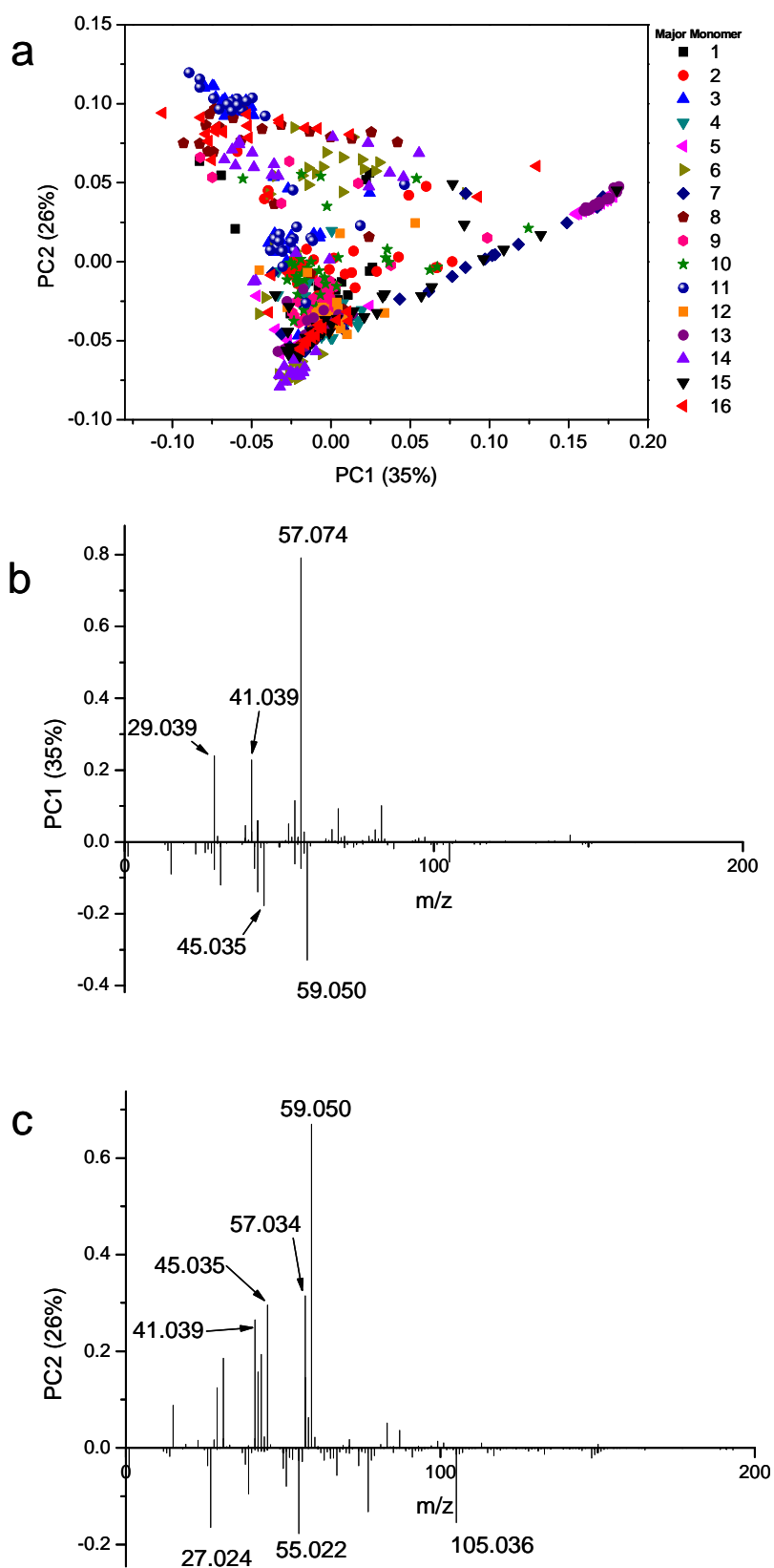


Figure 22. Principal component analysis of positive ion intensities from microarray. a) Scores biplot of PC1 and PC2. Polymers are group by their major monomer constituents. b) Loadings versus m/z on PC1. c) Loadings versus m/z on PC2.

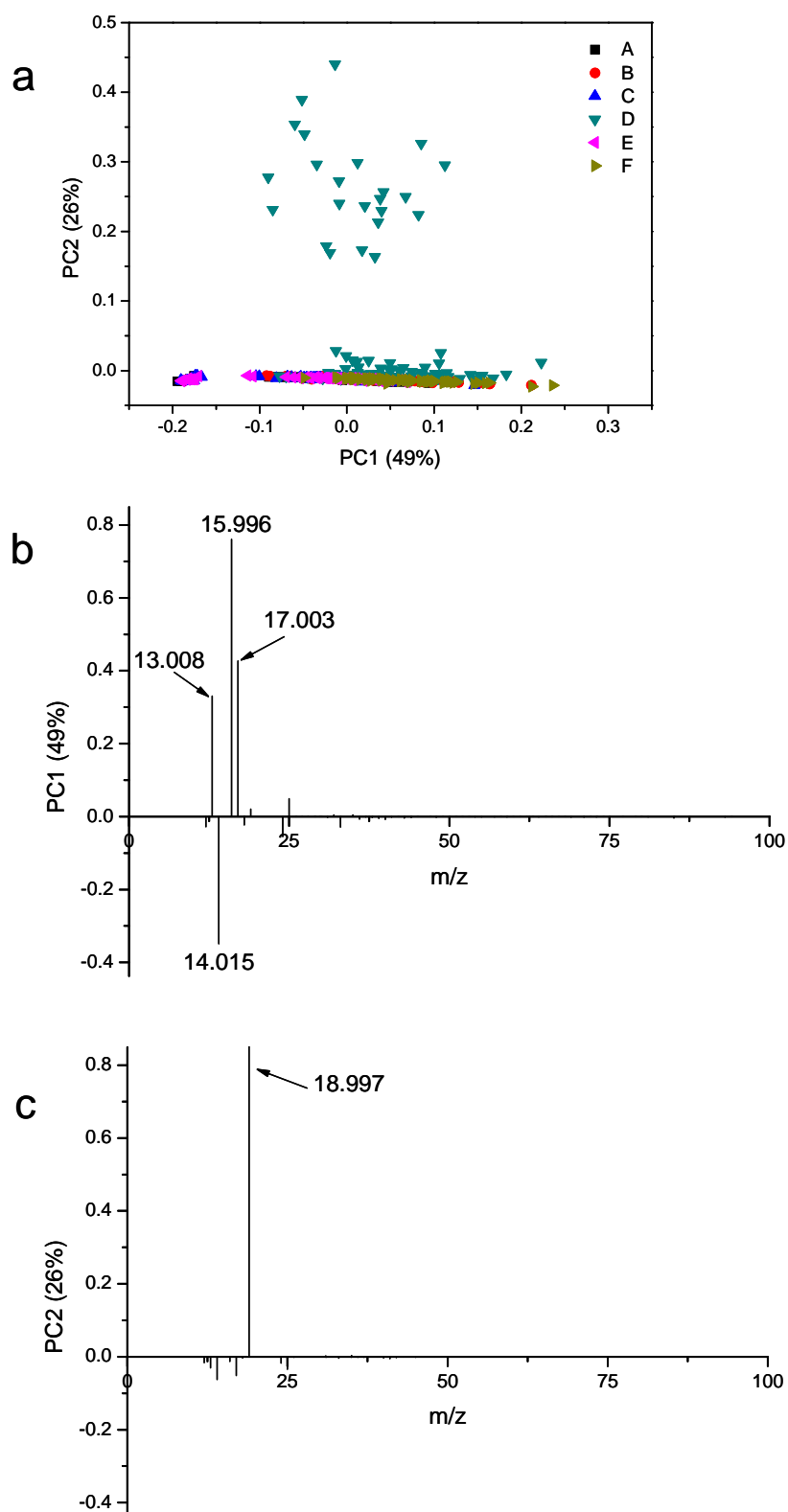


Figure 23. Principal component analysis of negative ion intensities from microarray. a) Scores biplot of PC1 and PC2. Polymers are group by their major monomer constituents. b) Loadings versus m/z on PC1. c) Loadings versus m/z on PC2.

The first two principal components in the PCA model for the negative ion dataset accounted for 75 % of the variance. The scores bi-plot is considerably simpler for the negatives than that for the positive ions, with polymers containing the fluorinated monomer D separating from the remaining polymers on the second principle component (Figure 23a). The loadings plots reflect this simpler picture with only m/z 18.997 having a significant loadings value on PC2 (Figure 23c). Ions with m/z 13.008, 15.996 and 17.003 have positive loadings on PC1, with only m/z 14.015 having a significant negative loading (Figure 23b).

3.3.2 X-ray Photoelectron Spectroscopy

XPS spectra, including survey and C1s high resolution scans, were obtained for all polymers on the microarray. The atoms visible in the survey scans of the polymers were carbon, oxygen, fluorine and nitrogen (Figure 25a & c). The presence of all these atoms can be explained with reference to the monomers used in the synthesis of the array (Figure 20). No silicon indicative of PDMS contamination was detected on any of the polymers on the microarray, in contrast to the ToF-SIMS results. Carbon and Oxygen was detected on all of the polymers, however fluorine was only observed in the survey spectra of polymers containing the fluorinated monomer D (Figure 25e). Nitrogen was detected in the survey spectra of some of the polymers containing monomer E, but at very low concentrations (~ 1-2 %). The polymers' C1s high resolution peaks were fitted with their component peaks, which for the majority of polymers consisted of the aliphatic peak at 285 eV, β shifted carbon peak at ~ 285.7 eV, ether peak at ~ 286.5 eV and the carboxylic ester peak at ~ 289 eV (Figure 25b). The majority of the fluorinated polymers also contained the F-C-F peak at ~ 290.9 eV (Figure 25d).

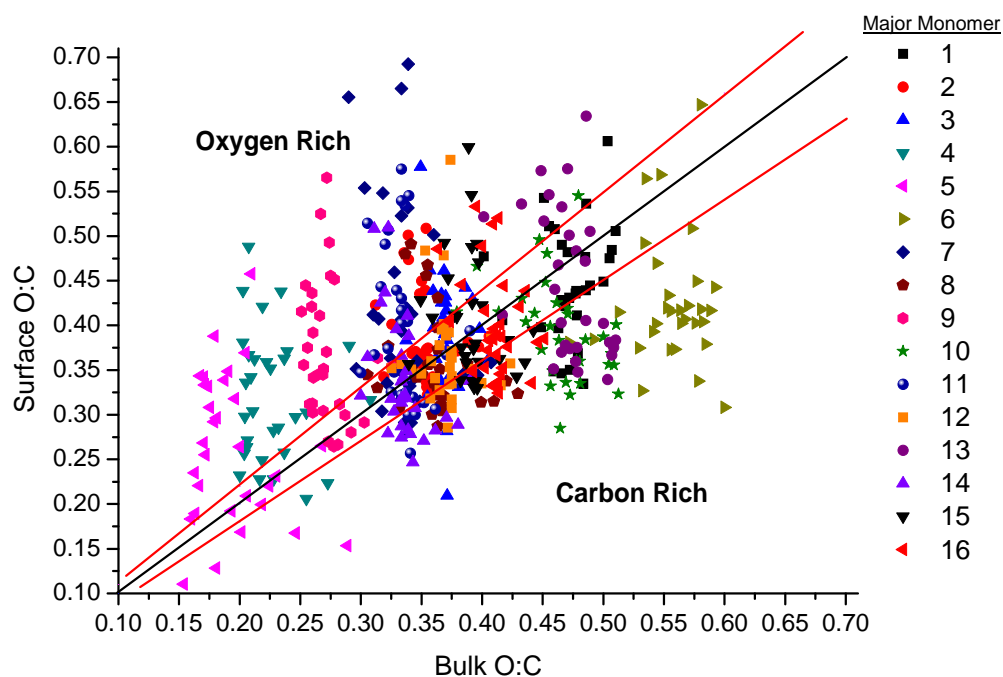


Figure 24. Comparison between polymer surface and bulk chemistries. The ratio of polymer surface O:C ratio is plotted versus bulk O:C ratio. Bulk is calculated from theoretical ratios based upon knowledge of the ratio of monomers used to synthesise each polymer (the radical initiator has been included in calculations).

To investigate the relationship between the surface and bulk chemistries of the polymers the theoretical bulk O:C ratio of the polymer was calculated and compared to the surface O:C obtained using XPS (Figure 24). XPS analysis for homogeneous surfaces can determine the atomic concentration of the surface with accuracies of $\approx 90\%$; [75] therefore a 10% confidence limited is given on Figure 24. It can be seen that only 36% of the polymers have a surface O:C which is similar to their bulk O:C ratio. Whereas 29% of the polymers have carbon rich surfaces and 35% have oxygen rich surfaces. For example, polymers containing monomers 4, 9 and 11 have oxygen rich surfaces, whereas those containing monomers 6 and 10 have carbon rich surfaces (Figure 24).

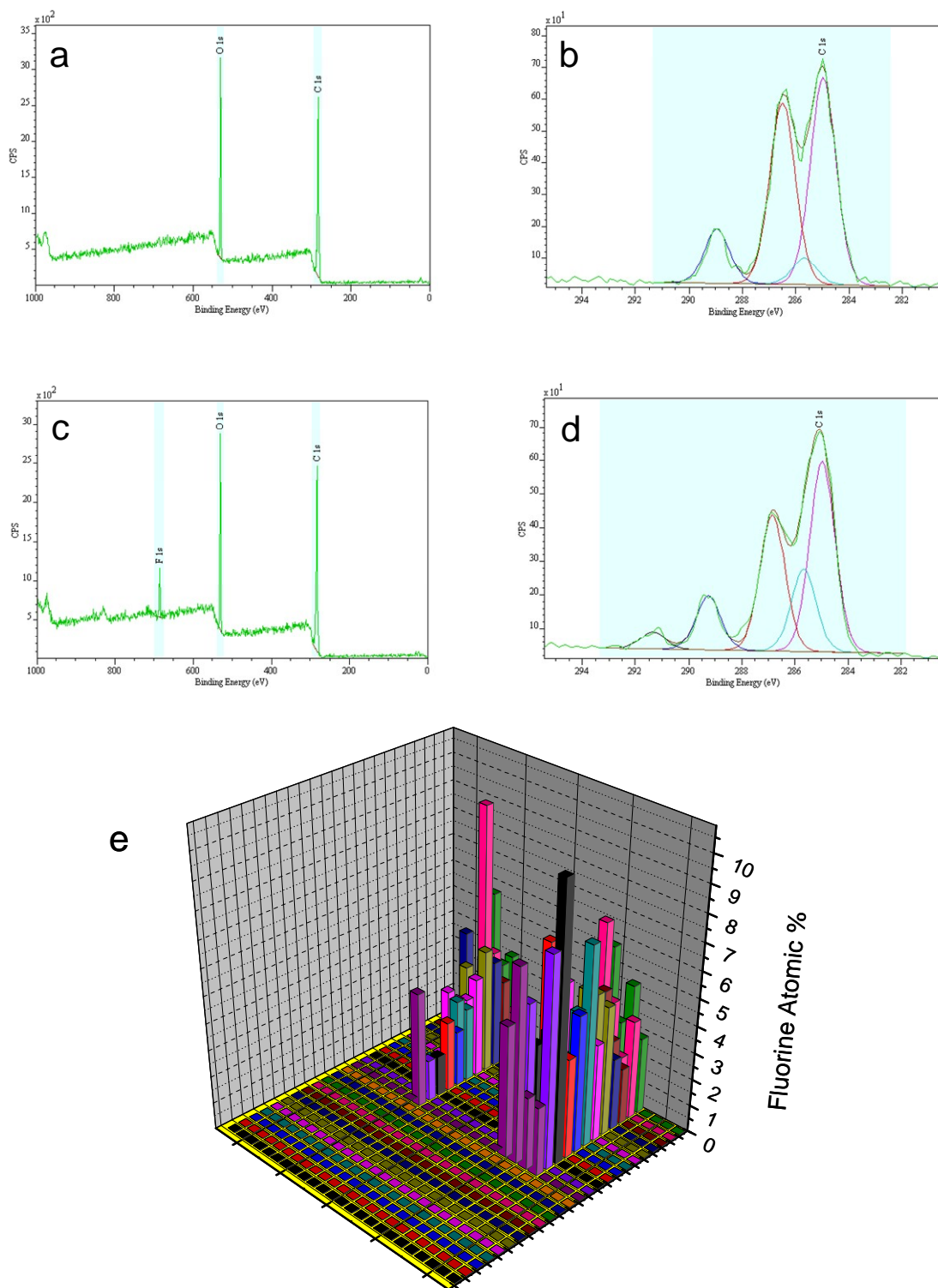


Figure 25. XPS analysis of the polymer microarray. a) Example survey spectrum of a representative polymer b) Example high resolution C1s spectrum of a representative polymer c) Example survey spectrum of a fluorinated polymer d) Example high resolution C1s spectrum of a fluorinated polymer e) Atomic percentage of Fluorine for all polymers on microarray.

PCA was carried out on the atomic and C1s component information gained from the microarray. The first two principal components described 57 % of the variance within the dataset. Analysis of the score values of the polymers on PC1 indicates that the majority of the polymers have a score value close to zero (Figure 26a). Polymers containing monomers 4, 5 and 14 have the greatest negative score values, whereas those containing monomers 1, 3, 6 and 16 have the greatest positive score values. Analysis of the score values on PC2 indicates that polymers containing monomer D have the greatest positive values, whereas the rest of the polymers have either negative score values or close to zero (Figure 26b). Analysis of the loadings values on PC1 indicates that the C-C and C1s % variables have positive loadings and the C-O and O1s % variables have negative loadings (Figure 26c). On PC2 the O-C=O, C-F and F1s % variables have the greatest positive loadings, whereas the C-O and C1s % variables have negative loadings (Figure 26c). The N1s % variable has a loadings value close to zero for both PC1 and PC2, suggesting that it has a minimal influence on the PCA model.

3.4 Discussion

XPS and ToF-SIMS spectra were obtained for all polymers on the microarray analysed within a period of approximately six days. This means that the surface chemical analysis of a polymer microarray can be achieved within the same time-frame as the biological evaluation (2 to 10 days),[34] which illustrates the high throughput nature of the analysis discussed in this chapter.

ToF-SIMS imaging provides information on the distribution of different secondary ions across a sample. This is particularly useful for microarray work as it enables confirmation that the polymers have been printed in the layout intended.

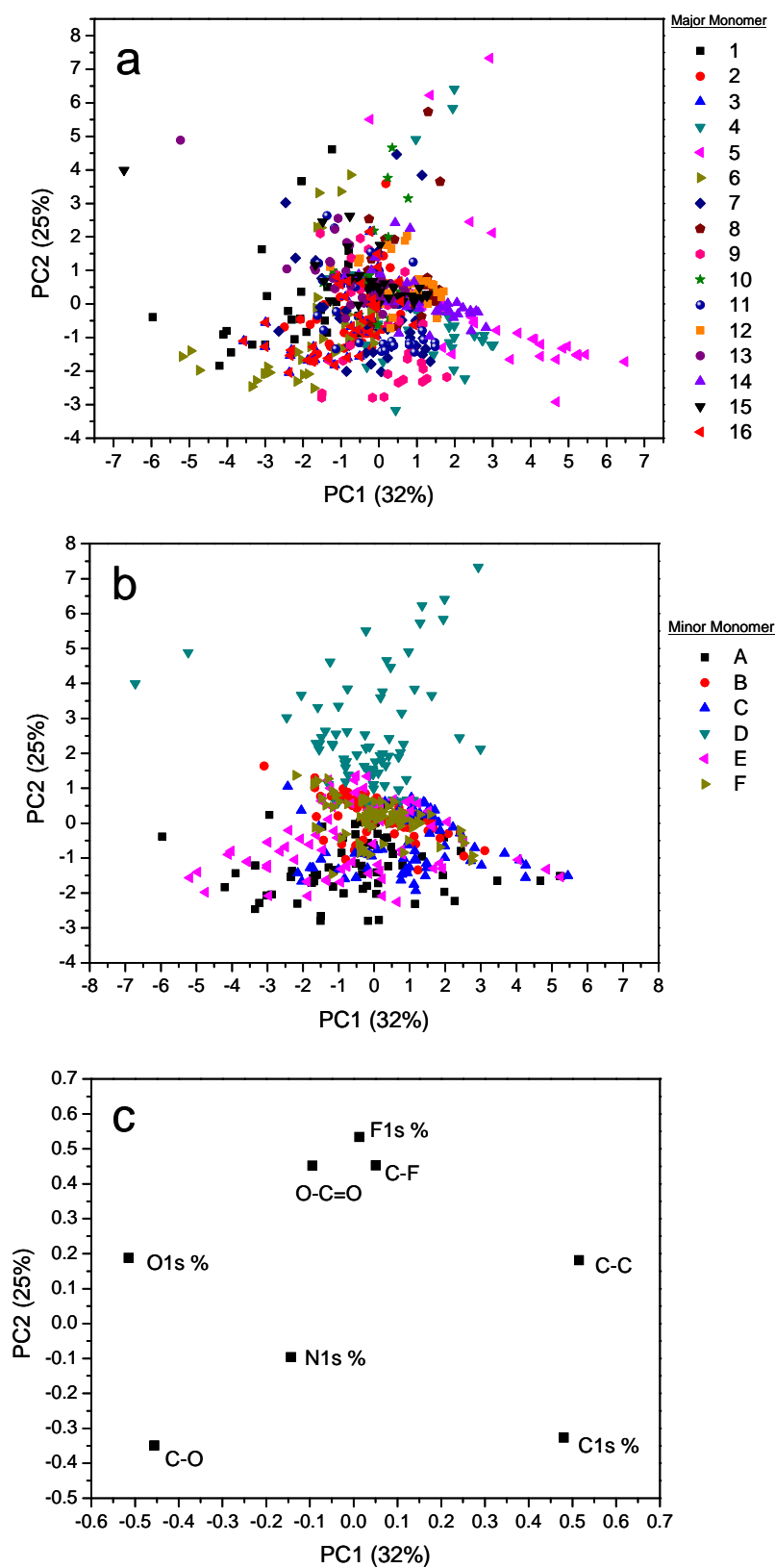


Figure 26. PCA of XPS data from the microarray. a) Scores biplot of PC1 and PC2. Polymers are grouped by their major monomer constituents. b) Scores biplot of PC1 and PC2. Polymers are grouped by their minor monomer constituent c) Loadings biplot of PC1 and PC2.

The most characteristic secondary ion on the microarray is the F^- ion, which is only seen at high intensities in polymers containing the fluorinated monomer D (Figure 21). This pattern is also seen for the CF^+ ion, although the intensities are much lower than that seen for F^- , which is probably due to the lower probability of this ion forming.[48] The ToF-SIMS CF^+ and F^- ion images correlate very well with the XPS Fluorine atomic concentration data (Figure 25e). The CH_3^+ fragment shows greatest intensity in polymers containing monomer 16 as their major monomer component (Figure 21). This monomer contains an ethane side chain and methoxyethane side chain, both of which are likely to fragment to form the CH_3^+ ion. This is confirmed by the observation of a particularly intense peak at m/z 15.023 in the positive ion spectra of polymers containing this monomer. The CH_3O^+ , $C_2H_3O^+$ and $C_3H_7O^+$ ions are all most intense for the majority of polymers containing either monomer 3 or 6 (Figure 21). Both of these monomers contain propylene oxide functionalities, which readily fragment to form the three ions mentioned above. Oddly this pattern is not observed for the $C_2H_3O^-$ and CHO_2^- ions which can also be formed from fragmentation of propylene oxide.

The OH^- ion is observed at high intensities across most of the polymers on the microarray and the PHEMA substrate as might be expected. However, exceptions include polymers containing monomers 5 and D which show relatively low intensities. This is intuitive as monomer 5 is a tertbutylcyclohexyl capped monoacrylate and monomer D is a fluorinated diacrylate (Figure 20). Nitrogen is commonly detected as the CN^- ion in the negative ion spectra of nitrogen containing polymers.[48] This is observed in the ToF-SIMS images of this microarray, where polymers containing the nitrogen containing monomer D have the highest intensity for the CN^- ion (Figure 21). The image for the $C_2H_6N^+$ ion shows a similar pattern, however other polymer spots not containing monomer D show relatively high intensities too. This could possibly be due to the fact that the peak at m/z 44 has multiple components, therefore there may be some overlap with other more commonly produced secondary ions such as $C_2H_4O^+$.

ToF-SIMS provides qualitative information regarding the molecular structure of a polymer surface. A ToF-SIMS spectrum for a single polymer

contains hundreds of molecular ion species, providing a significant challenge to the analyst. Conventional analysis of the spectra from these polymers would be very time consuming and ineffectual due principally to the large number of polymers in the library. To extract valuable information from an entire array in the required timeframe is unfeasible. There is also the added difficulty that the polymers are novel materials, therefore there is no previous work available to help identify ion fragments characteristic to these materials. Therefore, to investigate surface chemical similarities and differences within the polymer library PCA was performed on both the positive and negative ToF-SIMS datasets. In PCA analysis samples which have similar surface chemistries will have similar scores values and vice-a-versa. In the case of the positive ion spectra, the polymers are separated by their score values on PC1 and PC2 into approximately three general groups, with the majority grouping round the origin. It is obvious that for most polymers, both the major and minor monomer influences the surface chemistry as the polymers containing the same major monomer do not necessarily group very tightly (Figure 22a). Polymers containing monomers 5 and 8 as their major monomer component generally have positive scores on PC1 (Figure 22a). The ions with the highest positive loadings on PC1 are all hydrocarbons, i.e. 57.074 ($C_4H_9^+$), 41.039 ($C_3H_5^+$) and 29.039 ($C_2H_5^+$) (Figure 22b). Monomers 5 and 8 both contain tert-butyl functionalities which would likely fragment to form three ions mentioned above (Figure 20). The polymers with the greatest negative scores values on PC1 generally contain monomers 2, 3, 8, 10 and 11 as their major monomer component (Figure 22a). The ions with the greatest negative loadings on PC1 are 59.050 ($C_3H_7O^+$) and 45.035 ($C_2H_5O^+$) (Figure 22b). Monomers 2, 8 and 10 contain ethylene oxide functionalities, whereas monomers 3 and 11 contain propylene oxide functionalities (Figure 20). $C_3H_7O^+$ and $C_2H_5O^+$ are commonly formed from fragmentation of propylene oxide chains. $C_2H_5O^+$ can also be formed from fragmentation of ethylene oxide chains. It is possibly this cross-over which explains why polymers containing propylene oxide functionalities and those containing ethylene oxide functionalities do not separate on the PC1 scores (Figure 22a). It has previously been observed that PCA can be used to distinguish between polymers containing ethylene glycol chains of different lengths.[76] This does not appear to be the case in the PCA model of this group of polymers.

The ions with the greatest positive loadings values on PC2 are 59.050 ($\text{C}_3\text{H}_7\text{O}^+$), 57.034 ($\text{C}_3\text{H}_5\text{O}^+$) and 45.035 ($\text{C}_2\text{H}_5\text{O}^+$) (Figure 22c). Polymers with large positive score values on PC2 are mostly those containing monomers 2, 3, 8, 10 and 11 as their major monomer component (Figure 22a). Those containing monomer 3 and 11 (both containing propylene oxide functionalities) have the highest positive score values. Interestingly, $\text{C}_3\text{H}_7\text{O}^+$ and $\text{C}_3\text{H}_5\text{O}^+$ are both strongly characteristic of propylene oxide functionalities, and $\text{C}_2\text{H}_5\text{O}^+$ characteristic of ethylene oxide functionalities. Therefore like PC1 the polymers are again separating on the basis of these two functional groups, however unlike PC1 there is a degree of separation between those containing propylene and ethylene oxide functionalities. This is probably due to the considerably higher positive loadings values for $\text{C}_3\text{H}_5\text{O}^+$ compared to the other ions (Figure 22c). The ions with the greatest negative loadings on PC2 are 27.024 (C_2H_3^+), 55.022 ($\text{C}_3\text{H}_3\text{O}^+$) and 105.036 ($\text{C}_7\text{H}_5\text{O}^+$) (Figure 22c). These ions are characteristic of the fragmentation of acrylate functionalities.

The PCA model for the negative ion data is considerably simpler than that for the positive ion data (Figure 23a). The ions with the greatest positive loading values on PC1 are 15.996 (O^-), 17.003 (OH^-) and 13.008 (CH^-), whereas the ion with the greatest negative loading value is 14.015 (CH_2^-) (Figure 23b). This reflects the pattern seen in the positive ion PCA model where PC1 separates the polymers mainly in terms of oxygenated and non-oxygenated species (Figure 22). PC2 is dominated by the F^- ion which has a much greater loadings value than any other ion (Figure 23c). Unsurprisingly the polymers containing the fluorinated monomer D are separated on by the score values on this principal component (Figure 23c).

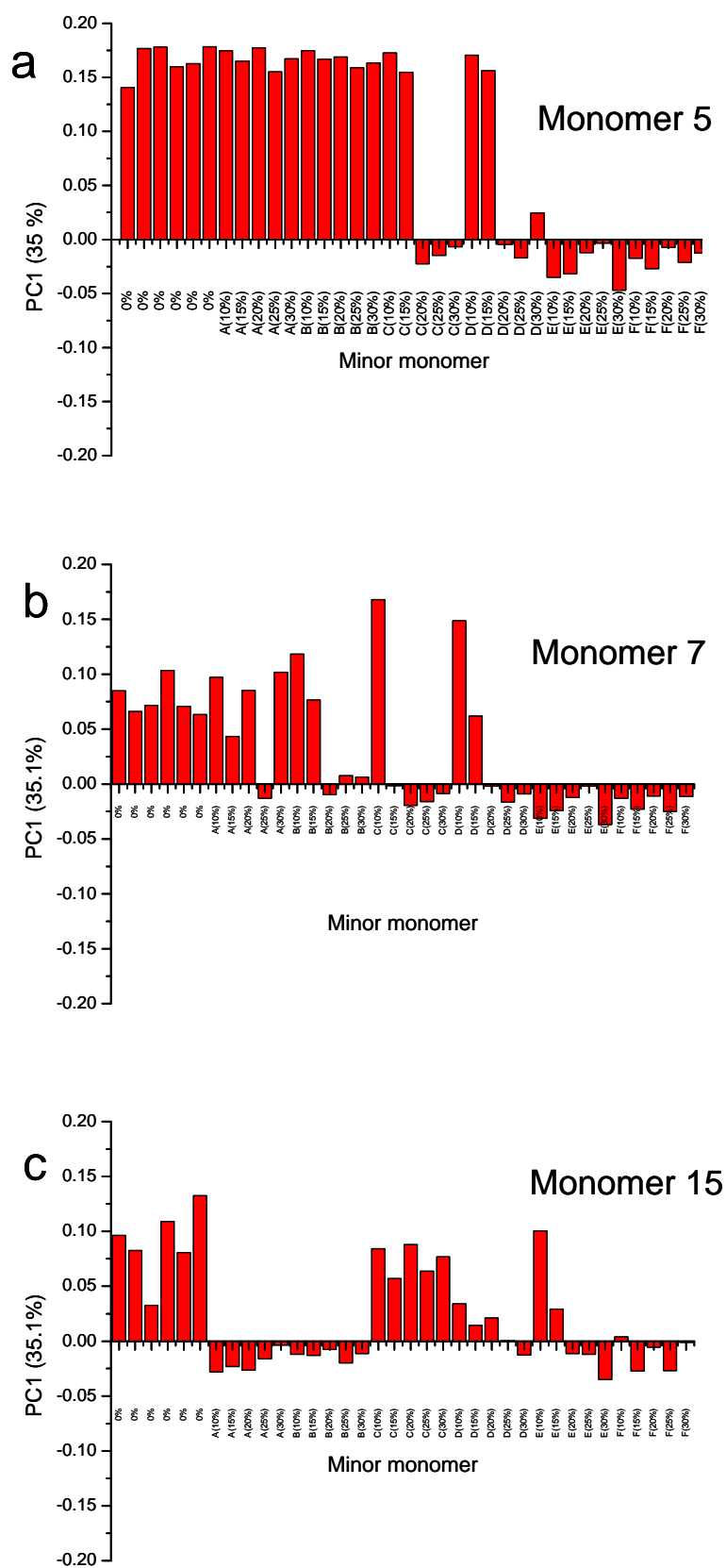


Figure 27. Influences of the addition of minor monomers on the PC1 score values of polymers containing major monomers a) 5 b) 7 and c) 15.

The score values from the PCA analysis can be used to study the influence on surface chemistry of varying the minor monomer constituent of a polymer. Analysis of the scores values in this context shows that the relationships between specific minor monomers and the corresponding polymers' score values are complex; perhaps reflecting the differing dynamics of the many different monomer combinations. Indeed there are few conclusions which may be made which are general for all of the polymers. The score values of polymers containing major monomer 5 are a good example. On PC1 the polymers containing 100 % monomer 5 all have relatively high score values (0.17 ± 0.02). Addition of any quantity of monomers A and B does not influence the score value on PC1, which could be due to depletion of these species from the polymer surfaces or similarities in the production of secondary ions from these species (Figure 27a). Addition of monomers C, D, E or F all result in a significant decrease in the polymers' score values on PC1. This is true for all concentrations of monomers E and F, but only for concentrations greater than 15 % for monomers C and D. The same relationships are also seen for polymers containing monomer 7 (Figure 27b). In contrast, for polymers containing monomer 15, addition of monomers A and B results in a decrease in the score values on PC1 (Figure 27c). Addition of monomer C results in no significant change, whereas addition of monomers D, E and F again result in a decrease in the score values.

XPS provides quantitative information regarding the atomic and functional group composition of a material's surface. Obtaining the elemental composition of a polymer's surface and comparing this to the polymer's bulk elemental composition is an important method of investigating whether a polymer's bulk chemistry reflects its surface chemistry. The majority of the polymers (64 %) have a surface O:C which differs from the bulk O:C, thus clearly demonstrating that the surface composition of these polymers cannot be inferred from their bulk composition (Figure 24). This is particularly important if surface structure-property relationships are to be studied for these polymers, as surface analysis will be a necessity. Approximately 29 % of the polymers have carbon rich surfaces, whereas 35 % of polymers had Oxygen rich surfaces. The polymers with a Carbon rich surface may preferentially adsorb air borne volatile organic compounds with

a high Carbon content.[42] Alternatively it may reflect depletion of Oxygen containing monomeric species from the surface of the polymer. The polymers with Oxygen rich surfaces may reflect the segregation of Oxygen containing mobile species, oxidation of surface functionalities or preferential orientation of functional groups.[42] These effects may also be monomer specific, for example, for polymers containing monomers 6 and 10 which have Carbon rich surfaces (Figure 24). Monomer 6 contains both hydroxyl and methyl functional groups on its side chain (Figure 20). In a UHV environment it is probable that this chain will rearrange to orientate the methyl functionalities towards the surface and the hydroxyl groups away from the surface, hence resulting in a Carbon rich surface. Likewise monomer 10 is a monoacrylate with a hydroxyl terminated side chain which will have the flexibility to orientate away from the surface in a UHV environment. Polymers containing monomer 4 have Oxygen rich surfaces which may be due to oxidation of the tricyclic ring structure that terminates this monoacrylate (Figure 20).

XPS data is considerably simpler than ToF-SIMS data in terms of the possible number of variables to be investigated. However, due to the number of samples on the polymer microarray there is still the problem of too much data to realistically analyse by traditional methods. Therefore, PCA was applied to the XPS data from the microarray to investigate the feasibility of this method to analyse such data. The first two principal components only accounted for approximately 57 % of variance within the data set, with the remaining principal components accounting for mainly noise. Different pre-processing regimes (such as mean-centering, auto-scaling and no pre-processing) were trialled to obtain a PCA model which described the maximum variance in the dataset. Mean centering with auto-scaling was found to maximise the variance described, particularly for PC2. Initial observation of the scores on these first two principal components may suggest that the PCA model is not discriminating between the polymers as well as the PCA model of the ToF-SIMS data (Figure 26a). However, due to the limited number of variables available to the PCA model the picture is actually a lot simpler and gives valuable information about the chemistry of the polymer surfaces. The polymers are separated on PC1 on the basis of their surface Oxygen/Carbon content (Figure 26a). C1s % and C-C % both have positive

loadings and O1s % and C-O % have negative loadings on PC1 (Figure 26c). The majority of the polymers have PC1 score values close to zero, however certain major monomer groups stand out as having surfaces that are particularly Carbon or Oxygen rich. For example, polymers containing monomer 4, 5 and 14 have the greatest positive score values on PC1 (Figure 26a). These three monomers all contain bulky, Carbon-heavy moieties which are probably the cause of the polymers high surface Carbon content compared to the rest of the library (Figure 20). Monomer 4 contains a side chain terminated with a tri-cyclic hydrocarbon ring structure, monomer 5 contains a side chain terminated with a tertbutyl functionality and monomer 14 has both an ethyl and phenyl terminated side chains. Polymers containing monomers 1 and 6 have the greatest negative score values on PC1 (Figure 26a). Monomer 1 consists of a side chain containing four ethylene oxide functional groups, whereas has a side chain consisting of multiple oxygenated functionalities such as hydroxyl, ether and ethylene oxide groups (Figure 20).

The minor monomer constituents of the polymers do not appear to influence the PCA model, with the exception of those polymers containing minor monomer D. Polymers containing monomer D have the greatest positive score values on PC2 and indeed separate almost entirely from the remaining polymers (Figure 26b). This separation is due to the high loadings values assigned to the F1s % and C-F % variables on PC1 (Figure 26c). PCA is very sensitive to the pre-processing of data prior to analysis, which can influence the results of the PCA model substantially. When the data were only mean-centered the PCA analysis was unable to discriminate the Fluorine containing polymers on any principal component. This was because the numerical values describing the variables in question (F1s % and C-F %) were considerably smaller than those of the other variables in the model. Auto-scaling of the data reduced this difference in scale; hence PC2 is now able to discriminate these polymers. Interestingly the surface Nitrogen content (in terms of N1s %) of the polymers containing monomer E is too low for the PCA model to discriminate these polymers, even when the data are auto-scaled prior to analysis (Figure 26b). This is evident from the very small loading values assigned to the N1s variable on both principal components (Figure 26c).

3.5 Conclusions

This chapter has demonstrated the feasibility of the high throughput surface chemical analysis of a polymer microarray using two complimentary surface analytical techniques. Importantly it is now possible to determine the surface chemistry of an entire microarray in the same time-frame as biological evaluation. The methods described here are applicable to any type of microarray, with similar spot dimensions. ToF-SIMS imaging has been shown to be useful for confirming the array layout and as a relatively rapid method of observing the layout of key secondary species. XPS analysis has confirmed the need for surface analysis of these arrays by demonstrating the difference between the bulk and surface chemistry of the polymers. Principal component analysis has been proven to be an ideal method for analysing the large amounts of data gained from such a large library and applicable to both ToF-SIMS and XPS data. In chapters 5 and 6 I will show how this surface chemical data can be applied to explain other surface properties of the polymers, such as cell adhesion, protein adsorption and wettability.

Chapter 4

Picolitre Contact Angle Measurement on Polymers

4.1 Introduction

Wettability, the degree to which a solid may be wet by a liquid, is a property of surfaces that influences many phenomena such as biological response to materials, and coating adhesion and durability.[42, 77] Usually wettability is assessed through the measurement of the contact angle (CA) of a liquid droplet placed on a surface, which is a quick, economical and relatively simple technique.[78] The CA is one of the most sensitive of all surface analytical techniques as only the top nanometre of a surface influences wettability.[79] The CA of a liquid on a solid depends on both surface chemistry and roughness.[80] When estimating the contact angle by fitting a function to the profile of a droplet, shape distortion by gravity must also be taken into account for larger droplets.[81]

The sessile drop method of CA measurement commonly utilises a few microlitres of a liquid (e.g. $\sim 2 \mu\text{L}$ giving a 2 mm base diameter when $\text{CA} = 90^\circ$) which are placed on a surface from a needle. This method is useful for relatively large, homogenous surfaces but lacks lateral resolution when analysing surfaces with chemical differences on the sub millimetre scale, due to the dimension of the base diameter of a droplet. Smaller regions will result in a drop shape that averages the response of areas along the circumference of the base.[82] With the miniaturisation of many areas of science (microarrays, surface chemical gradients and microfluidics) there is an increasing need to characterise surfaces that are small in area, which is consequently impractical for microlitre volume drops due to their size.

Recently a new method of CA measurement has been developed allowing the use of picolitre volume droplets of liquid. This allows for improved spatial resolution of wettability on a surface and an ability to measure CA on much smaller areas, such as microarrayed materials.[83] These picolitre volumes of liquid are dispensed using a piezo dosing unit similar to those used on inkjet printers and within biological array manufacture.[84] In the case of water as the dosing liquid, it is possible to produce 100 pL droplets with a base diameter of approximately 70 μm (when $\text{WCA} = 90^\circ$). In this chapter it is demonstrated that

water CAs measured from picolitre droplets are equivalent to those measured from microlitre droplets on 6 commonly used polymers. The high spatial resolution of the techniques is then demonstrated by mapping the wettability of a chemical gradient surface formed from consecutive deposition and making of plasma polymers.

4.2 Methods and Materials

4.2.1 Preparation of polymer films.

Solutions (1% w/v) of polystyrene (Mw 100,000), poly(L-lactic acid) (Mw 95,000), poly(DL-Lactic acid) (Mw 95,000), poly(methyl methacrylate) (Mw 60,000) and poly(2-hydroxyethyl methacrylate) (Mw 20,000) were prepared in chloroform. All polymers were purchased from Sigma Aldrich. Silicon wafers were cleaned using UV light, then sonicated in methanol. The polymer solutions were spin coated onto the clean silicon wafers at 3000 rpm. The polymer films were left for 24 hours under vacuum before CA measurements. The surface of a piece of poly(tetrafluoroethylene) (Krüss) was scraped clean before CA measurement.

4.2.2 Preparation of radial plasma polymer gradient.

The radial wettability gradient was prepared by plasma polymer deposition of allylamine (ppAAM) through an aperture onto a glass substrate coated with plasma polymerised hexane (ppHex). The radiofrequency plasma (13.56 MHz) was driven at a power of 20 W while the monomer pressure was kept at 300 mTorr for both hexane and allylamine. The chemicals were supplied by Sigma Aldrich and degassed prior to use. The glass substrate was cleaned with ultrasound, washed with acetone and treated with an oxygen plasma for 3 min before the deposition of ppHex. The radial gradient was obtained by a diffusion controlled deposition of ppAAM through a 1.2 mm hole in a non-conductive mask

that was placed at a distance of 0.1 mm over the ppHex-coated substrate. This is a development of a previously reported patterning technique.[85, 86]

4.2.3 CA measurements.

Images of the droplet profile were recorded from which the CA was determined using the angle of intersection between a baseline and a circle or Young-Laplace function fit to the drop profile. The Young-Laplace function models the droplet shape using two radii of curvature. The CA was also determined using a tangent placed at the intersection of the liquid and solid. A water droplet with a volume of 100 pL was dispensed by a piezo doser onto each polymer sample using a DSA100 (Krüss). Measurements were taken at 10 areas for each polymer sample from which average and standard deviation values were calculated. A CAM200 instrument (KSV instruments, Ltd) was used to dispense ~ 2 – 12 μ L volume water droplets onto each polymer sample. Again, 10 CA measurements were taken for each polymer sample at different areas. Ultra pure water was used for all CA measurements (18.2 MO resistivity at 25°C). To map the wettability of the polymer gradient the DSA100 was used to deposit 625 picolitre volume droplets onto the radial plasma polymer gradient in a 6 mm by 6 mm square grid. This was achieved with an automated stage and took 6 hours for automated dosing and fitting. The CAs of these droplets were fitted using a circle fitting function and the resulting CAs plotted to give a 2 D map of the gradient's wettability.

4.3 Results and Discussion

If picolitre volume droplets are to be routinely used for CA measurements it is useful to confirm experimentally that the CA data acquired from them are equivalent to that acquired from microlitre droplets. There are two major differences between small and large droplets, the influence of gravity on the droplet and the evaporation rate.[81, 87] To investigate the effect of droplet size, water droplets of different volume were placed on PMMA surface by controlling

the amount dispensed by the syringe. The droplet profile was fit using either a circle or Young-Laplace function and a tangent fitted by eye to the point of intersection with the surface. It is clear that the CAs estimated using the circle function decreases as the droplet volume increases (Figure 28a). The CA determined between the tangent and the surface did not vary significantly ($69 \pm 1^\circ$) with droplet volume (not shown). This is considered to be the actual contact angle and below the estimates based on fitting a function to the profile are discussed.

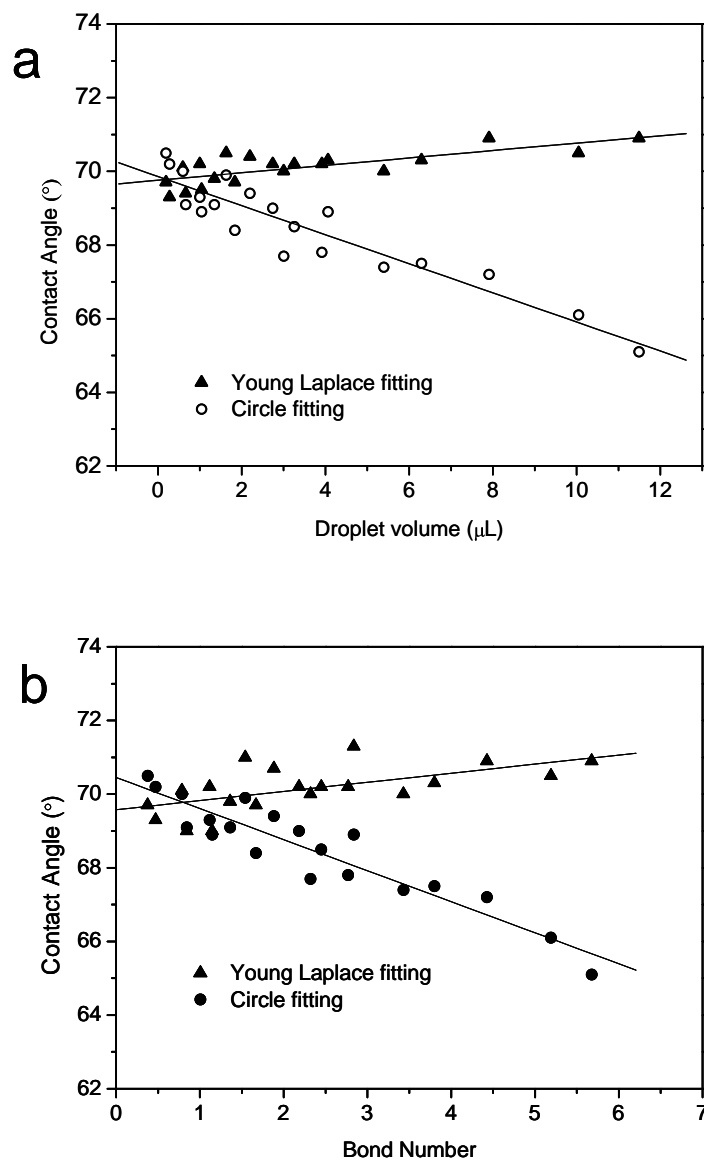


Figure 28. Water Contact Angle versus a) droplet volume and b) droplet Bond number on PMMA. Each water droplet was fitted using both circle and Young-Laplace function functions to model droplet shape. Linear regression fits have been provided to guide the eye.

Theory states that when a droplet is placed onto a surface a 3 phase equilibrium exists between the liquid, solid and vapour phases which is described by the classical Young equation.[88] However, this does not include droplet size which can influence the CA measured when fitting a function to a droplet profile.[81] If the droplet is small enough for the influence of gravity to be insignificant, the free energy of the system at equilibrium is minimised for a truncated sphere shape; thus the profile can be fitted to a segment of a circle. If it is large enough for the distortion of the shape by gravity to be significant, it is instead better fit using the Young Laplace equation. The Young Laplace equation describes the curved profile of a droplet using a 2 radius of curvature solution.[89] The Young-Laplace fit of the droplet shape resulted in a small increase of CA with time ($\sim 0.5^\circ$ between 0.2 and 12 μL as seen in Figure 1) which suggests that this method does not completely compensate for increase in droplet size. Compared with the measured variance of the CA, this is insignificant. In contrast, the circle fit provides an increasingly large underestimate of the CA compared to the actual CA ($69^\circ \pm 1^\circ$) as the droplet volume increased. As the droplet volume increases, the greater the effect of gravity and the less spherical the droplet becomes, causing the circle fitting model to become increasingly inaccurate. Comparison with the tangent method suggests that for droplets in this size range gravity is influencing the shape of the droplet, but not the CA itself. The Bond number (a numerical expression of the ratio of gravitational to surface tension forces) was calculated for 2 μL and 100 pL water droplets:

$$B_0 = \frac{\rho g L^2}{\gamma} \quad (5)$$

where B_0 is the bond number, ρ is the density of the liquid, g is the acceleration due to gravity, L is the diameter of the droplet and γ is the surface tension of the liquid. The values obtained are 1.51 for the 2 μL droplets and 6.58×10^{-4} for the 100 pL droplets respectively.[89] Figure 28b shows the relationship between the Bond number of a droplet and its CA on PMMA. It can be seen that at Bond numbers less than ~ 1 gravitational forces no longer influence the shape of the droplet. The Bond number for 100 pL droplets is much smaller than 1 which indicates that surface tension forces dominate over gravitational forces. Thus, for

the remainder of this paper the Young-Laplace method will be used for the 2 μL droplets and a circle fit for the 100 pL droplets. Although the Young-Laplace method would also be suitable for 100 pL droplets, its increased complexity compared to the circle fitting method makes the circle method preferable.

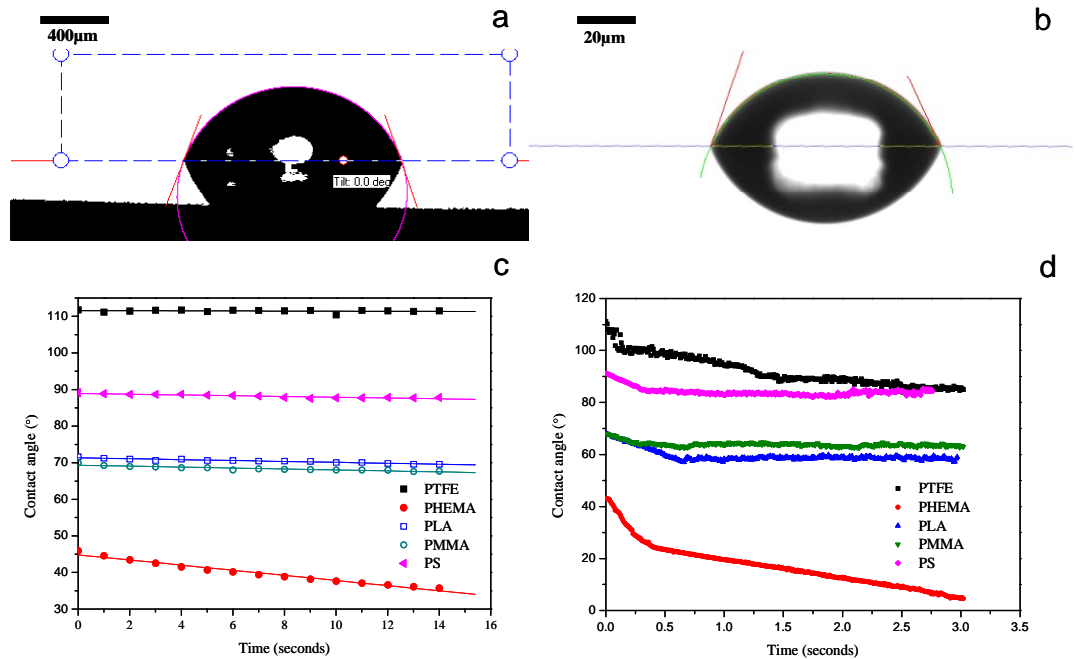


Figure 29. Images of the profile of a) 2 μL and b) 100 pL water droplets on PMMA to demonstrate difference in scale. Graphs of WCA versus time for c) 2 μL and b) 100 pL water droplets on five polymers.

To investigate the influence of evaporation, droplet images were collected using a high speed camera triggered to record as the droplets were released (Figure 29 a and b). It was possible to accurately record the droplet image at time intervals very much shorter than the timescale on which the droplets evaporated for both large and small droplets as seen in Figure 2c and d. The WCA has been plotted against time for both picolitre and microlitre volume droplets on five polymers. The different sized droplets show quite distinctly different CA profiles over time. The WCA of 2 μL droplets decrease slightly with time in a linear manner (Figure 29c), the decrease appears to be more pronounced with PHEMA which has the lowest WCA. The rapid evaporation of the picolitre droplets causes a rapid decrease of 10 to 20° in CA within approximately the first 0.5 second (Figure 29d). Subsequently, a second stage was observed where the WCA

decreases more slowly. Both stages are essentially linear and again the WCA of PHEMA appears to decrease more rapidly than the other polymers.

The observation of two distinct stages of WCA for picolitre volume droplets raises the question as to which WCA to measure, for example is it correct to take the WCA at time zero or at the start of the second stage. Examination of the videos revealed that as the picolitre droplets evaporate they initially decreased in height without movement of the perimeter, and then decreased in diameter, with a contraction of the perimeter. Very similar behaviour has been reported for microlitre droplets, although over much greater time periods (~ 30 mins) and has been rationalised in terms of contact angle hysteresis.[87, 90, 91] Thus, an initial constant contact area results due to pinning of the perimeter, causing the droplet height to decrease on evaporation and resulting in decreasing CA. When the CA reaches the receding value, the contact area decreases while the CA stays constant.[90] This description is valid for the size changes seen for picolitre droplets, although on shorter time scales since the decrease in volume occurs more rapidly for smaller drops.

It is apparent that this description of WCA with time after the droplet is dispensed is valid for PLA, PMMA and PS, whereas the PTFE and PHEMA WCA values do not enter a stable second phase. PHEMA is a mobile hydrogel which is known to modify its surface structure to minimise its interfacial energy by exposing methyl groups (hydrophobic) when in contact with air and hydroxyl groups (hydrophilic) when in contact with water.[92] This could explain why its WCA decreases so rapidly initially, possibly due to the reorientation of the polymer's surface upon contact with the water droplet and why the WCA continues to decrease. It is also possible that water sorption by the PHEMA could be responsible for the continued decline in WCA. A rapid decrease in the WCA on PTFE was observed that may be attributed to either droplet or surface instability. Despite this, within observed experimental variance, the initial contact angle is close to literature values.[93]

The WCAs of picolitre droplets taken from the first image of the droplet on the surface with the same image for the microlitre droplets are presented in

Table 1. A remarkably good correlation between the two techniques was observed. The average difference between microlitre and picolitre measurements for the five polymers is only 1.5° and in most cases the values were within the variance between measurements on the respective instruments. The precision of WCA measurement is often quoted as ± 1 degree and accuracy measurements are rarely provided. With due consideration of precision and accuracy the results gained with the two methods are comparable. There is much debate over the influence of line tension on the CA of droplets, particularly smaller droplets where the influence of line tension (and other surface forces) are theoretically greater.[94] Line tension is defined as a linear tension at the boundary where three phases meet at the perimeter of a droplet. It is interesting to observe that over the droplet size range 100 pL to 2 μ L there is no significant change in CA, suggesting that the influence of line tension on the contact angle in drops of this size range is negligible.

Polymer	CA measured from 100 pL droplet ($^\circ$)	CA measured from 2 μ L droplet ($^\circ$)
poly(2-hydroxyethyl methacrylate)	44.9 ± 1.0	43.5 ± 1.4
poly(L-lactic acid)	67.9 ± 0.5	71.5 ± 0.4
poly(DL-lactic acid)	73.5 ± 0.5	73.6 ± 0.7
poly(methyl methacrylate)	67.8 ± 0.6	69.7 ± 1.0
poly(styrene)	89.6 ± 0.4	90.2 ± 2.2
poly(tetrafluoroethane)	111.2 ± 1.5	111.3 ± 0.4

Table 1. Water contact angles of six polymers measured from picolitre and microlitre volume droplets (\pm standard deviation).

The polymer with the largest difference in WCA between microlitre and picolitre volume droplets (3.6°) was poly(L-lactic acid), whereas the difference for poly(DL-lactic acid) was negligible (0.1°). To investigate this difference both polymers were imaged in air using Tapping mode Atomic Force Microscopy. It was observed that the poly(L-lactic acid) was considerably rougher ($r_a = 29$ nm) than poly(DL-lactic acid) ($r_a = 7$ nm) (Figure 30). Contact angles have been observed to decrease on rougher surfaces with CAs below 90° . [80] Picolitre volume droplets with a base diameter of $70\ \mu\text{m}$ may be more sensitive to this surface topography than microlitre droplets, hence the 3.6° lower WCA measured on PLLA. This explanation is supported by the similarity of the WCA measured using the microlitre and picolitre droplets on the smoother variant of the polymer, poly(DL-lactic acid). A full study of the relative effects of roughness on WCA measurements with different sized droplets is warranted.

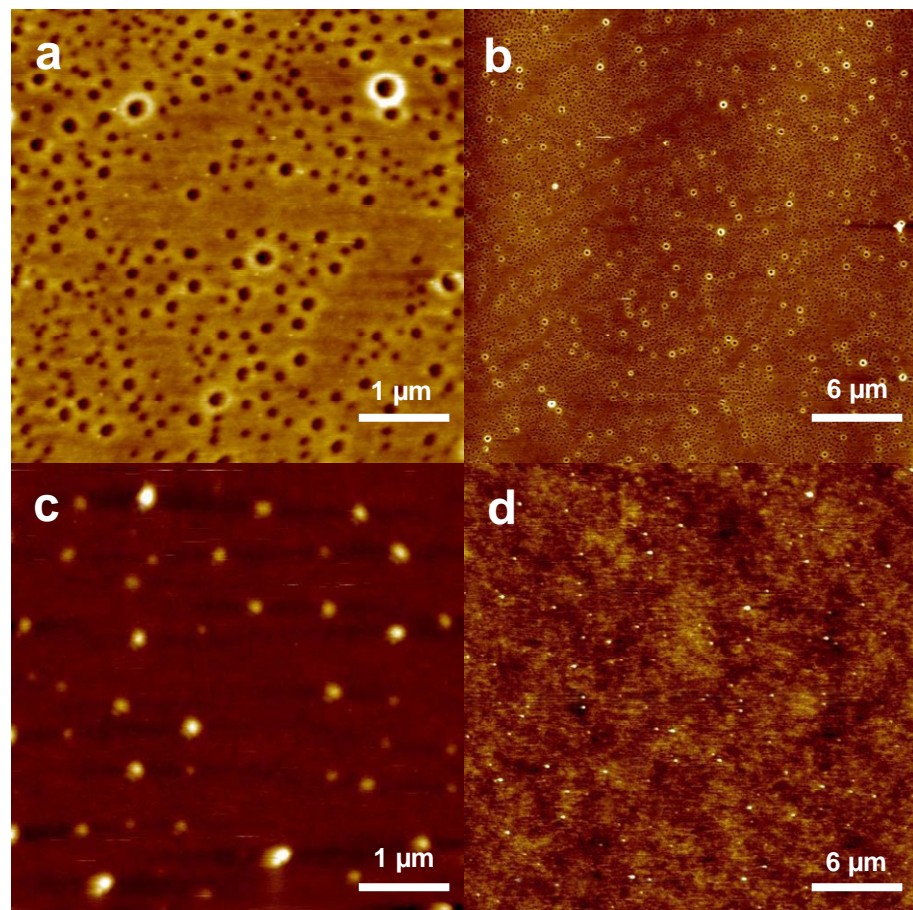


Figure 30. Tapping mode AFM height images of PLLA a) $5 \times 5\ \mu\text{m}$ b) $30 \times 30\ \mu\text{m}$ and PDLA c) $5 \times 5\ \mu\text{m}$ d) $30 \times 30\ \mu\text{m}$. The RMS roughness values for PLLA and PDLA were 29 and 7 nm respectively.

There is much interest in using gradients of surface chemistry and wettability to guide cellular response and biomolecular adsorption in scaffolds, sensors and devices.[19, 85] Using the above procedure developed to make measurements with picolitre droplets, the wettability of a radial chemical pattern was mapped to illustrate the utility of the approach. A circular plasma polymerised allylamine (ppAAM) (hydrophilic) area was deposited through an aperture acting as a raised mask on top of a pre-deposited plasma polymerised hexane (ppHex) coating (hydrophobic) to provide a radial wettability gradient. WCA measurements were acquired at 250 μm intervals within a 6 mm by 6 mm which gives a highly resolved picture of the change in wettability over the gradient. All WCA measurements were acquired under computer control using a motorised stage and the drop shapes were recorded and fitted automatically. It can be seen that the WCA reaches a minimum of 44 $^\circ$ in the centre of the radial gradient suggesting complete surface coverage with ppAAM (Figure 31). The WCA increased gradually from the centre of the gradient outwards reaching a maximum of 79 $^\circ$ at the periphery. The WCA of uniform samples of ppAAM is \sim 49 $^\circ$ and for ppHex is \sim 97 $^\circ$, therefore it can be reasonably assumed that the CA increase is due to the change in chemistry over the gradient formed by diffusion of the ppAAM from the centre outwards.[86]

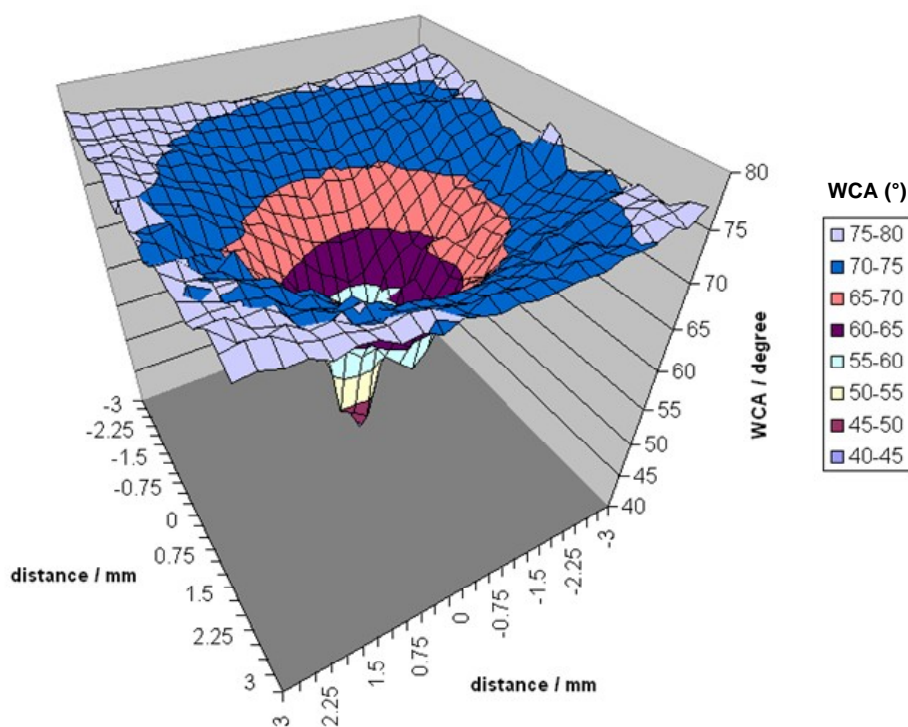


Figure 31. Three-dimensional wettability map of a radial plasma polymer gradient.

Using $\sim 2 \mu\text{L}$ volume droplets with a diameter of approximately 2 mm it would only be possible to take 9 CA measurements within the 6x6 mm area; therefore the wettability has been mapped with a resolution 70 times greater using the picolitre volume droplets than if conventional volume droplets were used. Historically surface analysts have been limited to making routine sessile drop WCA measurements on the millimetre scale. The development of this approach opens up a whole new world of applications at the sub millimetre length scale, with applicability to areas such as microarray and gradient surface analysis.[19, 83]

4.4 Conclusion

The use of microlitre and picolitre volume droplets of water for WCA measurement has been compared on six polymers: P_DLLA, P_LLA, PMMA, PS, PHEMA and PTFE. It has been demonstrated that the CAs measured from picolitre volume droplets are remarkably similar to those measured from microlitre volume droplets when appropriate consideration of evaporation and droplet shape are used. When the contact angle of the picolitre volume droplets are measured over a time period of three seconds, two stages are observed. It appears that the contact angle at the beginning of the second stage is probably the receding contact angle. More work is needed to investigate if the advancing and receding contact angle may be extracted from such experiments.

The high spatial resolution of wettability of this new approach has been demonstrated by mapping the wettability of a plasma polymer gradient. The polymer spots on a polymer microarrays generally have a diameter of approximately 300 μm , therefore it is obvious that conventional methods of contact angle measurement could not be used to analyse them. The application of picolitre contact angle measurements to determine the surface energy of microarrayed polymers is discussed in detail in Chapter 5.

Chapter 5

Surface Energy Analysis of Polymer Microarrays to Investigate the Chemical Basis of Polymer Surface Energy

5.1 Introduction

In previous Chapters methods have been described for the surface chemical analysis of polymer microarrays, measuring contact angles from picolitre volume droplets and using PLS to study surface structure/property relationships using the large datasets obtained from microarrays. In this chapter these methods will be applied to determine the surface energies of all the polymers on a microarray and then investigate how the surface chemistry of these polymers influences their surface energies. The microarray used in this study is a large combinatorial library of 496 novel copolymers, the first such array designed to generate through monomer selection a wide range of surface energies. This copolymer library has been synthesised *in situ* in a microarray format on a glass slide, as described in previous chapters. This new polymer library is used to investigate the relationship between copolymer surface energy (polar and disperse) and surface chemistry (determined using XPS and ToF-SIMS). Alternative methodologies used previously for investigating wettability include gradient surfaces of polymers and self-assembled monolayers that have been mixed in gradually changing proportions to vary wettability within a single system.[95, 96] Such approaches only allow investigation of a two component system, i.e. a change from one chemistry to another. Large multi-component material libraries such as the one described herein allow the study of surfaces with widely varying chemistries.[14]

The surface controls many important material performance properties such as biocompatibility and wettability. Material arrays provide challenges for surface characterisation, combining a large number of samples of a small size, spatially patterned. Previous attempts at high-throughput surface energy measurement of polymer libraries utilised microlitre volumes of liquids (with base diameters of 2-3 mm) which are not practical for the analysis of samples on a microarray, since space constraints necessitate that the sample spots have sub-millimetre dimensions.[16, 47, 97] In Chapter 4 the application of a new method of contact angle measurement from individually dosed picolitre volume droplets was demonstrated, which yield comparable contact angles to the conventional method

that utilises microlitre volume droplets.[98] This Chapter describes the first application of picolitre contact angle measurements to determine surface energy values using multiple liquid contact angle measurement. This picolitre contact angle approach has general applicability to surface energy determination of other materials, including pharmaceuticals, glasses and ceramics.

Surface energy (γ) is a fundamental property of surfaces and is defined as the work required to form an additional unit area of surface.[89] It has been shown to correlate with a wide range of surface phenomena such as wetting, adsorption and bioadhesion.[42] Surface energy can also be considered to be a measure of the attractive forces between the molecules of a surface and a liquid.[99, 100] Fowkes suggested that for many surfaces this attractive force can be considered to be made up of two primary types of contributing forces: dispersive and polar. The dispersive component is that due to London van der Waals forces which operate between all substances (polar and non polar), whereas the polar component is due to more discrete interactions such as hydrogen bonds.[101] Hence, a saturated hydrocarbon would be expected to have zero polar contribution to γ because it is purely disperse. Surface energy may be estimated using a number of experimental methods, including atomic force microscopy,[102] surface force apparatus[103] and inverse gas chromatography (for powders).[104] The most common method of γ estimation is by contact angle measurement, which can be achieved using a variety of methods including Owen and Wendt's model, which divides γ into its polar (γ^p) and dispersive (γ^d) components.[105, 106] Contact angle data from two or more liquids are entered into the extended Fowkes equation to form two or more simultaneous equations:

$$\gamma_l(1 + \cos\theta) = 2(\gamma_l^d \gamma_s^d)^{1/2} + 2(\gamma_l^p \gamma_s^p)^{1/2} \quad (6)$$

where γ_l is the surface tension of the liquid, θ is the contact angle of the test liquid on the solid, γ_l^d and γ_l^p are the disperse and polar components of γ of the liquid, γ_s^d and γ_s^p are the disperse and polar components of the γ of the solid respectively. The simultaneous equations generated are then solved graphically to yield the polar and disperse components of γ of the solid. The total surface energy (γ) can then be calculated by adding the two components:

$$\gamma = \gamma^p + \gamma^d \quad (7)$$

An array of micro patterned polymers was designed specifically for this study to investigate the effects of polymer composition on surface energy (see Methodology). Monomers were chosen with a variety of physicochemical properties with the aim of producing a library of copolymers which range from hydrophilic to hydrophobic. Information about the water contact angles of polymers from a previous acrylate/methacrylate library was also used when choosing the monomers.[83] The monomers used to create the 496 acrylate copolymers on the array analysed are listed in Figure 20. The polymer microarrays were created using an automated system, described in detail in Chapter 3.

5.2 Methodology

5.2.1 Polymer Microarray Synthesis.

The microarray under investigation comprised of 496 novel acrylate based polymers synthesised from 16 major monomers which were mixed pairwise with 6 minor monomers in the following ratios - 100:0, 90:10, 85:15, 80:20, 75:25 and 70:30 (Figure 20). A radical initiator was added to the monomer mixtures which were then spotted onto a pHEMA coated glass slide. They were then polymerised with ultraviolet light. Full details of array manufacture can be found in Chapter 3.

5.2.2 Contact angle Measurements.

Contact angles were determined for each polymer on the array using two liquids: Ultra pure water (18.2 MO resistivity at 25°C) and diiodomethane (= 99 % pure) (Aldrich). A DSA100 (Krüss) with a piezo-doser head was used to dispense a 100pL droplet of each liquid onto the centre of each polymer spot on the array. Data acquisition was automated with the spot side profile of the back lit spot being recorded. A dual camera system was used, one to record a profile of

the spot and the other to record a bird's eye view of the spot to ensure that the water droplet was deposited at the centre of each polymer. Modifications were made to the DSA100 reservoir position to allow dosing of liquids with low interfacial tension such as diiodomethane. Data analysis involved following standard contact angle measurement procedures except that due to the small droplet size circle fitting was used instead of Young – Laplace.[98]

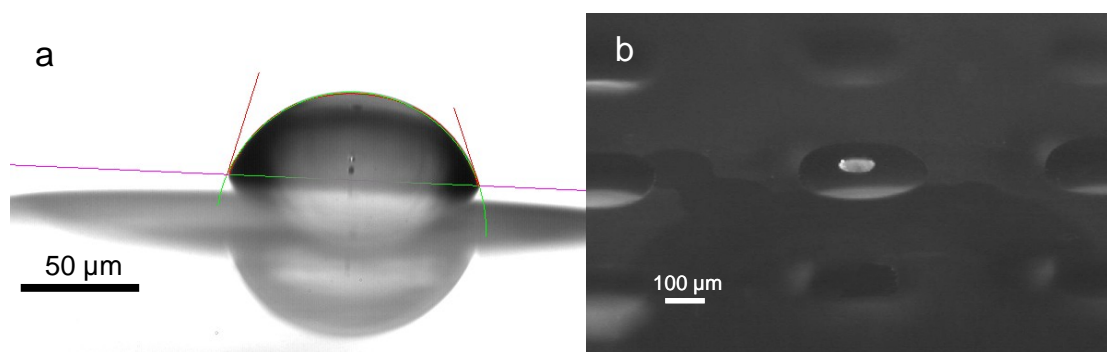


Figure 32. a) Side profile of a 100 pL water droplet sitting on a polymer spot which has been fitted with a circle function b) Birds eye view of a 100 pL water droplet sitting in the centre of a polymer spot.

Figure 32 shows a picolitre volume water droplet sitting in the middle of a polymer spot to demonstrate the relative size of the droplet to spot. The droplet image is fitted with a circle segment function to demonstrate the axisymmetry of the contact line. Polar and disperse γ values were calculated using the Owens and Wendt's model as described above. Macros were written to enable rapid γ calculations for the large dataset. The surface tension values of the liquids used are provided in Table 2.

Liquid	Surface tension (mN/m)	Dispersive component (mN/m)	Polar component (mN/m)
Ultra pure water	72.8	21.8	51.0
Diiodomethane	50.8	50.8	0

Table 2. Surface tension values (including dispersive and polar values) for test liquids.[107, 108]

5.2.3 X-ray Photoelectron Spectroscopy.

Analysis was carried out using a Kratos Axis Ultra equipped with a monochromated Aluminum X-ray source operated at 15 mA and 10 kV anode potential. Photoelectrons were sampled from a 110 x 110 μm area on each polymer spot on the array. Survey and high resolution C1s spectra were obtained from each polymer spot. Due to the large amount of polymers the analysis time per polymer spot was limited to 9 minutes for the survey and 3 minutes for C1s scan. Pass energies of 80 eV were used for the survey scans and 20 eV for the C1s high resolution scans. Full details of XPS analysis of polymer microarrays can be found in Chapter 3.

5.2.4 Time-of-Flight Secondary Ion Mass Spectroscopy.

Analysis was carried out using a ToF-SIMS IV spectrometer (ION TOF GmbH, Münster, Germany) using a Ga^+ primary ion beam (operated at 25 kV and in “bunched mode”). A 1 pA primary ion beam was rastered over a 100 x 100 μm area of each polymer spot on the microarray. A 60 second acquisition time was allowed for each polymer sample, ensuring that static conditions were maintained for every spectra acquired. Ion masses were determined using a Time-of-Flight analyser allowing very accurate mass assignment (to three decimal points). A macro was designed using instrument software to allow automatic acquisition of spectra from all polymer spots on the microarray.

The positive and negative ion spectra for all 496 polymers were automatically mass calibrated using ION-TOF ToF-Bat software. One peak list each was then created for both positive and negative ion spectra using mass spectra taken from a group of polymers from the array containing monomers with widely varying chemistries. These two peak lists were applied to all 496 polymers. The peaks were then integrated using ION-SPEC software and peak intensities exported to Origin Pro 7.5. The ion intensities for each polymer were normalised to the total ion count. The positive and negative ion data for all 496 polymers was then combined to form a concatenated data matrix. PLS analysis

was carried out using Eigenvector PLS_Toolbox 3.5 for Matlab. The ToF-SIMS and surface energy data was mean-centred before analysis.

The SIMPLS algorithm was used for the PLS analysis rather than the other commonly used algorithm NIPALS.[109] The two algorithms have been shown to give equivalent results when analysing a dataset where the independent variable is multivariate and the dependent variable is univariate.[110]

5.2.5 Atomic Force Microscopy Imaging of Polymer Spots.

A D3000 AFM (Veeco) was used in tapping mode to acquire 1 x 1 μm images. A Tap300 (Budget Sensors) tip was used. The mean root mean square (RMS) roughness was calculated from three images using instrument software. The images were plane corrected prior to analysis.

5.3 Results

5.3.1 Surface energy measurements.

The water contact angle (WCA), diiodomethane contact angle (DCA) and, upon solution of equation (1), the surface energy (γ^p & γ^d) was obtained for all of the 496 polymers. The WCA values of the polymers varied greatly from 31° to 104°, whereas the γ^p varied from zero to 24 mJ/m^2 . When WCA is plotted against γ^p for all the polymers (Figure 33a) it can be seen that as WCA measured on the copolymer decreases, the polar component of surface energy (γ^p) increased. Once the γ^p reaches zero the WCA continues to rise without change in γ^p . The DCA values of the polymers ranged from 13 to 47°, whereas the γ^d varied from 36 to 50 mJ/m^2 . The γ^d of the polymers is relatively invariant with WCA, with 90% of the polymers having a γ^d between 44 and 49 mJ/m^2 (Figure 33b).

If γ^p is plotted against γ^d it can be observed that the polymers have a narrow range of γ^d values with a wide range of γ^p values (Figure 34a). Polymers containing major monomer 13 have the largest range of γ^d values (~ 39 to 48 mJ/m^2) with a moderate variation in γ^p values (~ 0 to 9 mJ/m^2). In contrast, polymers containing major monomer 7 group quite closely with similar γ^p and γ^d values. Monomer 7 is notable as the only monomer containing a terminal phenyl group. Comparison with polymers that do have a large variation (e.g. those containing monomer 13) suggests that this reflects a lack of the minor monomer constituents at the surface, which is supported by ToF-SIMS analysis of polymers containing this monomer. Hence, all polymers in this group have similar γ^p and γ^d values to the polymer containing 100% major monomer 7.

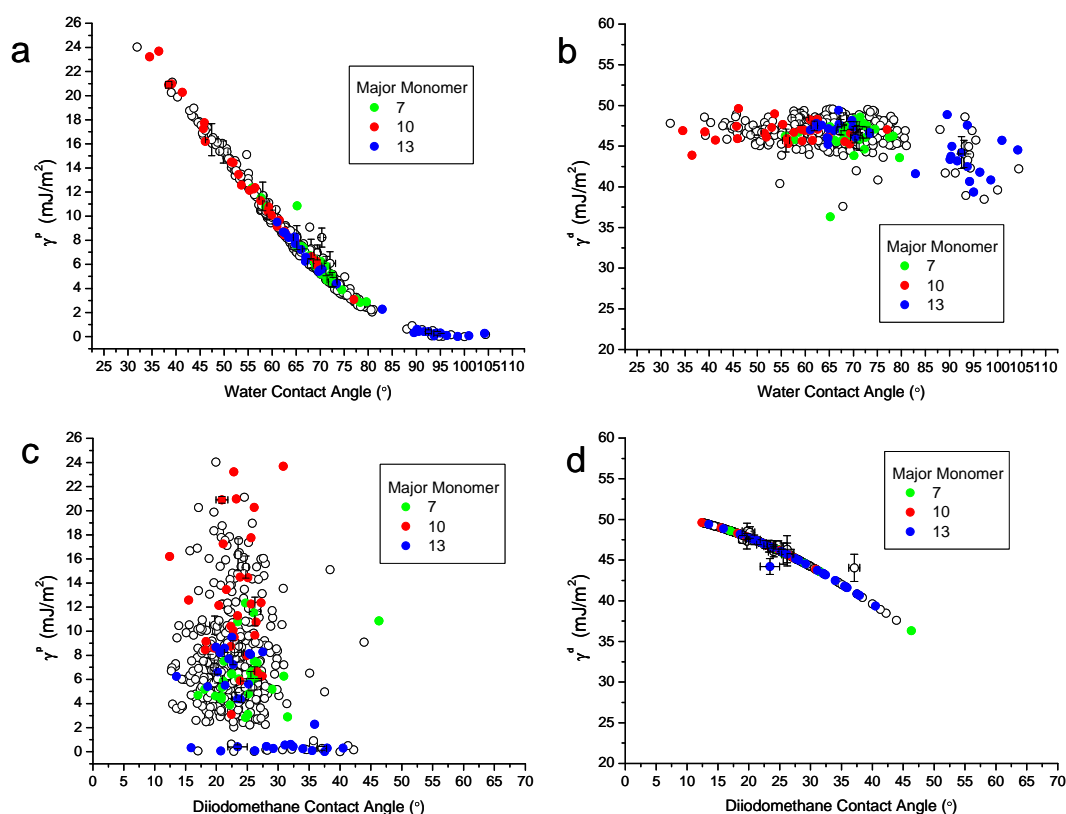


Figure 33. a) Water contact angle versus the polar component of surface energy b) Water contact angle versus dispersive component of surface energy for 496 polymers on array c) Diiodomethane contact angle versus the polar component of surface energy d) Diiodomethane contact angle versus dispersive component of surface energy. Polymers containing major monomers 7, 10 and 13 have been highlighted to illustrate differences between polymer composition. The array contained 6 repeats of each of the 16 100% major monomers. The error bars represent the standard deviations for these 16 polymers to give an indication of the error of the technique.

The addition of minor monomers had a significant effect on the γ^p for most of the copolymers. Minor monomer E generally increases the γ^p of a polymer (e.g.

major monomers 7 & 13) unless the copolymer already has a very high γ^p (e.g. 100% major monomer 10) in which case it will decrease it (Figure 34b-d). In contrast minor monomer D always decreases the γ^p of the polymer. Monomer D contains six fluorine atoms which have a weak hydrogen bonding ability when covalently bonded to carbon, hence a decreased γ^p when it is added as a minor constituent.[105]

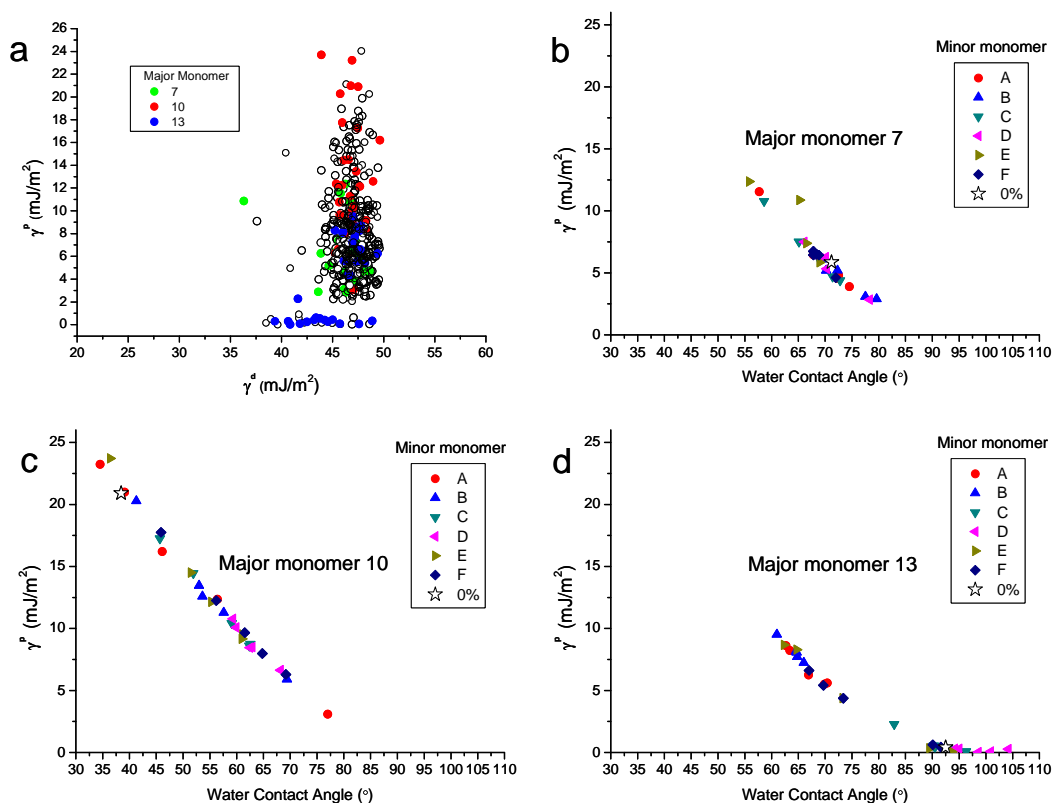


Figure 34. a) Polar versus dispersive component for all 496 polymers, and Water Contact Angle versus polar component of surface energy for b) polymers containing monomer 10 as their major constituent c) polymers containing monomer 13 as their major constituent d) polymers containing monomer 7 as their major constituent. For figures b) to d) the black star represents the polymer containing 100% of the major monomer, i.e. no minor monomer additions.

5.3.2 X-ray Photoelectron Spectroscopy.

Survey and high resolution C1s spectra were obtained for all 496 polymers on the microarray. Surface elemental compositions (C, O, F and N %) and high resolution C1s functional group compositions (C-C, C-O, C=O and C-F) were determined and related to polar and disperse surface energies. The surface O:C

ratio was calculated for all 496 polymers and plotted against the γ^p and γ^d values (Figure 35a & b). There is no obvious relationship observed between surface O:C ratio and γ^p and γ^d , which suggests that O:C ratio might be too simple a surface chemical descriptor for this task. A qualitative relationship between surface Nitrogen and Fluorine atomic concentrations and γ^p was observed. The polymers containing Nitrogen at their surfaces had the highest average γ^p values, whereas those containing Fluorine at their surfaces had the lowest average γ^p values.

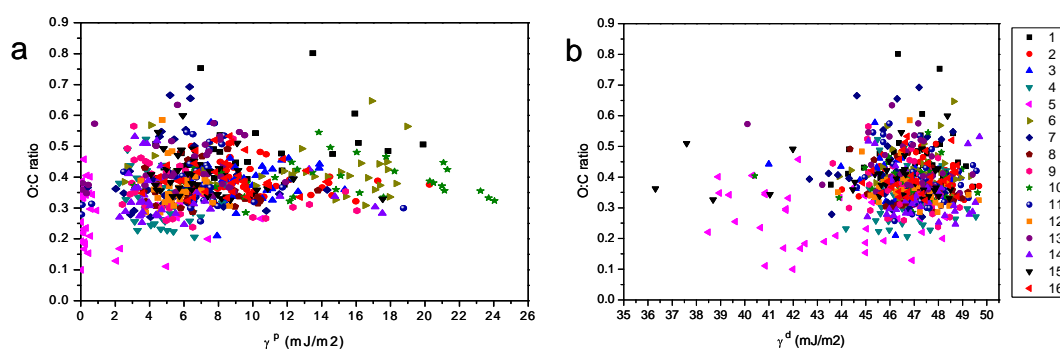


Figure 35. a) O:C ratio versus polar component of surface energy b) O:C ratio versus disperse component of surface energy for 496 polymers.

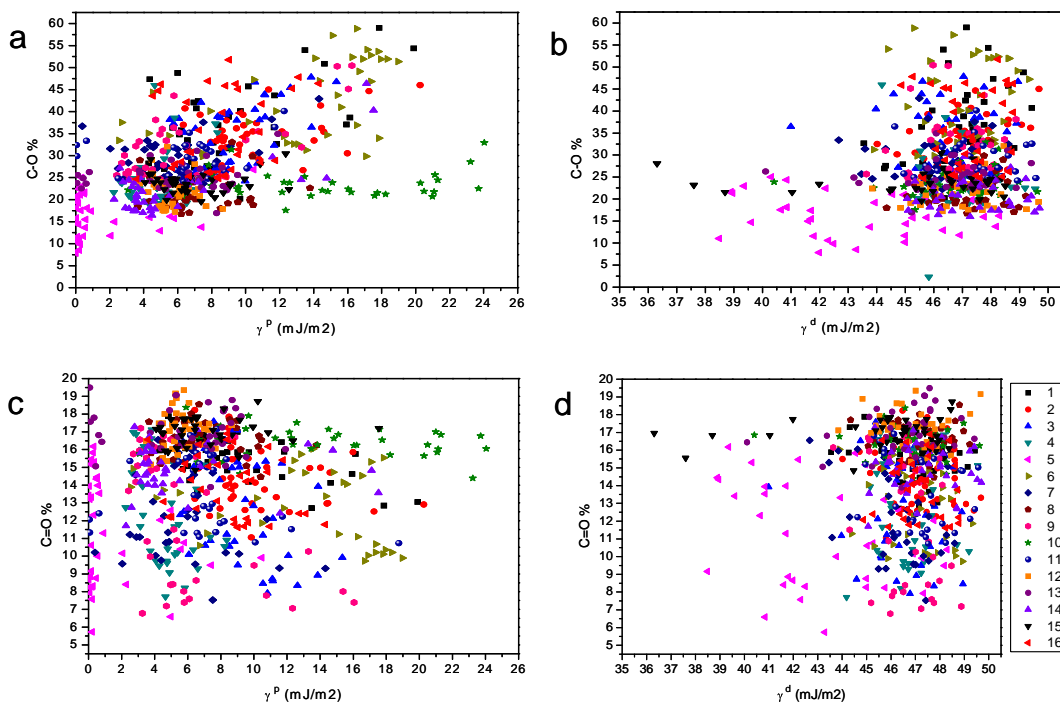


Figure 36. a) C-O % versus polar component b) C-O % versus disperse component c) C=O % versus polar component d) C=O % versus disperse component of surface energy for 496 components.

When C-O % is plotted against γ^p it can be observed that as the percentage of surface C-O increase so does polymer γ^p (Figure 36a). The one exception to this relationship is the group of polymers containing monomer 10 as their major component, where surface C-O % is invariant with γ^p . However, if C=O % is plotted against γ^p it can be seen that there is no such relationship (Figure 36c). Neither surface C-O nor C=O % appear to influence polymer γ^d (Figure 36b & d).

5.3.3 Time-of-Flight Secondary Ion Mass Spectroscopy analysis.

The positive and negative ion ToF-SIMS spectra obtained from the polymers contained secondary ions characteristic of acrylate polymers. Three PLS models were obtained using the positive and negative ion spectra from the polymer array and the γ^p , γ^d and total surface energy (γ). It was not possible to build a model with any predictive value using the γ^d data (as measured by plotting the experimentally determined values of γ^d against the predicted values). To determine the optimum number of latent variables for each PLS model the “leave one out” cross validation method was used. This involves leaving one sample out of the model then attempting to predict the value of this sample from the rest. This is done for all samples allowing the average error in prediction to be calculated - one measure of this error is the root mean square error of cross validation (RMSECV). Therefore the number of latent variables for each model was chosen by observing where the RMSECV reached a minimum. The RMSECV reached a minimum at 5 latent variables for γ and 4 latent variables for γ^p (Figure 37).

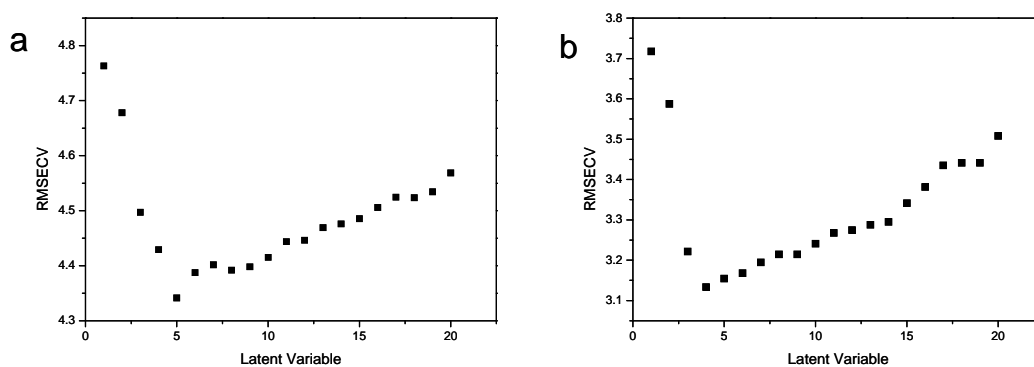


Figure 37. RMSECV versus latent variable for a) Total surface energy b) Polar surface energy.

The first PLS model built using ToF-SIMS spectra and polymer γ^p showed a relatively good auto-predictive ability (Figure 39a), as measured by plotting experimental versus predicted values (RMSPE = 2.1). However, the model appears to slightly underestimate γ^p values above 20 mJ/m². Figure 39b shows the regression co-efficients for the PLS model. The ions with the greatest positive regression co-efficients have m/z of 69.034, 45.034, 30.010, 34.992, 17.003 and 42.011. The ions with the highest negative regression coefficients have m/z of 15.023, 13.008, 55.055, 29.038, 53.038 and 41.039. The second PLS model built using ToF-SIMS spectra and polymer γ showed an equally good predictive ability (Figure 40a) to the first model (RMSPE = 2.3). Figure 40b shows the regression co-efficients for the PLS model. It can be seen that the ions with the highest positive regression co-efficients have m/z of 34.992, 69.034, 45.034, 22.991, 17.003 and 15.996. The ions with the highest negative regression coefficients have m/z of 13.008, 39.023, 41.039, 12.000, 15.023 and 57.071.

m/z	Positive correlation (au)	Ion structure	m/z	Negative correlation (au)	Ion structure
17.003	41	OH ⁻	13.008	-50	CH ⁻
22.991	26	Na ⁺	15.023	-97	CH ₃ ⁺
30.010	59	CH ₂ O ⁺	29.038	-36	C ₂ H ₅ ⁺
31.019	31	CH ₃ O ⁺	41.039	-20	C ₃ H ₅ ⁻
34.992	44	Cl ⁻	41.039	-28	C ₃ H ₅ ⁺
41.005	25	C ₂ HO ⁻	43.056	-27	C ₃ H ₇ ⁺
42.011	40	C ₂ H ₂ O ⁺	53.038	-36	C ₄ H ₅ ⁺
45.031	66	C ₂ H ₅ O ⁺	55.055	-41	C ₄ H ₇ ⁺
55.021	18	C ₃ H ₃ O ⁻	71.081	-23	C ₅ H ₁₁ ⁺
57.033	29	C ₃ H ₅ O ⁺	73.053	-19	SiC ₃ H ₉ ⁺
69.033	91	C ₄ H ₅ O ⁺	77.032	-20	C ₆ H ₅ ⁺
83.046	21	C ₅ H ₇ O ⁺	147.071	-18	Si ₂ C ₅ H ₁₅ O ⁺

Table 3. Ion assignment for the ions with the largest regression coefficients for γ^p PLS model.

m/z	Positive correlation (au)	Ion structure	m/z	Negative correlation (au)	Ion Structure
15.996	21	O ⁻	12.000	-22	C ⁻
17.003	33	OH ⁻	13.008	-82	CH ⁻
22.991	34	Na ⁺	15.023	-22	CH ₃ ⁺
30.010	19	CH ₂ O ⁺	27.023	-17	C ₂ H ₃ ⁺
31.019	32	CH ₃ O ⁺	39.023	-38	C ₃ H ₃ ⁺
34.992	53	Cl ⁻	41.039	-31	C ₃ H ₅ ⁺
45.034	41	C ₂ H ₅ O ⁺	43.056	-8	C ₃ H ₇ ⁺
57.033	13	C ₃ H ₅ O ⁺	53.038	-14	C ₄ H ₅ ⁺
69.033	51	C ₄ H ₅ O ⁺	55.055	-10	C ₄ H ₇ ⁺
42.031	5	C ₂ H ₄ N ⁺	57.071	-18	C ₄ H ₉ ⁺
42.011	8	C ₂ H ₂ O ⁺	67.050	-14	C ₅ H ₇ ⁺
43.019	12	C ₂ H ₃ O ⁺	147.071	-15	Si ₂ C ₅ H ₁₅ O ⁺

Table 4. Structural assignments for the ions with the largest regression coefficients for γ PLS model.

5.4 Discussion

The automated acquisition and processing of all contact angle data and surface energy calculations were completed within three days. Since this is well within the timeframe required for biological evaluation of such a polymer microarray (2-10 days), this is considered to illustrate the *high-throughput* nature of the method for this application.[34] The large range of WCA (31 to 104°) confirms the strategy of monomer selection - generating copolymer surfaces which ranged from hydrophilic to hydrophobic (Figure 33a). Rawsterne *et al* reported a relationship between the calculated $\log P$ of amino acid-modified surfaces and their resulting water contact angle.[111] $\log P$ is the partition coefficient of a molecule between water and octanol, and therefore gives an indication of its relative hydrophilicity. If there was such a relationship between monomer $\log P$ and the WCA of the resulting polymer, this would be a useful method of predicting the WCA of a polymer without the need to synthesise it. To investigate if polymer surface energy can be predicted from the $\log P$ value of its constituent monomer, the $\log P$ of each major monomer (1 to 16) were calculated.

Many methods exist for calculating the $\log P$ of a molecule, however the most widely used method is that developed by Leo *et al.*[112] The $\log P$ values for each major monomer were then compared to the WCA of the 16 polymers containing 100 % of each monomer to see if a similar relationship was observed (Figure 38). No clear relationship between $\log P$ and WCA is seen for this group of 16 polymers, where for the majority of the polymers there is a significant change in $\log P$ values without a corresponding large variation in WCA. Indeed two polymers with the highest WCA ($\sim 90^\circ$) have significantly different $\log P$ values (Figure 38). This probably reflects the change in the chemistry of the monomers upon polymerisation.[113] In contrast the chemistry of the amino acids will not change as dramatically once chemically linked to a surface.

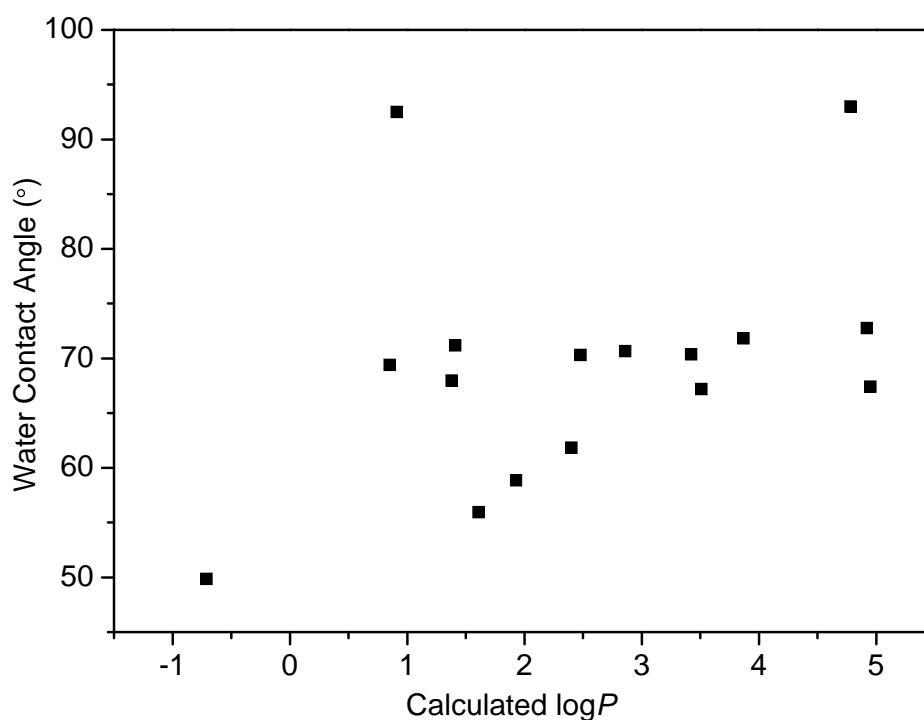


Figure 38. Calculated $\log P$ versus water contact angle for the 16 major monomer polymers.

Polar liquids (e.g. water) have low contact angles on materials with a high polar component because of increased affinity for the liquid with the surface due to increased hydrogen bonding between the liquid and the surface. Adhesive forces between the liquid molecules and the surface dominate over cohesive forces between the liquid molecules, hence a low contact angle.[100] Figure 33a

illustrates the large range of γ^p values achieved, ranging from 0 to 24 mJ/m², demonstrating a significant ability to tune the polar component of a polymer surface by choice of monomeric constituents. In contrast the γ^d of the polymers is relatively invariant with WCA, with 90% of the polymers having a γ^d between 44 and 49 mJ/m² (Figure 33b). The magnitude of γ^d is strongly related to the average atomic mass of the atoms at a surface, because London van der Waals forces increase in strength with increasing atomic size.[89] Therefore, considering that the majority of the monomers used in this study have backbones containing only carbon and oxygen it is unsurprising that there is so little variation in γ^d between the different polymers.

The diiodomethane contact angle (DiCA) of the polymers varied from ~ 13 to 47°, with no relationship evident between DiCA and γ^p for the polymers considered (Figure 33c). The attractive force between the diiodomethane and the surface only arises due to London van der Waals forces. The polarity of the surface (and consequently the potential for hydrogen bonding) will therefore not govern the DiCA of a surface.[100] Conversely, with increasing γ^d the DiCA of the polymers decreases due to the increasing adhesive force between the diiodomethane and the co-polymer surfaces. This increase in dispersion force is due to the increasing strength of London van der Waals forces between the liquid and the surface as the surface becomes more hydrophobic.

Liquid contact angles can be influenced by surface roughness,[80] therefore the polymer spots were imaged using optical and atomic force microscopy (AFM) to investigate their macro and nanoscale topography. Viewed through an optical microscope (20x magnification) the polymer spots were relatively uniform in size and smooth in appearance, with an average thickness of approximately 50 μm . There was no indication of dewetting of the monomer solutions which could have caused incomplete coverage of the substrate on polymerisation. AFM analysis of a sample group of 24 polymer spots described in chapter 7 suggests that the nanoscale roughness of the polymers was low and uniform ($r_a \sim 2\text{-}5\text{ nm}$).[61] Polymer solubility is unlikely to be an issue, due to the timescale of the contact angle measurements, i.e. the contact angle is measured

from an image taken less than one hundredth of a second after the droplet contacts the surface.

Simplistic comparisons can be made between the surface energies of the polymers and their bulk chemistries. Indeed a review of the contact angle data from the copolymer array reveals that monomer structure has a major influence on surface energies as would be expected. To illustrate this point, three major monomer groups (7, 10 & 13) have been selected in Figure 33a to highlight the effect of monomer chemistry on WCA and γ^p of the resultant copolymer surface. Major monomer 7 is a monoacrylate with a pendent chain containing phenyl and hydroxyl functionalities. Major monomer 10 is another monoacrylate, but in this case its pendent chain only terminates with a hydroxyl functionality. Finally, major monomer 13 is a triacrylate containing a hydroxyl functional group. All three monomers have a polar hydroxyl functional group within their structure, yet the polymers containing the three major monomers differ greatly in WCA ($\sim 35 - 105^\circ$). Polymers containing monomer 10 as their major constituent are grouped towards the hydrophilic end of the scale, whereas those containing major monomer 13 tend towards the hydrophobic (Figure 33a). The large difference in the wettability of these polymers can be related to their chemical structure and specifically their potential for crosslinking. Monomer 10 shows the most hydrophilic WCA range which may be consistent with preferential orientation of the polar hydroxyl end groups towards the polymer surface. This phenomenon has been observed previously for a monoacrylate monomer with hydroxyl end groups.[83] The monoacrylate monomer 7 has a side chain with both hydroxyl and phenyl functional groups and interestingly sits in a WCA range between monomer 10 and polystyrene ($\sim 90^\circ$),[98] which would indicate an energetic compromise between surface hydroxyl and phenyl groups. Finally monomer 13 shows the most hydrophobic range in WCA which would indicate that the triacrylate nature of the monomer increases the degree of copolymer cross-linking and thus the hydroxyl group is not presented at the surface due to steric hindrance. This exercise suggests that variations in the amount of cross-linking within a polymer may have a considerable effect on polymer surface energy.

To understand the influence of surface chemistry on polymer surface energy, the arrayed polymers were analysed by XPS and ToF-SIMS. A number of previous studies have attempted to use XPS to study the relationship between surface composition and surface energy, although with much smaller datasets. Liu *et al* observed a linear relationship between the surface O:C ratio of wood samples and their γ^d , i.e. as O:C ratio increased so did γ^d , however this was only the case for six samples with a limited spread of γ^d values.[114] A similar observation was made for a group of 8 oxygen plasma treated polycarbonate wafers by Baytekin *et al*. [68] In another study Araujo *et al* reported a strong relationship between the WCA of various silane treated glass slides and the surface atomic C %.[115] Priest *et al* used ToF-SIMS to make rather facile comparisons between WCA measurements on SAM modified surfaces and the intensity of secondary ion peaks specific to these surfaces.[116] The authors reported linear relationships between PO_x^- fragments (from the phosphonic acid terminus of the SAM) and the advancing and receding WCA. A more advanced study used PCA to analyse the ToF-SIMS spectra of a group of plasma treated samples and then related the principle component score values of these samples to their WCA (i.e. a simple form of principal component regression).[68] The principle component loadings were used to identify secondary ions which were characteristic of high and low WCA. There is however two major differences between these studies and that described in this chapter: the number and chemical diversity of samples analysed.

No definitive trends were observed between the XPS and surface energy data which may be due to the differences in surface sensitivity of the two approaches. Contact angle measurement is sensitive to the top nanometre of a surface,[79] whereas the sampling depth of XPS is ~ 10 nm.[51] However, some interesting qualitative observations were noted. As surface C-O % of the polymers increased, the γ^p appears to also increase, however with considerable spread in the data. No relationship was noted between surface C=O % and polymer γ^p (Figure 36a & c) Logic suggests that as γ^p is dependent upon hydrogen bonds being formed between a test liquid and the polymer surface, therefore the quantity of polar functionalities at the surface such as C-O and C=O would influence measured γ^p . A survey of the monomer structures used to create the polymers

(Figure 20) suggests that the C-O measured will be predominantly from ester and ether groups, whereas the C=O measured will only be from carbonyl groups in the monomer acrylate functionality. Both these functionalities are capable of forming hydrogen bonds, however there are significant differences in number and flexibility. Ester and ether groups are far more numerous in the monomer structures than the carbonyl groups, therefore are likely to be responsible for the majority of hydrogen bonding. Also, the oxygen atom in ester functionalities will have greater flexibility to orientate towards the polymer surface, rather than the oxygen atom in the carbonyl functionality. This is because the double bond in the carbonyl groups will make the geometry of that part of the molecule more rigid. It is interesting that the one group of polymers where surface C-O % did not increase at all with increasing γ^p were those containing major monomer 10. This monomer contains a hydroxyl end group, therefore it might be expected that the more of these groups that orientate towards the surface, the more polar the surface. This may be a good example of the problems of the greater analysis depth of XPS (1-10 nm), i.e. all hydroxyl groups from this monomer within this 10 nm range will be detected by the XPS, however only those orientated towards the surface (top nanometre) will influence γ^p .

The presence of Nitrogen at the polymer surfaces was observed to increase γ^p . The only Nitrogen containing monomer is minor monomer E which contains a dimethyl amine end group (Figure 20). Tertiary amine groups such as this have a positive charge in water,[117, 118] therefore polymers with this functionality at their surface would be expected to have a high γ^p . The presence of Fluorine at the polymer surfaces was observed to decrease γ^p . The only monomer which contains Fluorine was minor monomer D. This monomer contains six fluorine atoms which have a very weak hydrogen bonding ability when covalently bonded to carbon, hence a decreased γ^p when it is added as a minor constituent.[105, 119]

In summary XPS analysis has been of limited use in explaining the influence of polymer surface chemistry on surface energy values, therefore multivariate statistics in the form of PLS was applied to ToF-SIMS data from the array to see if this technique allowed any greater insight. The ToF-SIMS spectra from polymeric materials are very complex, generally containing hundreds of

secondary ion peaks in both the positive and negative spectra.[48] Multivariate statistical methods have therefore been applied as a means of extracting information from these complex spectra, as demonstrated in chapter 5. Hence we have used PLS to study the influence of polymer surface chemistry on surface energy.

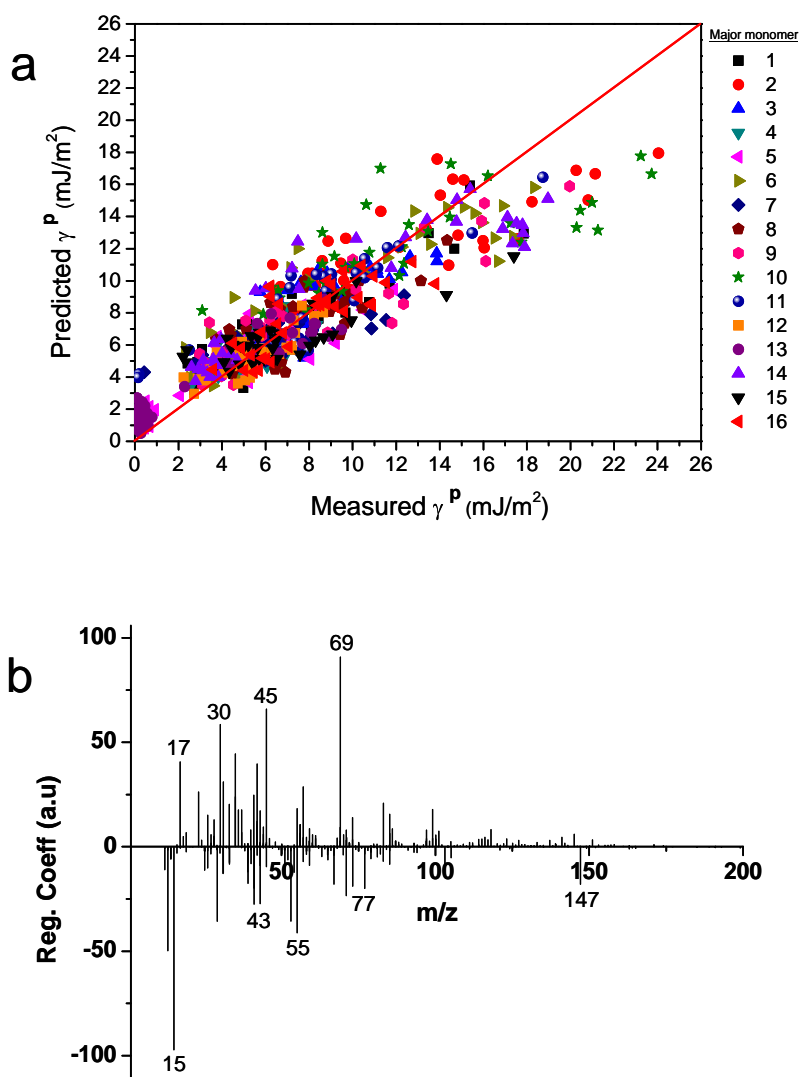


Figure 39. PLS model for γ^p (4 latent variables). a) Measured versus predicted γ^p (Linear fit shown, $R^2 = 0.82$) b) Regression vector plotted as regression coefficient versus peak m/z for the concatenated data set.

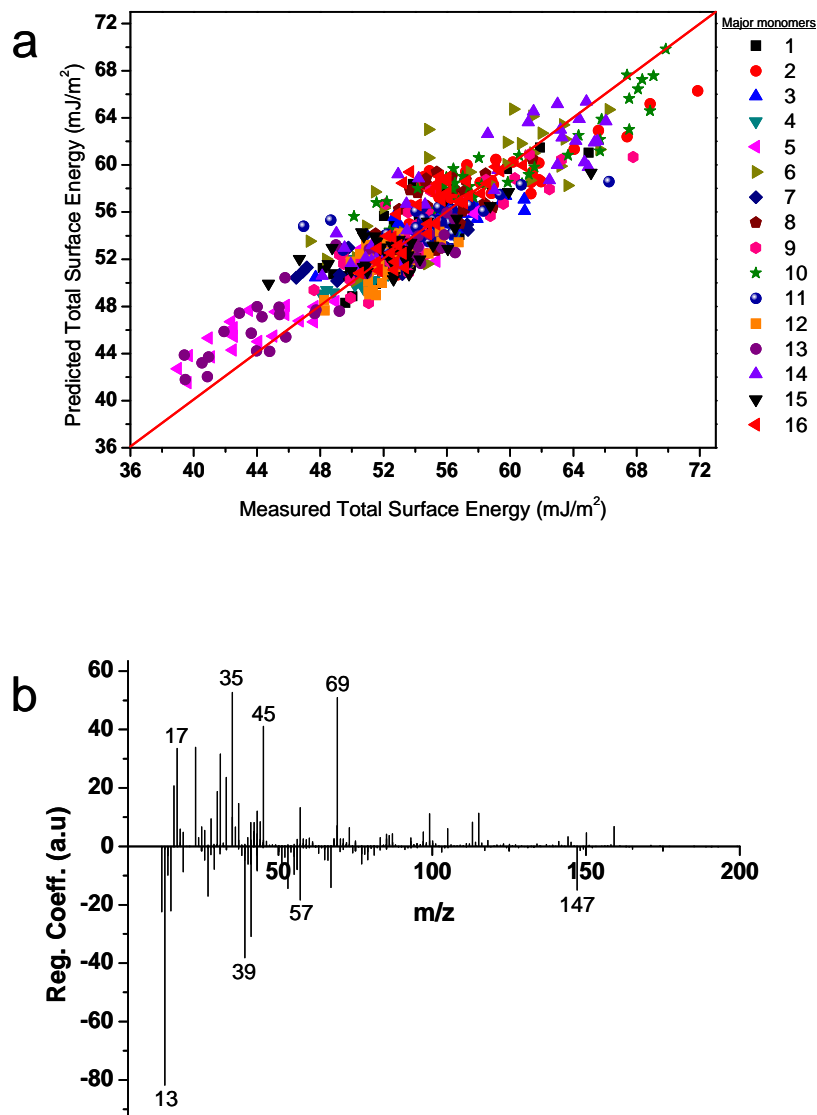


Figure 40. PLS model for γ (5 latent variables). a) Measured versus predicted γ (Linear fit shown, $R^2 = 0.87$) b) Regression vector plotted as regression coefficient versus peak m/z for the concatenated data set.

When PLS models were obtained to describe the relationship between the ToF-SIMS data and γ^d , the RMSPE was high (> 15). This may be a result of the relative lack of variation in γ^d in this group of polymers, hence there can be very little covariance between the ToF-SIMS and γ^d data matrices. It is also probable

that information about the molecular structure of the surface obtained using ToF-SIMS is of little use in explaining differences in surface van der Waals forces, which are the origin of dispersive surface forces. In contrast PLS models with a good predictive ability ($\text{RMSPE} < 3$) were obtained to describe the relationship between ToF-SIMS and γ^p and γ data, suggesting that the molecular structure of polymer surfaces does strongly influence γ^p and γ . Table 3 shows the structures of the ions with the highest positive and negative regression coefficients for the γ^p PLS model. Ions positively correlating with γ^p are predominantly oxygen containing species. These include ions which are associated with ethylene glycol functionalities such $\text{C}_2\text{H}_5\text{O}^+$ and acrylate functionalities such as $\text{C}_4\text{H}_5\text{O}^+$. Oxygen containing species are able to form hydrogen bonds, therefore it is intuitive that surfaces that contain these species would have a higher γ^p . Secondary ions from surface contaminants also had positive regression coefficients, such as Na^+ and Cl^- . Ions negatively correlating with γ^p are predominantly non-oxygenated hydrocarbons, for example CH_3^+ . These functionalities do not contain the lone pairs of electrons necessary for hydrogen bonding, resulting in a low polar surface energy. Ions which are associated with poly(dimethylsiloxane) (PDMS) such as SiC_3H_9^+ also negatively correlate with γ^p . PDMS has a low γ^p because the oxygen in the polymer backbone does not form hydrogen bonds due to steric hindrance.

The information obtained from the γ^p PLS model can be directly related to the ToF-SIMS spectra of the polymers on the microarray. To illustrate this fact the positive ToF-SIMS spectra of two polymers are shown in Figure 41: the polymer synthesised from 100 % monomer 10 which has a very high γ^p ($\sim 21 \text{ mJ/m}^2$) and the polymer synthesised from 100% monomer 13 which has a very low γ^p ($\sim 0 \text{ mJ/m}^2$). The positive spectrum of the polymer synthesised from 100 % monomer 13 is dominated by hydrocarbon ions, with C_2H_3^+ and C_4H_7^+ being the two most intense ion peaks (Figure 41b). Two ions characteristic of PDMS contamination are also present. Indeed the only prominent ion that does not fit the pattern predicted by the PLS model is $\text{C}_3\text{H}_6\text{O}^+$. The positive spectrum of the polymer synthesised from 100 % monomer 10 is considerably different (Figure 41a). Although the two most prominent ions are again hydrocarbons (C_2H_3^+ and C_3H_5^+), the spectrum is dominated by oxygenated hydrocarbon species such as $\text{C}_2\text{H}_5\text{O}^+$ and CHO^+ . Na^+ is visible in the spectrum which had one of the greatest positive

regression coefficients in the γ^p PLS model. Again, low level PDMS contamination is visible in the form the $\text{Si}_2\text{C}_5\text{H}_{15}\text{O}^+$ ion.

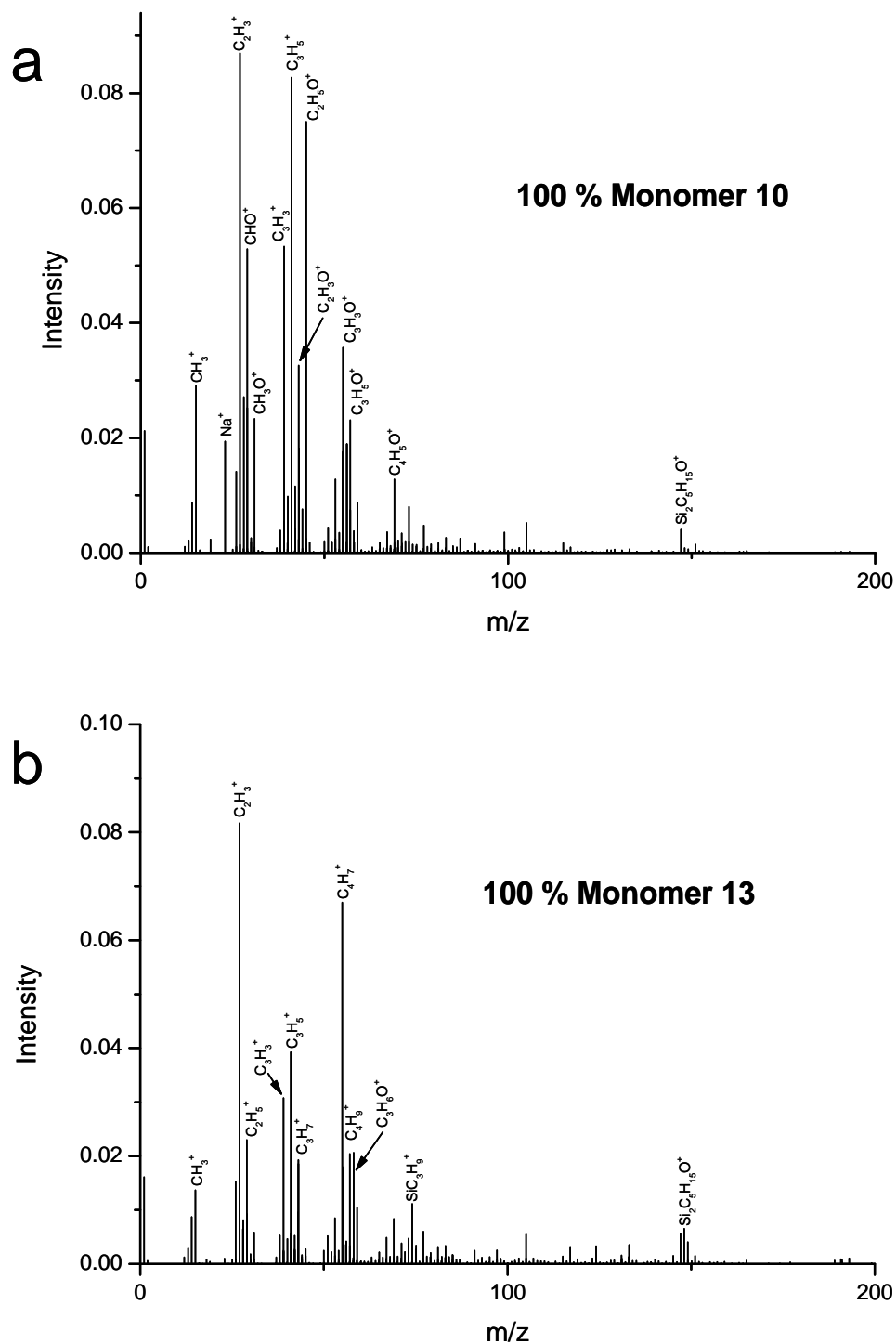


Figure 41. ToF-SIMS positive ion spectra of a) polymer containing 100 % monomer 10 and b) polymer containing 100 % monomer 13.

The XPS results indicated that polymers containing Nitrogen at their surfaces had the highest average γ^p . However, although Nitrogen containing secondary ions (e.g. $C_2H_4N^+$) do have positive regression coefficients, they are not amongst the highest for the γ^p PLS model. Likewise polymers with Fluorine at their surfaces had the lowest average γ^p , yet Fluorine containing secondary ions (e.g. CF^+) do not count amongst the ions with the most negative regression coefficients. It is possible that these observations are due to the fact that these ions are common to only a small number of polymers in the library, therefore the model gives these ions a lower weighting in the regression vector relative to more common ions. It is apparent that the ions which positively and negatively correlate with both γ^p and γ are similar (Table 3 and

Table 4). Again, oxygen containing ions positively correlate with γ and non-oxygenated hydrocarbon ions negatively correlate. In this chapter γ has been calculated by addition of γ^p and γ^d . It has been noted below that the majority of variance in polymer γ has been in γ^p , whereas γ^d is relatively invariant between polymers. Therefore it is not surprising that the PLS model attributes the variance in γ to ions which account for the greatest amount of variance, i.e. those which influence polymer γ^p .

5.5 Conclusions

In summary, the results presented here demonstrate that the acquisition of WCA and surface energy values for a large group of copolymers in a microarray format is possible within a relatively short period of time, using picolitre contact angle measurement. It has been shown that surface atomic and functional group information from XPS has limited value in explaining the differences in surface energy within the copolymer library studied. However, molecular information from ToF-SIMS analysis has been proven to provide an insight into the way the molecular structure of a polymer surface influences surface energy.

The surface properties of materials are important for many applications, including the important field of biomaterials science. This chapter has demonstrated that micro-arrayed copolymer libraries are an excellent platform to

study surface structure-property relationships in copolymer systems, suggesting the feasibility of designing new materials with tuneable surface energies. Information gained from investigating such a large group of materials could be used as a basis to design materials with optimised surface properties. The techniques described in this chapter could readily be applied to the study of the interactions of cells and biomolecules with polymers printed in a microarray format. It would be hoped that this may provide a valuable insight into how the molecular structure of a polymer (and indeed any material) surface influences the important processes of cell adhesion and protein adsorption. This would be a major step-forward towards the goal of the rational design of new biomaterials.

Chapter 6

Partial Least Squares Regression as a Tool for Investigating Large Combinatorial Polymer Libraries

6.1 Introduction

In the field of combinatorial polymer research there has sometimes been a lack of emphasis on the characterisation of surface properties, probably due to the practical difficulties of analysing large numbers of separate samples. Analysis of the surface properties of combinatorial polymers is important because it is the surface of a material that determines many of its properties. With the advent of polymer microarrays, where the entire library is on one flat support, some of these practical issues are reduced, particularly when combined with automated acquisition. In Chapter 3 a *high throughput* methodology for the surface analysis of a copolymer microarray on one glass slide by the surface analytical techniques of Time-of-Flight Secondary Ion Mass Spectrometry (ToF SIMS), X-ray Photoelectron Spectroscopy (XPS) and water contact angle measurement is described.[83] In Chapter 7 methods for assessing the polymers' protein adsorption properties are also described.[61] Once these data have been collected the challenge is to develop the existing statistical data handling approaches to relate this large amount of surface analytical information to other properties such as wettability, cell adhesion assays and protein adsorption.

High throughput polymer development may take the form of simple identification of 'hit' polymers which have a property of interest (e.g. high cell attachment). Alternatively, they may aim for the development of quantitative structure-property relationships which aim to improve our understanding of the key causal factors underlying the properties of 'hit', 'miss' and intermediate performance polymers. In this case, the surface chemical data (ToF SIMS and/or XPS) is termed the independent variable and the data describing the surface property to be predicted is termed the dependent variable. If the independent variable is composed of multiple observations such as spectral data from ToF-SIMS (i.e. it is multivariate in nature), it is necessary to use multivariate regression techniques to identify correlations. These include Multiple Linear Regression (MLR), Principal Component Regression (PCR) and Partial Least Squares (PLS) regression.[120]

PLS has been used previously in the field of biomaterials to study the relationship between surface chemistry and endothelial cell adhesion on plasma polymer deposits,[121] and to investigate the relationship between surface chemistry and protein adsorption.[122-124] PLS is a multivariate statistical method allowing models to be built that relate a set of multivariate data to a set of univariate data.[125] Multivariate techniques such as PLS use factors to describe the variance in the dataset, thereby reducing the dimensionality of the data. PLS specifically finds factors (called latent variables) that describe variance in both the independent and dependent variables. i.e. to maximise the covariance described by the model. Covariance is a measure of how closely the independent and dependent variables follow the same trends. The data used to build the PLS model is termed the training set. The predictive ability of a PLS model can be assessed using a test set of samples which have not been included in the training set; this is called validation. An alternative method is cross-validation which does not require a test set, only the original data in the training set. The most common form of cross-validation is the Leave One Out (LOO) method which involves leaving one sample out of the training set at a time, then repeating the PLS model. The error in the predictions of the samples left out can then be determined. LOO cross-validation is commonly used to determine the optimum number of factors used to build a PLS model, i.e. the number which gives a model that adequately describes the variance within the training set data, without including any variance due to noise in the data. Using too many latent variables inevitably leads to a model which over fits the data.

In ToF-SIMS data analysis, a PLS model assigns each ion with a regression coefficient which quantifies the influence it is having on the model. If an ion has a positive regression coefficient it is positively correlated with the univariate variable and the opposite is true for ions with a negative regression coefficient. Ions with a regression coefficient close to zero do not significantly influence the model. These regression coefficients can be used to build an understanding of the relationship between the two datasets. It is important to emphasise that although PLS can help predict a response, it does not actually explain any underlying relationships between variables. The theory of PLS is described in greater detail elsewhere.[126, 127]

In this Chapter various aspects relating to PLS modelling of data from large datasets are investigated, such as how the conclusions reached from this type of PLS model are affected by the number of different samples in the polymer library and importantly the chemistry of the monomers making up the polymers included in the training set. Also investigated is whether the information gained has any predictive application outside the group of copolymers used to build the model. This is done using test copolymers synthesised from the same monomers as the training set and other polymers that are chemically different.

6.2 Methodology

6.2.1 Polymer Microarray Synthesis

The microarray under investigation comprised of 496 novel acrylate based polymers synthesised from 16 major monomers which were mixed pairwise with 6 minor monomers in the following ratios - 100:0, 90:10, 85:15, 80:20, 75:25 and 70:30 (Figure 20). A radical initiator was added to the monomer mixtures which were then spotted onto a pHEMA coated glass slide. They were then polymerised with ultraviolet light. Full details of array manufacture can be found elsewhere.[34] Each polymer is synthesised from two monomers, therefore to avoid confusion in this paper we will refer to the monomer comprising the majority (90, 85, 80, 75 & 70%) of a polymer as the “major monomer” and the monomer comprising the other 30, 25, 20, 15 or 10 % as the “minor monomer”. The microarray was printed in triplicate on the slide, therefore the water contact angle, diiodomethane contact angle and ToF-SIMS measurements were each conducted on one of the three microarrays.

6.2.2 Preparation of Polymer Films

Solutions (1% w/v) of polystyrene (Mw 100,000), poly(L-lactic acid) (Mw 95,000), poly(methyl methacrylate) (Mw 60,000), poly(dimethylsiloxane) (Mw 1,000) and poly(2-hydroxyethyl methacrylate) (Mw 20,000) were prepared in chloroform. All polymers were purchased from Sigma Aldrich. Silicon wafers were cleaned using UV light, then sonicated in methanol. The polymer solutions were spin coated onto the clean silicon wafers at 3000 rpm. The polymer films were left for 24 hours before contact angle measurements. The surface of a piece of poly(tetrafluoroethylene) (Krüss) was scraped clean before contact angle measurement.

6.2.3 Time-of-Flight Secondary Ion Mass Spectrometry

An ION-TOF ToF-SIMS IV instrument was operated using a monoisotopic $^{69}\text{Ga}^+$ primary ion source operated at 25 kV and in “bunched mode”. A 1 pA primary ion beam was rastered over a 100 x 100 μm area of each polymer spot on the microarray. A 60 second acquisition time was allowed for each polymer sample, ensuring that static conditions were maintained for every spectra acquired. Ion masses were determined using a Time-of-Flight analyser allowing accurate mass assignment (to typically 40 ppm). The typical mass resolution (at m/z 41) was just over 6000. ToF-SIMS analysis of the microarray was fully automated via the design of a macro using ION-TOF ToF-Bat software, allowing completely unattended operation. ToF-SIMS analysis of polymer microarrays has been described in greater detail in Chapter 3. One positive and one negative spectrum were obtained for each polymer on the microarray. The reproducibility of these measurements has been determined previously using principal component analysis and found to be very good.[76]

6.2.4 Partial Least Squares Regression

The positive and negative ion spectra for all 496 polymers were automatically mass calibrated using ION-TOF ToF-Bat software.[73] Mean deviations of < 40 ppm from true mass for m/z 0-100 were noted after automatic calibration. One peak list each was then created for both positive (344 peaks) and negative (92 peaks) ion spectra using mass spectra taken from a group of polymers from the array containing monomers with widely varying chemistries. This group included polymers synthesised using all of the monomers in Figure 20. This peak list was then applied to all 496 polymers. The peaks were then integrated using ION-SPEC software and peak intensities exported to Origin Pro 7.5. The positive and negative ion intensities for each polymer were normalised to the total ion count separately, to account for normal variation in secondary ion yield between polymers. The positive and negative ion data for all 496 polymers was then arranged into one concatenated data matrix. PLS analysis was carried out using Eigenvector PLS_Toolbox 3.5 for Matlab. The ToF-SIMS and surface energy data were mean-centered before analysis. The Root Mean Square Error of Prediction (RMSPE) was calculated to quantify how well each model predicted the training set or test set polymers:[128]

$$\text{RMSPE} = \left[\frac{\sum (y_p - y_m)^2}{n} \right]^{1/2} \quad (8)$$

where y_p is the predicted value, y_m is the measured value and n is the total number of samples in the training set.

The SIMPLS algorithm was used for the PLS analysis rather than the other commonly used algorithm NIPALS.[109] The two algorithms have been shown to give equivalent results when analysing a dataset where the independent variable is multivariate and the dependent variable is univariate.[110]

6.2.4 Surface Energy Measurements

Contact angles were determined for each polymer on the array using two liquids: Ultra pure water (18.2 MO resistivity at 25°C) and diiodomethane (= 99 % pure) (Aldrich). A DSA100 (Krüss) with a piezo-doser head was used to dispense a 100pL droplet of each liquid onto the centre of each polymer spot on the array. Data acquisition was automated with the spot side profile of the back lit spot being recorded. A dual camera system was used, one to record a profile of the spot and the other to record a bird's eye view of the spot to ensure that the water droplet was deposited at the centre of each polymer. Data analysis involved following standard contact angle measurement procedures except that due to the small droplet size circle fitting was used instead of Young-Laplace.[98] Polar and disperse surface energy values were calculated using the Owens and Wendt's model as described elsewhere.[105, 106] Total surface energy was calculated by the addition of the polar and disperse values. Macros were written to enable rapid γ calculations for the large dataset. Although more than two probe liquids may be used when using the Owen-Wendt method, the use of only two liquids is common in the literature and it has been demonstrated that providing a polar and non-polar pair of liquids is used accurate surface energy measurements can be obtained.[106]

6.3 Results and Discussion

The use of PLS as a tool in surface analysis is well established, however the number of samples analysed using this method have been relatively small, with closely related chemistries through the range of samples.[121-124] The application of PLS to large polymer libraries containing hundreds of samples of very different chemistries is a new development and the limits of this approach have not yet been systematically investigated. Thus, a dataset acquired from a 496 member copolymer library printed in microarray format, comprising ToF-SIMS spectra and surface energy values was used. The positive and negative ToF-SIMS spectra were obtained in an automated fashion using a methodology described in Chapter 3 over an acquisition period of approximately 6 hours.[83] The surface

energy values were calculated from water and diiodomethane contact angles measured from picolitre volume droplets over an acquisition period of approximately 24 hours. The polar and dispersive components of the surface energy were calculated using the Owen and Wendt's model, although only the total value is used in this study. A PLS model was built using these two datasets with ToF-SIMS ions intensities as the multivariate parameter and total surface energy as the univariate parameter.

PLS models were constructed using either no pre-processing, with mean centring or with auto-scaling of the ToF-SIMS and surface energy data. The models constructed using data which was auto-scaled or underwent no pre-processing had a very low predictive ability for samples within the training set ($\text{RMSPE} > 20$), therefore mean centering was chosen. The model was cross-validated using the "leave one out" method, which indicated that the root mean square error of cross validation reached a minimum at 5 latent variables. When the experimental values of γ are plotted against those predicted by the PLS model (Figure 42a), a linear relationship with a relatively low RMSPE is observed, suggesting a good predictive ability for the copolymers within the training set ($\text{RMSPE} = 2.3$). Figure 42b shows the regression co-efficients for the PLS model. It can be seen that the ions with the greatest positive regression co-efficients have m/z of 34.992 (Cl^-), 69.034 ($\text{C}_4\text{H}_5\text{O}^+$), 45.034 ($\text{C}_2\text{H}_5\text{O}^+$), 22.991 (Na^+), 17.003 (OH^-) and 15.996 (O^-). The ions with the largest negative regression coefficients have m/z of 13.008 (CH^-), 39.023 (C_3H_3^+), 41.039 (C_3H_5^+), 12.000 (C^-), 15.023 (CH_3^+) and 57.071 (C_4H_9^+). The ions positively correlating with γ are predominantly oxygenated hydrocarbons (Table 4). Ions negatively correlating with γ are all hydrocarbons with the exception of C^- and $\text{Si}_2\text{C}_5\text{H}_{15}\text{O}^+$ (Table 4). These results agree with theory concerning the molecular basis of polymer surface energy (see Chapter 6).[42] The disperse surface energy of the copolymers in the library is relatively invariant (between ~ 40 and 50 mJ/m^2), therefore it is changes in the polar component that is responsible for most of the differences in total surface energy.[129] Oxygenated groups at a polymer surface can form hydrogen bonds, increasing the polar contribution to total surface energy. Attractive forces at surfaces that are predominantly composed of hydrocarbon containing moieties

will mainly be due to dispersive London-van der Waals forces, hence the polar contribution will be very small.

Two aspects relating to PLS modelling of such a large and varied library of copolymers are investigated. The first issue that will be investigated is whether the number of the samples in the library influences the ions identified to control the surface energy through assignment of large positive or negative regression coefficients. Secondly, the limits of the PLS model in predicting the surface energies of polymers outside of the training set will be studied.

6.3.1 The influence of sample number on ions identified in regression vector

To investigate the effect of sample number on the key ions identified in the regression vector, the PLS model of the 496 copolymer dataset above was split in half to produce two new data sets, each one containing 8 major monomer groups (major monomers 1-8 or 9-16, i.e. 248 copolymers each). Each copolymer in the library under investigation contains one of 16 monomers as its major constituent (major monomer) and one of 6 monomers as a minor constituent (minor monomer). New PLS models were then constructed for each of these two datasets. The number of latent variables used for each new model was again decided by the LOO cross validation method. When the surface energy values predicted by each of these two new models were plotted against the measured values, the RMSPE were higher (average = 3.0) than the original model (Table 5), indicating a lower predictive ability for polymers within the two smaller training sets (Figure 42c & e). Analysis of the regression vectors of these two new models showed that the dominant ions contained in both were the same and were also identical to the original 496 copolymer model (Figure 42d & f). The ions positively correlating with surface energy were still predominantly oxygenated hydrocarbons and those negatively correlating were still hydrocarbons. However, it was noted that there were differences in the relative and absolute magnitude of the regression coefficients of these ions.

The 496 copolymer dataset was then split into quarters: major monomers 1-4, 5-8, 9-12 and 13-16, each containing 124 copolymers. Each of these groups was then used to build a new PLS model. The RMSPE of the new models (mean = 5.2) are higher than that of the model describing all 496 copolymers (Table 5). Analysis of the regression vector of these models identified the same ions as the full and half datasets; however there are some subtle differences in the regression vector for major monomers 1-4 (Figure 42h). For example, the ion at m/z 55.055 corresponding to $C_4H_7^+$ has a positive regression coefficient and the ion at m/z 43.019 corresponding to $C_2H_3O^+$ has a negative regression coefficient: the inverse of which is observed in the full and half models.

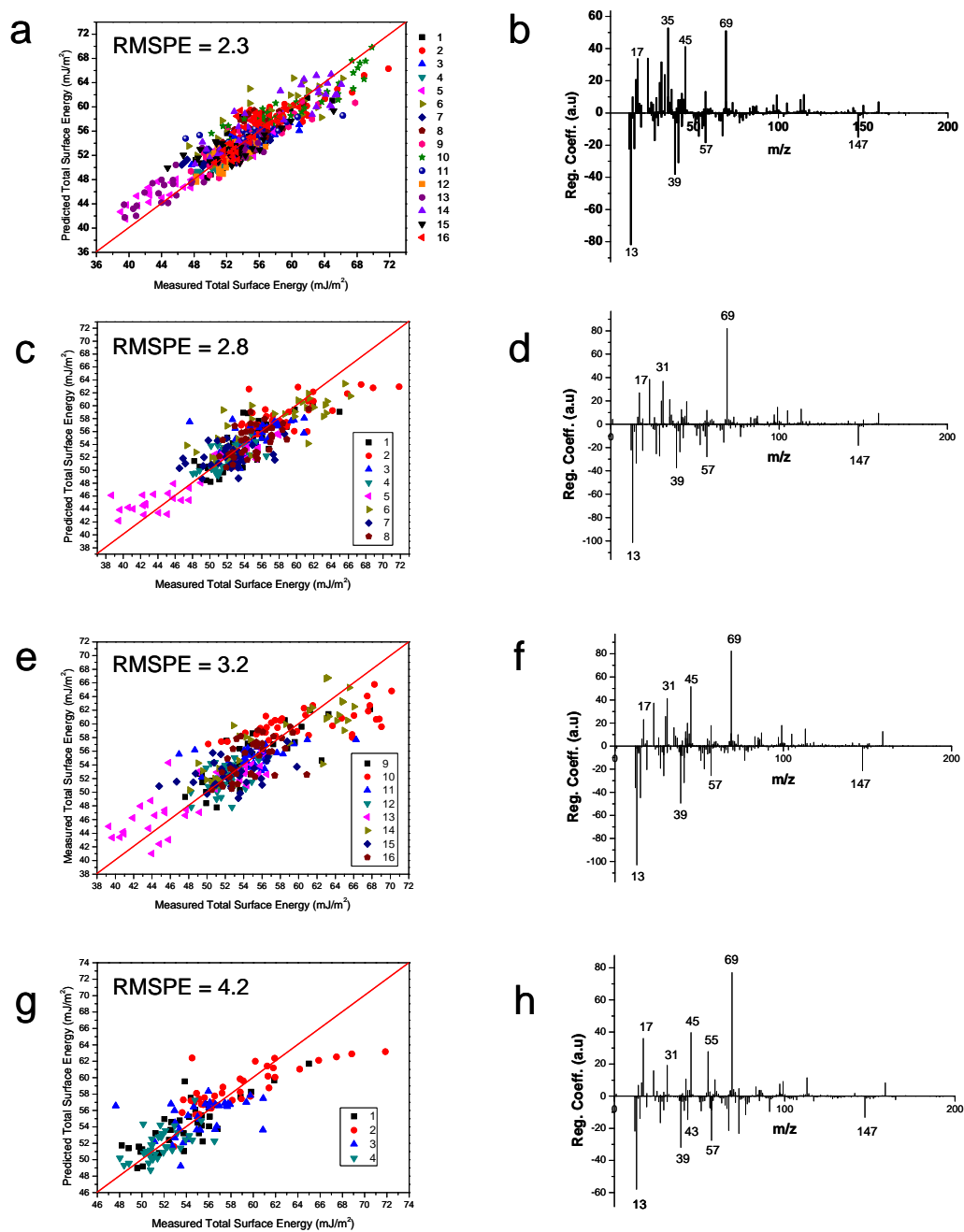


Figure 42. PLS models constructed using a) & b) 496 polymers, c) & d) 248 polymers (Major monomers 1 to 8), e) & f) 248 polymers (Major monomers 9 to 16) and g) & h) 124 polymers (Major monomers 1 to 4). Measured versus Predicted surface energy and Regression coefficient versus m/z is shown for each PLS model. $X = Y$ lines are provided to guide the eye.

There also appears to be a systematic underestimate of predicted surface energies for polymers containing monomer 2 in this model (Figure 42g). This result could suggest that reducing sample number might lead to anomalies in the regression coefficients obtained, due to the more limited range of chemistries in the training set. Therefore, to test this observation the 31 polymers containing major monomer 1 were used to construct a PLS model. The RMSPE value of this model (1.2) is lower than that of the original model (Figure 43a). The regression coefficients of this model are very similar to the model of all 496 copolymers, without the anomalies seen in the model for major monomer 1-4 (Figure 43b). The main difference is the complete absence of the peak at m/z 69.033 corresponding to $C_4H_5O^+$. This is combined with the large increase in the positive regression coefficient of the peak at m/z 59.050 corresponding to $C_3H_7O^+$. These changes do not contradict the results of the original model and are probably due to the decrease in the variety of surface chemistries included in this model (i.e. only 7 out of 22 monomers). It is also possible that for this group of polymers the peak at m/z 59.050 correlates more strongly with surface energy than the peak at m/z 69.033.

Dataset	RMSPE	Number of Latent Variables
496 polymers (Full)	2.3	5
248 polymers (Major monomers 1 to 8)	2.8	4
248 polymers (Major monomers 9 to 16)	3.2	4
124 polymers (Major monomers 1 to 4)	4.2	5
124 polymers (Major monomer 5 to 8)	5.9	4
124 polymers (Major monomers 9 to 12)	5.0	5
124 polymers (Major monomers 13 to 16)	5.5	5
31 polymers (Major monomer 1)	1.2	5
336 (minus minor monomers E & F)	3.2	5

Table 5. Comparison of PLS models with different numbers of samples.

It is postulated that the change in RMSPE values seen above (i.e. a maximum error is observed for intermediate sample numbers in the training set) reflects a changing balance between two competing influences on the PLS models and the number of latent variables used. This balance is between the number of samples included and the chemical diversity of the polymers in the training sets. The model describing all 496 copolymers is very chemically diverse, but this is balanced by the large number of samples included in the training set. Conversely the model containing 31 polymers has a significantly lower sample number but also much less chemical diversity. Indeed, the high RMSPE value seen in this model is probably the result of using 5 latent variables to describe the variation of only 7 monomers within this group of polymers. The models containing 248 and 124 polymers contain significant diversity, however have much fewer samples in the training set; hence exhibit an increase in the RMSPE values. In summary changing sample number influences the auto-predictive capabilities of the PLS models due to the changing balance between the diversity of the training sets and the number of latent variables used to model them.

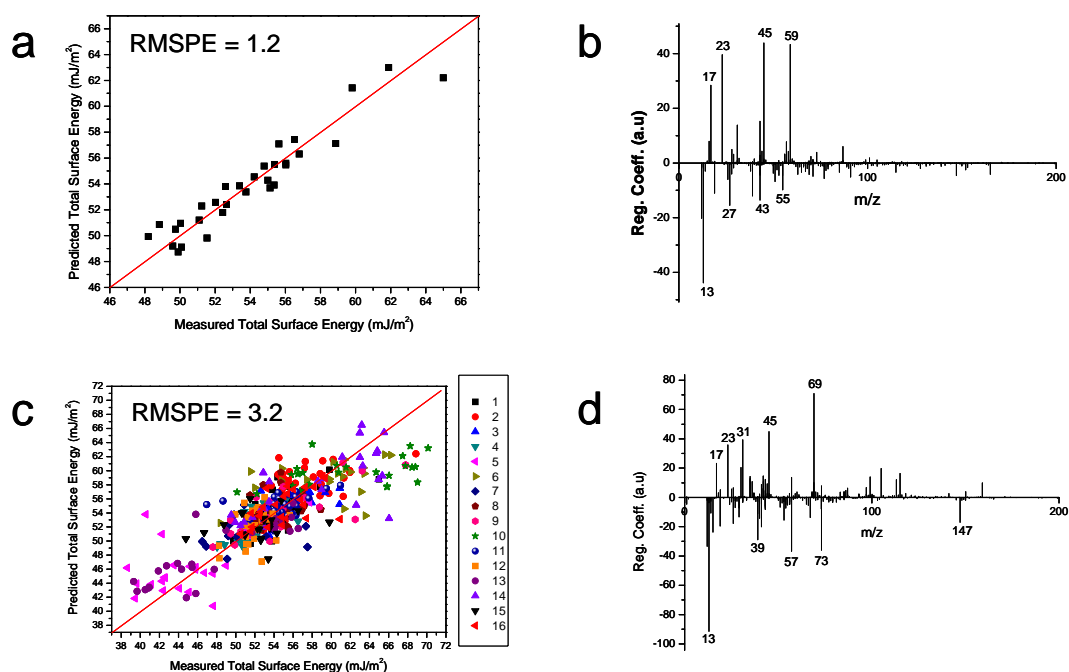


Figure 43. PLS models constructed using a) & b) 31 polymers (Major monomer 1), c) & d) 336 polymers (Minor monomers A to D). Measured versus Predicted surface energy and Regression coefficient versus m/z is shown for each PLS model. $X = Y$ lines are provided to guide the eye.

It can be concluded from this exercise that a reduction in sample number does appear to systematically affect the auto-predictive capabilities of the model, i.e. the ability to predict surface energy of polymers within the training set (as judged by the RMSPE value). However, analysis of the regression vectors of the reduced sample models indicate that the same general chemical conclusions can be drawn from regression coefficients of the different models, even though there is a change in the relative magnitude of the regression coefficients for each ion. Unsurprisingly the ions observed in the regression vector is dependent upon the chemistry of the polymers included in the training set.

6.3.2 Investigating the predictive ability of the PLS model outside of the training set

Analysis of the PLS models obtained has provided further understanding of which ions govern the surface energy of the acrylate copolymers, and therefore an indication of which surface structure are influential. The fact that the results from this analysis make chemical sense, e.g. hydrocarbon $C_nH_n^{+/-}$ ions correlate with low surface energy and polar oxygenated hydrocarbon $C_nH_nO_n^{+/-}$ ions correlate with high surface energy, gives confidence in the method. Plotting the measured surface energy values versus those predicted by the PLS model (and calculating RMSPE) has demonstrated the model has good quantitative predictive ability for those polymers within the training set (Figure 42a). However, the model has limited use in predicting surface energy if it is only applicable to polymers within the initial training set. To investigate the extent of the predictive ability of the above PLS model outside of the library of acrylate copolymers used in the training set, three test sets were used. The first set contained acrylate copolymers containing the same monomers as the training set, but in different proportions. The second group contained acrylate copolymers synthesised using minor monomers not included in the training set. The third test set comprised six commercially available linear polymers. Hence, predictions using test polymers with varying degrees of similarity to those in the training set were investigated.

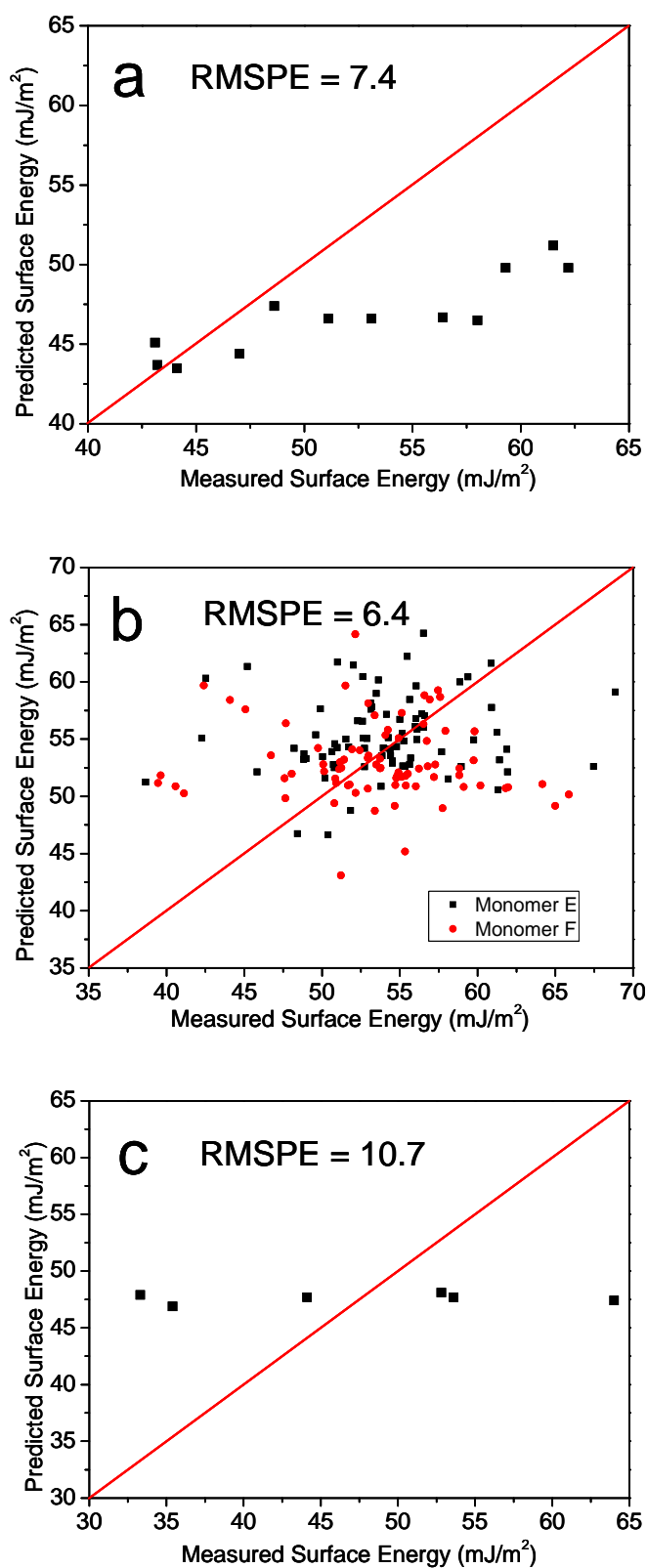


Figure 44. Measured versus predicted surface energy values for a) 12 acrylate copolymers synthesised from monomers common to training set b) 160 acrylate copolymers synthesised from monomers not used in training set c) 6 commercially available linear polymers, using data mean-centered using means from the training set. X = Y lines are provided to guide the eye.

6.3.2.1 Acrylate copolymers synthesised using monomers included in the training set

The PLS model of the full 496 copolymer dataset was used to predict the surface energies of 12 acrylate copolymers from a different library. The error in the predictions ranged from ~ 1 to 20 % compared to an error of approximately ± 10 % in predictions for polymers within the training set (Figure 42a). The error in the predictions for the 12 test polymers appears to be systematic, i.e. the predictions for the polymers with relatively low surface energies is low (< 5 %), whereas the error increases linearly as polymer surface energy increases (Figure 44a). This is more apparent when the error in prediction is plotted against polymer surface energy (Figure 45).

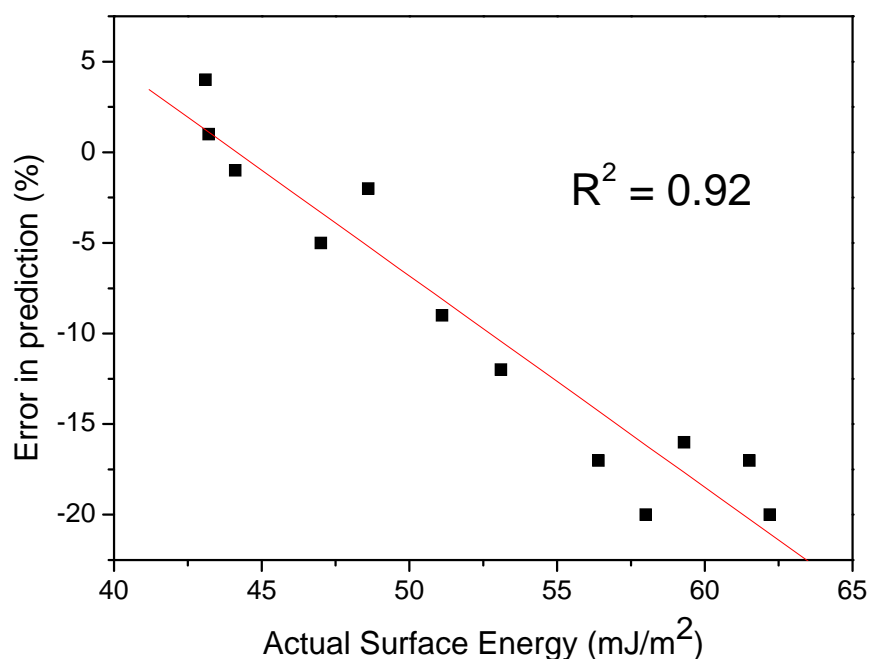


Figure 45. Actual surface energy of a polymer versus the error in the predicted surface energy using PLS model.

There are a number of things that could explain this error in surface energy prediction. For example, the error may possibly be due to the pre-processing of the data prior to analysis; both the ToF-SIMS and surface energy data was mean-centered, which is common prior to multivariate analysis to ensure that numerically larger variables do not unduly influence the statistics.[130, 131] This

data transformation sets the origin of the model arbitrarily to the mean of the training set (46.6 mJ/m^2), therefore the model will describe deviations from this mean. However, the mean surface energy of the polymers in the test set is 52.3 mJ/m^2 . To test this theory the ToF-SIMS ion intensities of the test data set were mean-centered using the means from the training set. Predictions were then obtained using these data and rescaled using the mean of the surface energy values from the training set. This time the model over-estimated the surface energy values of the polymers, with a considerably higher RMSPE (Figure 46a).

6.3.2.2 Acrylate copolymers containing minor monomers not included in the training set

Although the twelve polymers used in the test set above were not included in the 496 copolymer training set, they are chemically related, i.e. all monomers used to synthesise the test set polymers are represented in the training set. To test the predictive ability of this approach on copolymers that were more chemically disparate, predictions for acrylate copolymers synthesised from monomers not used in the training set were obtained. To achieve this aim a PLS model was constructed using data from the 336 copolymers in the library that were synthesised using minor monomers A to D. The resulting PLS model has an RMSPE value of 3.2 which is greater than the full model generated from all 496 polymers (Table 5). Analysis of the regression vector indicates that again predominantly the same ions positively and negatively correlate with surface energy, with the same variation in magnitude of regression coefficients observed in the other reduced sample datasets. However, ions with m/z 29.028 (CH_3N^+), 42.031 ($\text{C}_2\text{H}_4\text{N}^+$) and 58.068 ($\text{C}_3\text{H}_8\text{N}^+$) (Figure 43d) are completely absent from the regression vector. These ions can only be formed by cleavage of the tertiary amine group in monomer E; therefore it is unsurprising that the removal of polymers containing this monomer results in the disappearance of these ions from the regression vector.

This model was then used to predict the surface energies of the remaining 160 copolymers that contain minor monomers E and F (Table 5). Monomer E contains a tertiary amine functionality and monomer F contains a phenyl group.

Therefore the copolymers in this test set contain monomers not included in the training set. The predicted values for the test set are considerably different from the actual surface energy values (Figure 44b), with a much greater apparently random error than previously obtained. The predictions for the polymers containing either monomers E or F are equally inaccurate. This inaccuracy might be expected for those samples containing monomer E as there are no similar chemical functionalities within the training set. However, monomer F is a phenyl diacrylate therefore it might be expected that monomers included in the training set such as 7, 9 and 14 would produce similar secondary ions. These data suggest that it is probable that the model only has a predictive capability for polymers that are chemically related to those in the training set, i.e. contain the same monomers, as noted above.

As above the ToF-SIMS data for these polymers were then mean-centered using the means from the training set and predictions obtained (Figure 46b). Although the RMSPE is considerably higher than previously, the relatively random error in the predictions has disappeared. Indeed the predictions appear to differ systematically from the measured values, i.e. approximately 20 mJ/m² higher, which may suggest that the rescaling of the predictions may be at fault.

6.3.2.3 Polymers which are chemically unrelated to the training set

To investigate if the PLS model has any predictive application in polymers that are chemically unrelated to the test set, the exercise was repeated for six commercially available linear polymers: polystyrene (PS), poly(L-lactic acid) (PLLA), poly(methyl methacrylate) (PMMA), poly(dimethylsiloxane) (PDMS), poly(2-hydroxyethyl methacrylate) (PHEMA) and poly(tetrafluoroethylene) (PTFE). All of the predictions are within 1 mJ/m² of the average surface energy of the training set, suggesting that the model does not have the ability to discriminate between them and returns an estimate based on this average (Figure 44c). It is probable that this is due to the fact that the spectra of these polymers contain secondary ions not found in the training set, which may be equally or more correlated with surface energy for these samples than those modelled above.

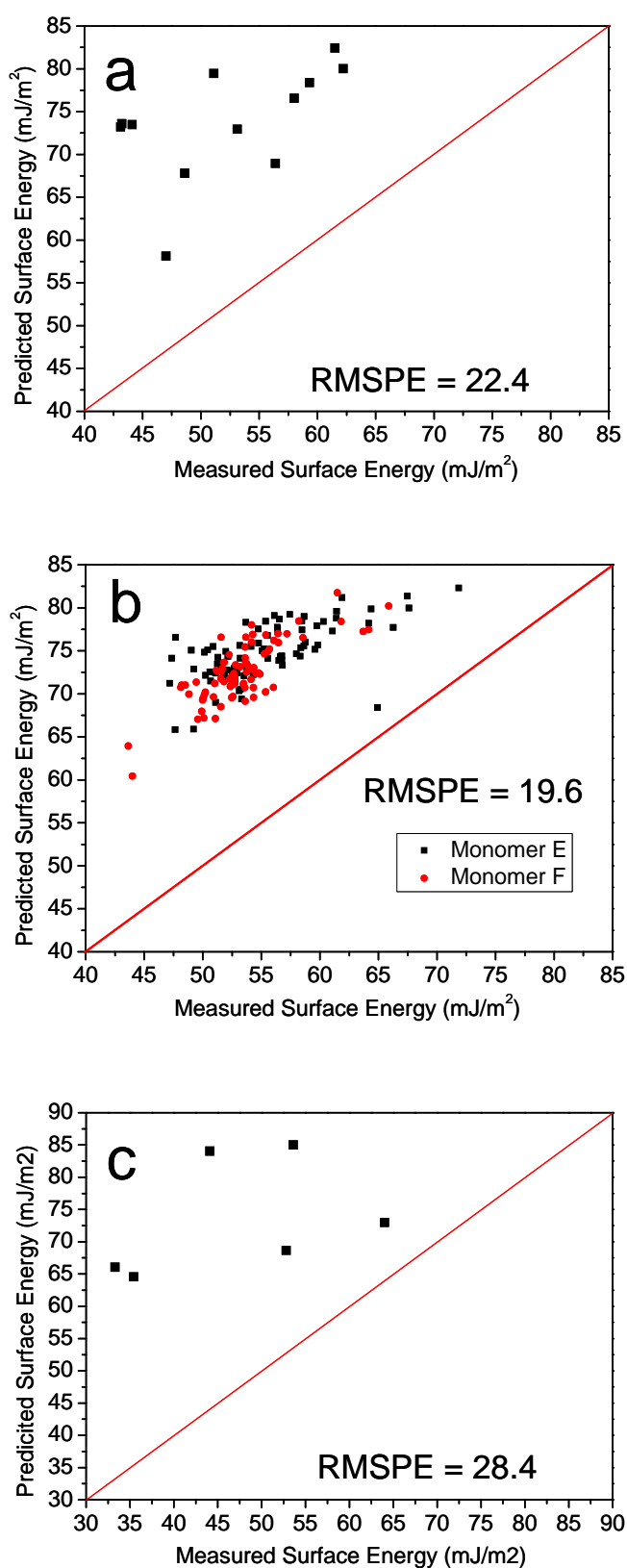


Figure 46. Measured versus predicted surface energy values for a) 12 acrylate copolymers synthesised from monomers common to training set b) 160 acrylate copolymers synthesised from monomers not used in training set c) 6 commercially available linear polymers, using data mean-centered using means from the test set. X = Y lines are provided to guide the eye.

When the exercise was repeated using data mean-centered using means from the training set, the RMSPE was considerably higher (Figure 46c). Although the predictions are no longer approximately identical to the mean of the training set, there is no correlation with polymers' measured surface energy values.

The above exercise has given an indication of the limits of the predictive power of PLS for the type of co-polymer dataset tested here. When the model was predicting samples that were synthesised from monomers that were included in the training set, the model gave the best predictions (with an error of 1 to 20 %). When the model was used to predict polymers synthesised from monomers that were not used in training set the predictions are very poor. Unsurprisingly when the model is used to predict the surface energy of linear polymers with significant chemical differences from the training set, the predictions all approximated to the mean value of the training set because it does not have the information to explain the differences in the test set. Mean-centering using the mean from the training set may help to improve the predictions in some cases; however more work is needed to investigate the effect of rescaling the data. Indeed changing the pre-processing method for these models has demonstrated just how sensitive these predictions are to the way the data is scaled (Figure 46).

The importance that the training set is chemically related to the samples on which predictions are to be made has been demonstrated. More specifically, for this dataset it has been demonstrated that it may be possible to use PLS to make predictions for copolymers synthesised from the same monomers as used in the training set. It is expected that these predictions may be improved by more sophisticated data pre-processing.

6.4 Conclusions

PLS has been shown to be able to identify surface moieties important in controlling surface energy. These are chemically intuitive, with high surface energy coming from moieties that relate to polar surface species while low surface energy correlates with hydrocarbons. It has been demonstrated that the results

obtained from PLS modelling of large combinatorial polymer libraries are equivalent to those obtained from much smaller datasets, in terms of the ions identified in the regression vector. The work in this Chapter has shown that removing acrylate copolymers with unique chemistries from the training set does not largely affect the ions identified in the regression vector significantly, although of course secondary ions specific to those polymers are not present. This is consistent with the supposition that PLS can only model information which has been included in the training set.

There is very little research in the chemometrics literature dealing with the use of PLS to make quantitative predictions; hence the work discussed in this Chapter has given a valuable insight into the limits of prediction achievable using this method. The PLS model underestimated the surface energy values for acrylate copolymers synthesised from monomers used in the training set, probably due to the pre-processing of the data prior to analysis. The predictive error increased substantially when predictions were made for acrylate copolymers that were synthesised from monomers not used in the training set, suggesting that no predictions could be made for these polymers. Finally, when predictions were made for six commercially available polymers that were chemically unrelated to the training set the values obtained were very poor.

Further work could include repeating this study using a polyatomic primary ion beam rather than the Ga^+ used here. This would likely give more chemical information, particularly at higher mass ranges, which may improve the predictions obtained.

Chapter 7

A Methodology for Investigating Protein Adhesion and Adsorption to Micro-arrayed Polymers

7.1 Introduction

Protein adsorption to surfaces is of significant importance in the fields of biomedical devices and tissue engineering since most biological fluids encountered *in vivo* and used in cell culture contain serum proteins.[132] Adsorbed proteins have a significant effect on how cells interact with materials. The adsorption of adhesion proteins, such as fibronectin, is generally thought to control cellular adhesion in combination with displacement of non cell-adhesive proteins such as albumin.[133] For many biomedical devices the non-specific adsorption of protein to their surface causes a cascade of events resulting in harm to the patient, e.g. thrombus formation.[134] Hence understanding why different proteins adsorb to different surfaces and the effect this has on cell adhesion and proliferation is of major importance. Protein adsorption to surfaces is dependent on various molecular interactions including van der Waals interactions, electrostatic interactions, hydrogen bonding and hydrophobic interactions.[135] AFM has become an important method of quantifying these various, non-specific forces.[52] By coating an AFM tip or colloidal probe with proteins the technique has been used to directly measure the protein adhesion properties to polymers,[56, 136, 137] metals[138] and self-assembled monolayers (SAM).[139] Protein coated AFM probes have also been applied to investigate the effect of surface wettability of a range of SAMs on protein adhesion.[140] The theory underlying AFM is discussed in some detail in chapter 2. Methods used to quantify the amount of protein adsorbed to a surface from solution include fluorescent and radioactive labelling of proteins, of which the former is readily adaptable to micro arrays using commercially available fluorescent slide readers.[141, 142]

When measuring protein adhesion forces with an AFM a standard tip may be coated directly with proteins or a micrometre diameter sphere may be attached first and then coated with proteins.[143-145] Attaching the colloid sphere is advantageous as it can help overcome problems with variable tip geometry or non-homogenous sample coating. The increased radius of the sphere in comparison with the bare AFM tip gives a higher sensitivity, allowing much

smaller forces to be measured.[146] The disadvantage with this method is that the lateral resolution of the technique is reduced to the diameter of the sphere, i.e. micrometres.

This chapter describes the application of two approaches for characterising protein-surface interactions; AFM force measurement of adhesion and fluorescence measurement of adsorption from solution to a library of novel copolymers printed on a poly(hydroxyethyl methacrylate) coated glass slide. The mechanism of protein-surface interactions is beyond the scope of this proof-of-concept study; these important issues will be addressed in future application of the methods developed in this chapter. Here, the protein adhesion and adsorption data are used to investigate the relationship between these two measurements and surface wettability to illustrate how such data may be used to relate protein interactions and a surface property. The polymer array was created using an automated system which produces spots of $\sim 300 \mu\text{m}$ diameter from mixtures of acrylate monomers polymerised *in situ*. [34] The structure of the monomers that were combined pair wise in the v/v ratio 70:30 to create the polymer library are presented in Figure 47.

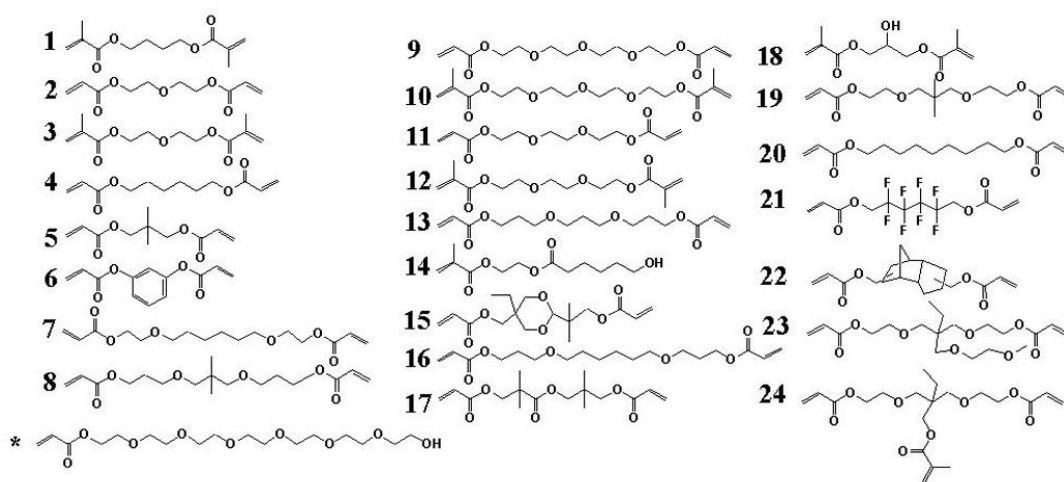


Figure 47. The 24 monomers used to synthesis the polymer library. Monomer 17 was substituted for * as a minor monomer to increase hydrophilicity.

7.2 Methods and Materials

7.2.1 Array synthesis.

The microarray under investigation comprised of 576 novel acrylate and methacrylate polymers synthesised from 24 monomers. Stock solutions of each monomer were prepared by mixing 75 % monomer, 25 % DMF and 1 % (w/v) 2,2-dimethoxy-2-phenyl acetophenone. These solutions were then mixed pairwise in all possible combinations at a ratio of 70:30. Monomer mixtures were then printed onto a poly(hydroxyethyl methacrylate) coated glass slide and polymerised by exposure to long-wave UV, to form spots with a diameter of ~ 300 μm and a centre-to-centre spacing of 740 μm . Monomers used to create the polymer library analysed can be found in Figure 47. Full details can be found in chapter 3. Each polymer is synthesised from two monomers, therefore to avoid confusion in this chapter we will refer to the monomer comprising 70 % of a polymer as the “major monomer” and the monomer comprising the other 30 % as the “minor monomer”.

7.2.2 AFM imaging and force measurements.

A 5 μm diameter borosilicate sphere was glued to the tip of a standard silicon nitride AFM cantilever (spring constant = 296.9 pN/nm) with epoxy resin. Acrylic acid was plasma polymerised and deposited on to the cantilever at 282 mTorr pressure and 20 W power.[147] The AFM probe was then reacted with 6 mM 1-ethyl-3 (3-dimethylaminopropyl) carbodiimide hydrochloride and 15 mM N-hydroxysulfosuccinimide in pH 7 phosphate buffered saline (PBS) (Figure 48). The probe was then reacted with human fibronectin (0.1mg/ml) in PBS for two hours, then washed in fresh PBS. A D3000 AFM (Veeco) was then used to take 100 force-distance measurements from each of 48 polymers on the polymer array in PBS. All measurements were taken using a preset maximum load to keep contact force constant. The deflection of the AFM cantilever was converted into force using Hooke’s law: $F = -k\Delta D$, where k = spring constant and ΔD = tip

deflection. To monitor for any deterioration or change in the state of the AFM probe, force-distance measurements were taken at the beginning and throughout the experiment on three control surfaces: glass, poly(tetrafluoroethylene) (PTFE) and fibronectin adsorbed onto silicon. The 24 polymer spots containing monomer 1 as their major monomer were imaged in tapping mode using a D3000 AFM (Veeco) in air (Tap300 tip). A scan size of 1 x 1 μm was used at a scan rate of 1 Hz. RMS roughness (r_a) was calculated using instrument software.

7.2.3 Contact angle measurements.

All contact angle measurements were taken using a DSA100 (Krüss) fitted with a piezo dosing head. A 100 pL water droplet was dispensed onto each polymer spot and the droplet profile recorded. The contact angles of these droplets were fitted using a circle fitting function.[98] Contact angle measurement from arrayed materials has been described in Chapter 5 in greater detail.[83]

7.2.4 Fluorescently labelled protein adsorption.

Human fibronectin (1mg/ml) was prepared in a 0.1M sodium carbonate buffer (pH 9). Fluorescein Isothiocyanate (FITC) was dissolved in Dimethyl sulfoxide (1mg/ml) and 50 μL added to the fibronectin solution. This fibronectin-FITC solution was incubated for 8 hours at 4 $^{\circ}\text{C}$. Ammonium chloride was then added to a final concentration of 50 mM and then incubated for a further 2 hours at 4 $^{\circ}\text{C}$. The unbound FITC was then removed by dialysis. A polymer array was immersed in a 0.01mg/ml solution of the fibronectin-FITC for 1 minute, after which it was removed and rinsed with fresh PBS. A Genepix 4000B scanner (laser wavelength 488 nm) was used to measure the fluorescence of the polymer spots before and after immersion. The intensity before immersion was then subtracted from the intensity after to account for background fluorescence of the polymers.[142] The intensities were then normalised by dividing all values by the maximum intensity.

7.3 Results and Discussion

Force measurements were made on 48 polymer spots of the microarray in PBS using a fibronectin coated colloidal AFM probe (recording 100 force-distance measurements on each polymer). The surface of the colloidal probe was first coated with plasma poly(acrylic acid) (ppAA). Fibronectin molecules were then covalently bound to the surface after activation of carboxyl groups with EDC and NHS (Figure 48). In a previous study ppAA deposited on glass has been shown to be stable in PBS for 24 hours.[145]

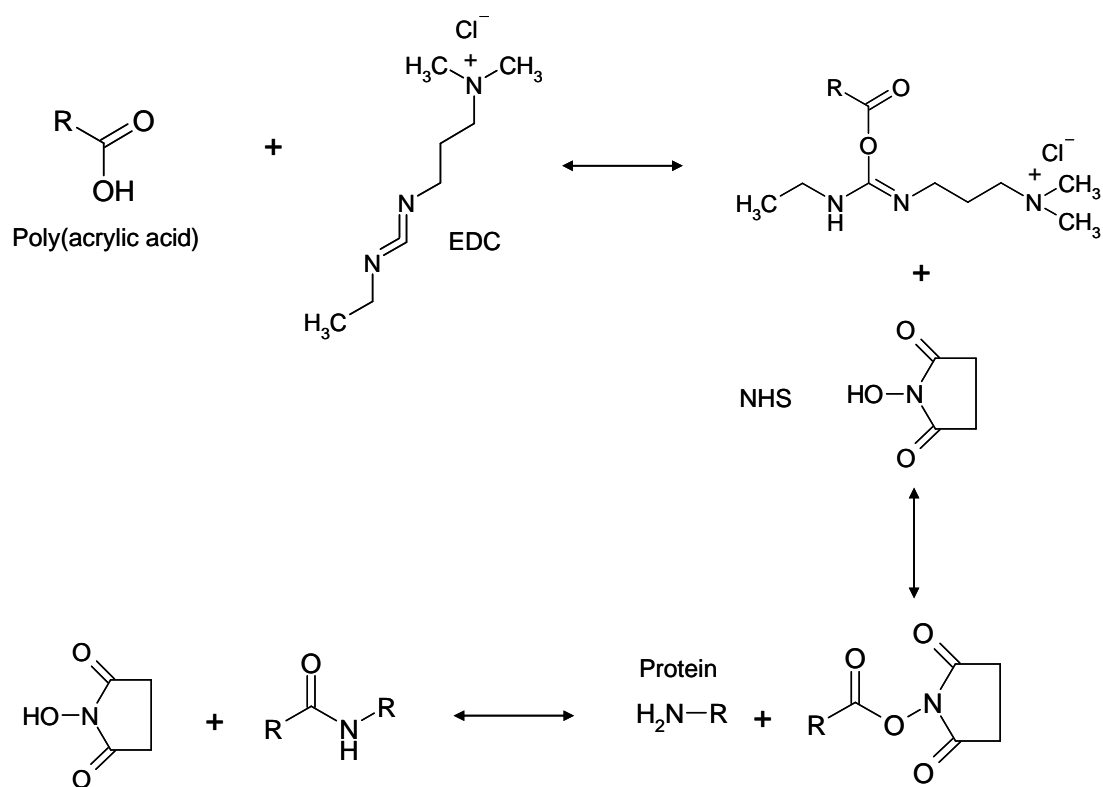


Figure 48. Formation of an amide bond between carboxylic groups on ppAA and amine functionalities on fibronectin (Figure adapted from Tsapikouni *et al*[145]).

All measurements were taken using a preset maximum load to keep the contact force constant. Force-distance measurements were taken on three control surfaces at the beginning and throughout the experiment to monitor any deterioration or changes in the AFM probe (Figure 49). These control surfaces were glass, PTFE and fibronectin adsorbed to silicon. The fibronectin coated probe adhered most strongly to the control PTFE surface (~ 5.5 nN), which can

be explained by the presence of strong hydrophobic forces between the surface and the probe. The adhesion force on glass (~ 1 nN) was less than that measured on PTFE which is probably due to its more hydrophilic nature. No adhesion force was measured between the fibronectin coated probe and the fibronectin pre-adsorbed to silicon. The fibronectin molecules on the AFM probe and on the silicon surface will have the same charge in the phosphate buffer, hence the two surfaces do not adhere. No significant changes in maximum adhesion forces on glass, PTFE and fibronectin coated surfaces was noted throughout the experiment. This provides a good indication that the probe coating remained intact during the experiments and will have given reproducible force measurements on the arrayed polymers.

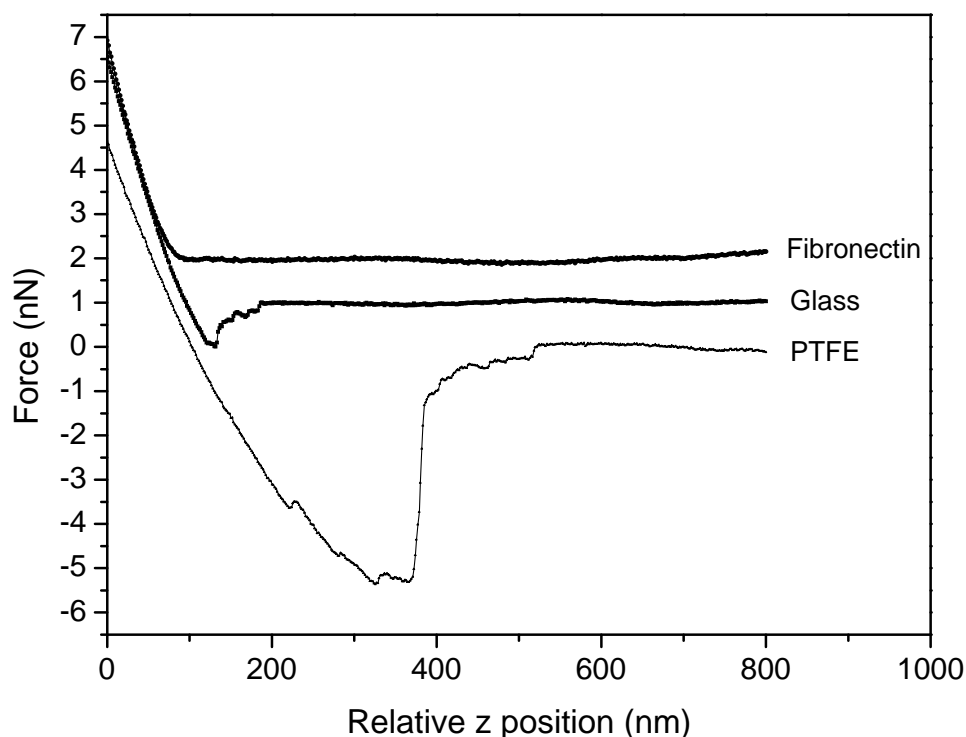


Figure 49. Typical force-distance curves measured between a fibronectin coated AFM probe and three control surfaces: glass, PTFE and fibronectin adsorbed to silicon.

No attractive forces were detected between the fibronectin coated probe and any of the 48 polymers analysed during the approaching cycle of the force measurements (Figure 50). This suggests that there were no significant long-range

interactions between the fibronectin molecules on the AFM probe for any of the polymers. This is consistent with any electrostatic forces being screened by the PBS buffer. Weaker, secondary forces such as van der Waals will only act when the AFM probe is in very close proximity to the surface. Hence all of the polymers analysed would adsorb fibronectin from solution to the surface that arrives by diffusion and Brownian motion alone, rather than be electrostatic attraction to the surfaces.[137] Occasionally, rupture points can be observed on the retracting part of the force-distance curves measured on the polymers (Figure 50). These may be due to different parts of the AFM probe detaching from the polymer surface in succession.

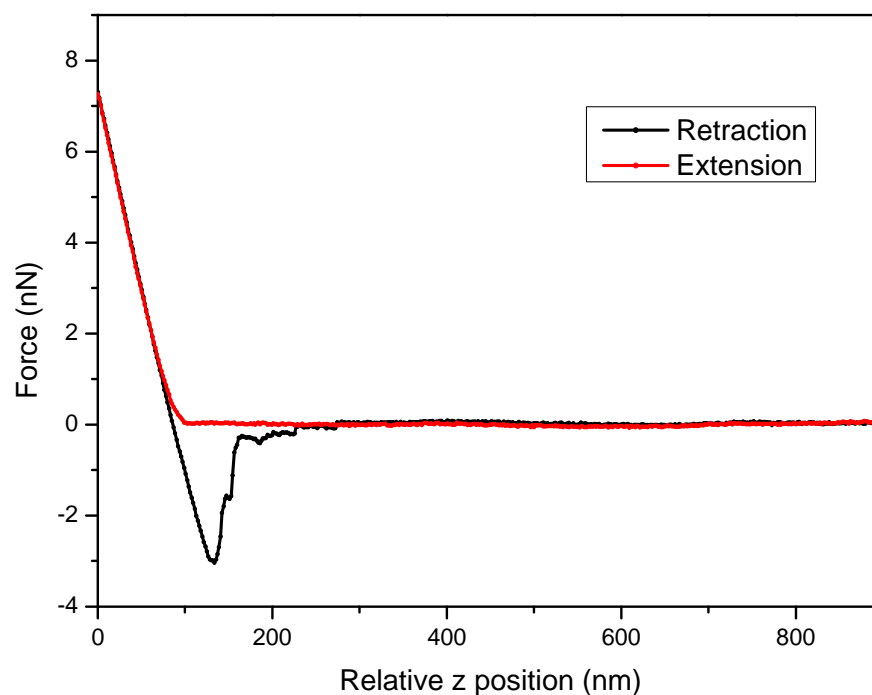


Figure 50. Example force-distance curve for the polymer containing 70 % monomer 21 and 30 % 1.

The maximum adhesion forces of the fibronectin coated AFM probe to each of the 48 polymers were measured and are presented in Figure 51. The values presented are the mean forces measured from 100 force-distance measurements with the error bars representing the standard deviation. The adhesion forces varied greatly from 0.15 to 2.65 nN within the sample set of

polymers, suggesting significantly differing affinities of the fibronectin for the range of polymers.

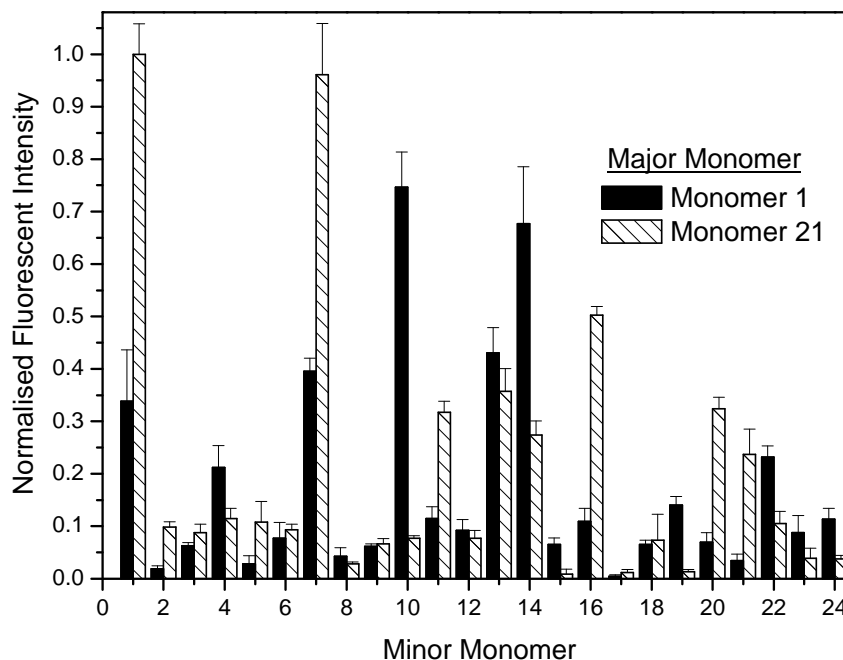


Figure 51. Graph displaying the maximum adhesion force between a fibronectin coated probe and 48 polymers.

The adhesion forces measured exhibited a normal distribution for nearly all of the polymers, suggesting that the use of the mean adhesion force is appropriate (Figure 52a). The only exception was the polymer containing 70% monomer 21 and 30% monomer 7 (Figure 52b). This polymer is also notable for having the largest standard deviation in adhesion measurements (Figure 51). The histogram for this polymer shows a bimodal distribution, which explains the large standard deviation observed in the data. This distribution suggests that the surface of this polymer is heterogeneous in such a way as to produce two distinct adhesion forces at ~ 1 and ~ 7.5 nN. This heterogeneity may be chemical, for example phase separation of the polymer or physical, for example microscale roughness. To investigate this further the polymer was imaged using tapping mode AFM. The RMS roughness of the polymer was calculated as 11 nm. The phase images of the polymer show no surface morphology indicative of phase separation.

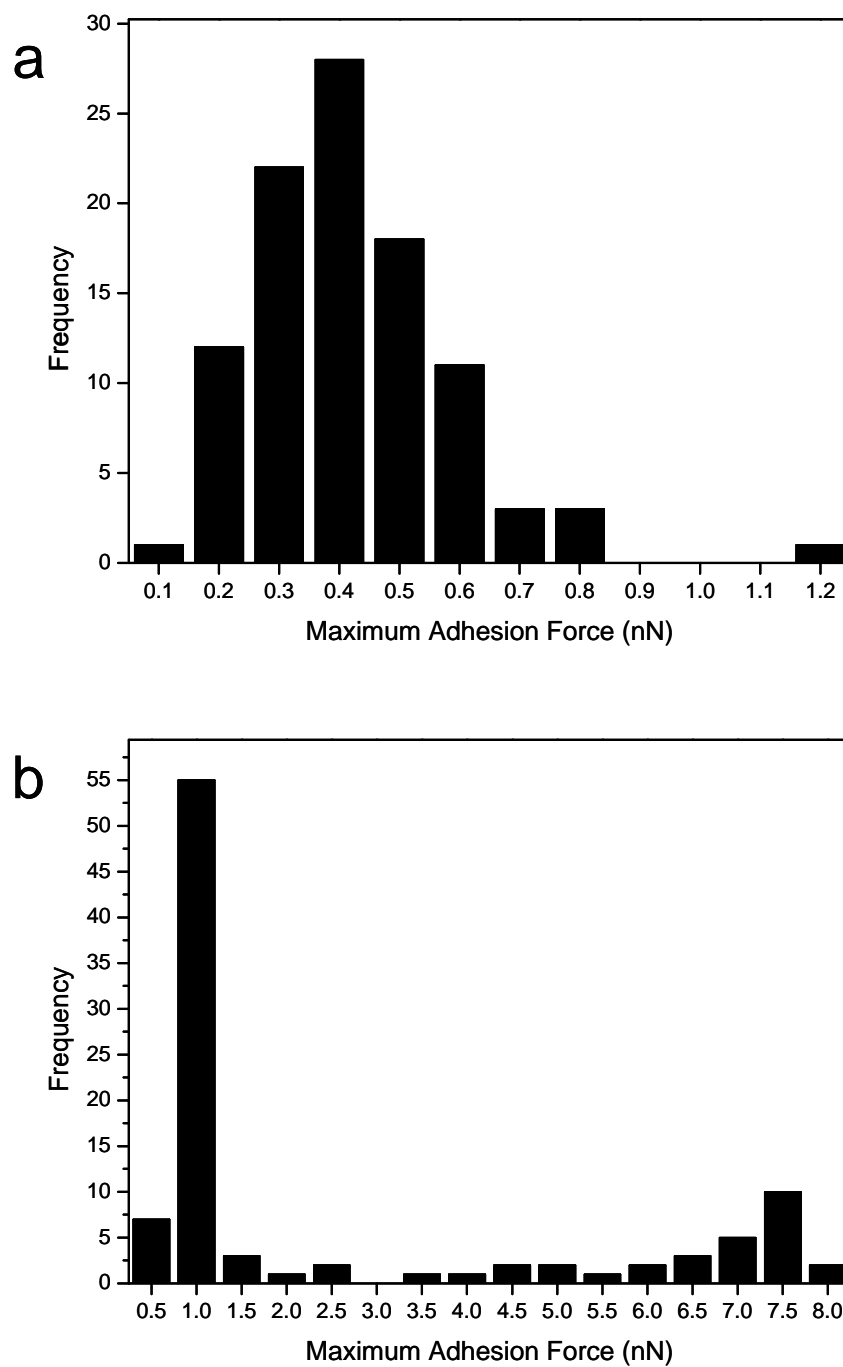


Figure 52. Histograms displaying adhesive forces (nN) between a fibronectin coated AFM probe and polymers synthesised from a) 70 % monomer 21 & 30 % monomer 2 b) 70 % monomer 21 & 30 % monomer 7.

To measure the relative amount of fibronectin adsorption from solution, a polymer array was immersed in a 0.03 mg/ml solution of human fibronectin-FITC for 1 minute, after which it was removed and rinsed with fresh PBS.[148] A Genepix 4000B scanner (laser wavelength 488 nm) was used to measure the fluorescence intensity of the polymer spots before and after immersion to quantify the relative amount of retained protein. The intensity before immersion was subtracted from the intensity after to account for any auto-fluorescence from the polymers and normalised to the maximum intensity (Figure 53).[142] Proteins adsorb to a surface from solution within seconds of exposure and the speed of adsorption depends upon the chemistry of the surface.[2, 132]

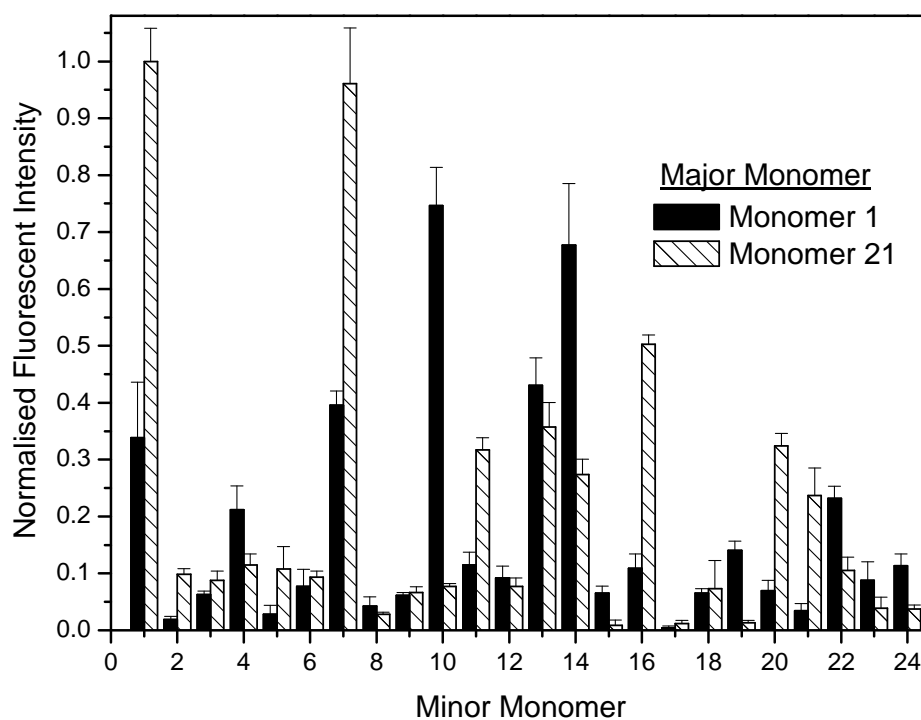


Figure 53. Graph displaying the normalised fluorescent intensities of 48 polymers after adsorption of fluorescent labelled fibronectin.

An adsorption time of 1 minute was chosen to provide a fixed amount of time in which to measure initial protein adsorption to the polymers, to allow a measure of relative affinity of fibronectin to each polymer. Longer adsorption times could be studied as the microarrays are stable in aqueous media for up to six days.[34]

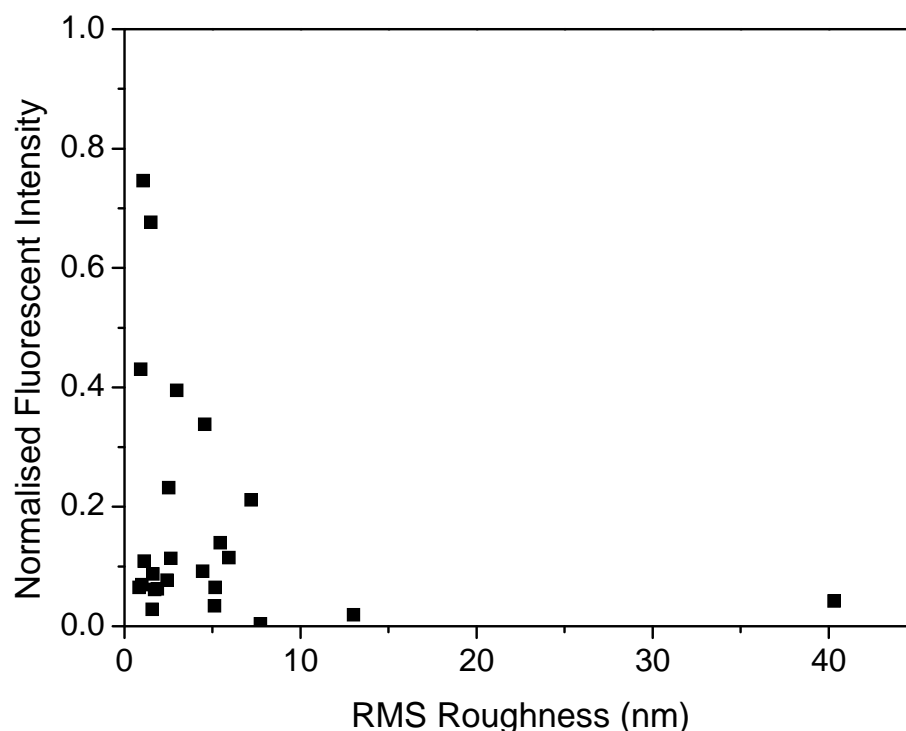


Figure 54. RMS roughness versus normalised fluorescent intensity for 24 polymers containing monomer 1 as their major constituent.

The roughness of the polymer surfaces could potentially influence the amount of fibronectin adsorbed by increasing the surface area available for adsorption. To investigate whether surface roughness influenced the amount of protein adsorbed, the 24 polymers containing monomer 1 as their major component were imaged using tapping mode AFM and their r_a values were calculated from $1 \times 1 \mu\text{m}$ scans. No relationship was observed between polymer roughness and amount of fibronectin adsorbed (Figure 54).

To investigate the relationship between the adhesion force of the protein coated probe to a polymer and the quantity of protein adsorbed, these two parameters were plotted against each other (Figure 55). It can be seen that there is a linear relationship between the two with a correlation coefficient $R^2 = 0.89$.

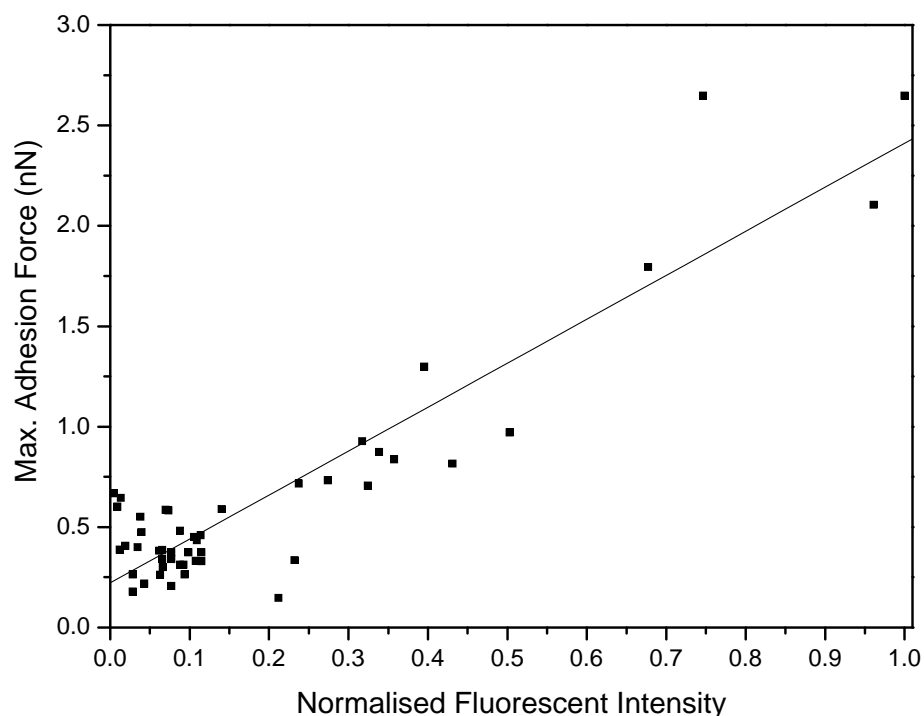


Figure 55. Adhesion force versus normalised fluorescent intensity for 48 polymers ($R^2 = 0.89$).

This correlation between the data from the two experiments is interesting because the two are related but very different measurements of protein-surface interactions: one measuring the strength of the interaction between fibronectin and a surface, and the other measuring the *amount* of fibronectin adsorbed after solution exposure and rinsing. This linear relationship suggests that proteins that strongly adhere to a surface will adsorb and on washing be retained in greater numbers than proteins which only have a weak affinity for a surface. Bremmell *et al* have previously reported a similar relationship between protein adhesion and amount of protein adsorbed using radiolabelling on a small group of large scale plasma polymer samples.[141] The data reported in this chapter combined with previous work relating protein adhesion measurements to protein adsorption using surface plasmon resonance,[143] demonstrates the value of fluorescently labelled protein adsorption as a method to investigate protein affinity for biomaterials.

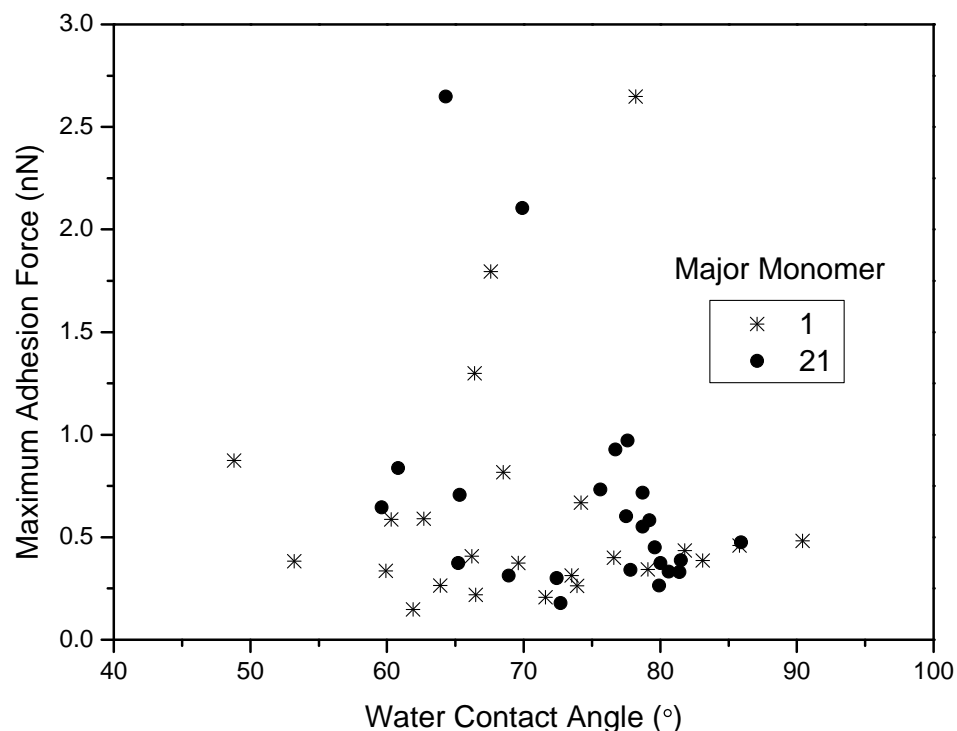


Figure 56. Relationship between protein adhesion force and water contact angle for 48 polymers.

To demonstrate the utility of protein adhesion data from microarrays the relationship between protein adhesion and surface wettability was investigated. The water contact angles of the 48 polymers were measured using picolitre volume water droplets and compared with the adhesion forces (Figure 56). All contact angle measurements were taken using a piezo dosing head to produce 100 pL droplets. The WCA of the polymers varied from ~ 48 to 91° , demonstrating that the polymers ranged from relatively hydrophilic to hydrophobic. It has previously been reported on SAM surfaces (alkanethiolates on gold terminated with different functional groups) that large proteins such as fibronectin adhere greatest to hydrophobic surfaces, as the protein molecules are able to expose more internal hydrophobic residues during adhesion.[140, 149, 150] This is not observed in this group of polymers, where it can be seen that protein adhesion was generally low with higher values at WCA between 65 to 85° . This indicates that the conclusions on protein adhesion drawn from studies using well ordered SAM surfaces cannot be extended to this set of polymers. A more complex surface

chemistry than the well ordered SAM systems is likely to be at the root of this difference; including variable cross-linking, steric consideration and specific moieties.

7.4 Conclusions

A wide range of protein adsorption properties within the 48 combinatorial polymers synthesised and analysed in a microarray format has been observed. Since protein adsorption to materials is such an important stage in cellular adhesion, it is essential that protein interactions with microarrayed materials are studied, in order to more greatly understand cellular response. Both methods described in this chapter show promise for the analysis of arrayed polymer libraries. The correlation between the two sets of data appears to validate both. This proof of concept study indicates that these may be used in combination with surface analysis methods to further study the relationship between surface properties and protein adsorption. It will be necessary to extend the protein adsorption experiments to more realistic competitive and sequential multi-protein experiments which more closely mimic actual serum conditions encountered in cell culture.

Chapter 8

Conclusions

8.1 General Conclusions

The aim of this thesis was to develop methods for the characterisation of the surface properties of polymers printed as microarrays. Chapter 3 described the surface chemical analysis of a library of 496 polymers *in situ* in microarray format using ToF-SIMS and XPS. Importantly the acquisition of this data was possible within the timeframe of cell adhesion and proliferation assays, thus suggesting that the screening of the biological and surface chemical properties of these libraries could run in parallel. ToF-SIMS was used to image the whole microarray, thereby showing the distribution of key secondary ion species across the array. It could easily be envisaged using this technique as a rapid method of confirming the correct array layout prior to printing – an essential step before conclusions can be made from data acquired from the arrays. A comparison of the bulk and surface chemistries of the polymers on the microarray showed great differences for a large proportion of the polymers. This confirms the importance of surface analysis procedures for these arrays, as it is obvious that the polymers' surface chemistries can not be inferred from their bulk chemistries.

Principal component analysis was applied to both the ToF-SIMS and XPS spectral data with great success, suggesting that this is an ideal method for analysing the vast amounts of information gained from these arrays. PCA allowed the similarities and differences in the surface chemistries of the polymers to be easily visualised. Analysis of the principle component score values of the polymers gave a great deal of information about how the monomer composition of the polymers influenced their surface chemistries. It could be imagined that this kind of study could easily be used to 'tune' the surface chemistry of a new polymer to an ideal for a particular use, by studying how the relative amounts of certain monomers will change the resulting polymer surface. PCA could also be used to investigate whether the surface chemistry of polymers with identical constituent monomers are equivalent, i.e. test the repeatability of the method of polymer synthesis.

In Chapter 4 a new technique allowing contact angle measurement from picolitre volume droplets was described. The contact angles measured using these very small droplets was shown to be equivalent to those measured from the more conventional microlitre volume droplets, with appropriate consideration of their rapid evaporation. With the miniaturisation of many areas of science it is becoming increasingly necessary to characterise surface with very small dimensions. To demonstrate the ability of this new technique to achieve high spatial resolution, the wettability of a radial chemical gradient was mapped at intervals of only 250 μm . This indicated the utility of this technique in countless applications where sample size or the unit change in wettability is very small, for example, gradient surfaces microfluidic devices and microarrays.

The new technique for contact angle measurement described in Chapter 4 allowed the contact angles of individual polymers on a microarray (diameter of $\sim 300 \mu\text{m}$) to be measured for the first time. Chapter 5 described the estimation of the surface energies of all 496 polymers on a microarray using contact angle data from picolitre volume droplets of water and diiodomethane. As with the surface chemical data, the surface energy data can be acquired well within the time required to screen the polymers' biological properties. The water contact angles and polar surface energies of the polymers varied greatly, demonstrating the power of combinatorial methods to produce polymers with a wide range of properties. To investigate what the chemical basis is for this large range in surface energies, the ToF-SIMS and XPS data from the polymers was related to their surface energy values. It was noted that atomic and functional group information from XPS was unable to explain the variation in surface energy values probably because of the lower surface sensitivity of the technique. In contrast when ToF-SIMS ion intensity data was related to surface energy using partial least squares regression some interesting conclusions could be made. It was observed that oxygenated hydrocarbon secondary ions were strongly associated with high surface energy values, whereas non-oxygenated hydrocarbon secondary ions were strongly associated with low surface energy values. These conclusions were confirmed by reference to the raw spectra of the polymers. This exercise demonstrates the massive potential the combination of PLS and arrayed polymer libraries have for studying surface structure-property relationships. For example,

PLS could be used to identify the surface chemistries of polymers which promote cell adhesion, inhibit non-specific protein adsorption or even direct the differentiation of stem cells into specific lineages. This information could then be used to design new polymers with the desired polymers, i.e. moving towards the intelligent design of new biomaterials.

If PLS is to be used as a tool to study large combinatorial polymer libraries it is essential that the limits of the technique are known. In Chapter 6 two important issues relating to the use of PLS in large datasets were investigated. Firstly, the influence of the number and type of samples in the training set on the results obtained was investigated. Secondly, the ability of PLS to give accurate, quantitative predictions was studied. Importantly it was observed that changing the number of samples included in the training set does not appear to influence the key ions in the regression vector, only their relative and absolute magnitude of the regression coefficients. This suggests that the results obtained from large libraries of polymers are equivalent to those from smaller, more conventional sized datasets. It was noted that if polymers with unique chemistries are removed from the training set, secondary ions specific to these polymers are not observed in the regression vector, as would be expected.

There has been very little research in the chemometrics field investigating the use of PLS to make quantitative predictions. Therefore in the second part of Chapter 6 different test sets of polymers were used to test the ability of PLS to predict surface energy. It was observed that the best predictions obtained were for polymers that were closely related chemically to the training set. The predictions were seen to decrease in accuracy as the test polymers became more chemically dissimilar to the training set. These observations are intuitive as a PLS model is only able to make predictions on the basis of the information it has been given in the training set. It can be concluded from this exercise that the potential for using PLS as a predictive tool is perhaps limited. However with knowledge of these limits and the correct choice of training sets there is scope for obtaining predictions within groups of closely related polymers. More research is needed into the influence of data pre-processing and rescaling on the predictions obtained.

Protein adsorption to surfaces is a vitally important step in the function of biomaterials, therefore it is important that methods exist for studying the interaction of proteins with new polymer libraries that are printed in microarray format. Hence in the final experimental chapter two methods are described for studying protein interactions with arrayed polymers. AFM was used to measure the adhesion force between a fibronectin-coated probe and a group of polymers on a microarray. The microarray was then incubated in a solution of fluorescently labelled fibronectin to obtain a relative measure of the amount of fibronectin adsorbed to each spot. Interestingly there was a linear relationship between the adhesion force of fibronectin to a polymer and the amount of fibronectin adsorbed (as measured by fluorescence). This suggests that if a protein is strongly attracted to a surface it will adsorb in greater quantities. As the adsorption of adhesion proteins to polymers is such an important stage in cellular adhesion, it is hoped that using techniques such as those described above to study the protein adsorption properties of arrayed polymers will aid further understanding of cellular response.

8.2 Final Comments

This thesis has demonstrated the feasibility of a thorough characterisation of the surface properties of a polymer microarray, within the timeframe of their biological assessment. It is worth noting that the techniques described here could also be applied to microarrays of other types of materials. The methods described in this thesis have two principal applications. Firstly they enable an understanding of the surface properties of hundreds of novel materials to be obtained, which otherwise would remain uncharacterised. Importantly this allows confirmation that any desired properties have been achieved and gives reassurance that the array is laid out as intended. Secondly, knowledge of the surface properties of these polymer libraries allows surface structure-property relationships to be studied, using techniques such as PLS. This will aid greater understanding as to why materials exhibit certain properties and allow the intelligent design of new materials.

Acknowledgements

I would like to begin by thanking Prof. Martyn Davies and Dr. Morgan Alexander for their supervision and continued encouragement over the past three years. It has truly been a privilege to have been given the opportunity to work in such a well-renowned and equipped laboratory. Thanks to Dr. Ying Mei, Dr. Daniel Anderson and Prof. Robert Langer at MIT for providing the polymer microarrays used in this thesis. Special thanks must go to Dr. Andrew Urquhart for his constant advice and support (and also for his occasional moments of stress-induced madness that provided ample entertainment for the lab!).

I have made many good friends during my time in the LBSA, without whom life would have been very dull and coffee breaks lonely! So to name a few, thanks to Andrew, Big Dave, Ryo, Dave S, Jeff, Chris, Niall, Declan, Vicky, Darren, Mischa, Lee and Matt. Likewise outside of the lab special thanks to Pete, Ginger Ian, Powley and John for the many random nights out and for enduring my piano playing after a few pints! Thanks also to my mates back in Wallasey who still don't really understand what I've been doing for three years, but never-the-less have continued to provide a welcome break from Nottingham whenever I venture back home.

Thanks to Dave and Ruth for not only being a great brother and sister, but also for being my best friends – it still surprises me that after 26 years we can still get together and have such entertaining conversations! Finally I would like to thank my Mum and Dad, who are without-a-doubt the best parents I could have hoped for. Your constant encouragement and genuine interest in whatever I have been doing has been amazing.

References

1. Griffith LG. Polymeric biomaterials. *Acta Materialia* 2000 Jan;48(1):263-277.
2. Ratner BD, Hoffman AS, Schoen JF, Lemons JE. *Biomaterials Science, an Introduction to Materials in Medicine*. San Diego: Academic, 1996.
3. Blaine G. The Uses of Plastics in Surgery. *Lancet* 1946;251(OCT12):525-528.
4. Ingraham FD, Alexander E, Matson DD. Synthetic Plastic Materials in Surgery. *New England Journal of Medicine* 1947;236(10):362-368.
5. Langer R, Tirrell DA. Designing materials for biology and medicine. *Nature* 2004 Apr;428(6982):487-492.
6. Langer R, Vacanti JP. Tissue Engineering. *Science* 1993 May;260(5110):920-926.
7. Stevens MM, George JH. Exploring and engineering the cell surface interface. *Science* 2005 Nov;310(5751):1135-1138.
8. Young RJ, Lovell PA. *Introduction to Polymers*. 2nd ed. London: Chapman & Hall, 1991.
9. Walton D, Lorimer P. *Polymers*. Oxford: Oxford University Press, 2000.
10. Dumitriu S. *Polymeric Biomaterials*. 2nd ed. New York: Marcel Dekker, 2001.
11. Kohn J, Welsh WJ, Knight D. A new approach to the rationale discovery of polymeric biomaterials. *Biomaterials* 2007 Oct;28(29):4171-4177.
12. Eisenberger P. *Biomaterials and medical implant science*. Bethesda MD: NIH; 1995 October 16-17.
13. Webster DC. Combinatorial and high-throughput methods in macromolecular materials research and development. *Macromolecular Chemistry and Physics* 2008 Feb;209(3):237-246.
14. Meredith JC. A current perspective on high-throughput polymer science. *Journal of Materials Science* 2003 Nov;38(22):4427-4437.

15. Brocchini S, James K, Tangpasuthadol V, Kohn J. A combinatorial approach for polymer design. *Journal of the American Chemical Society* 1997 May;119(19):4553-4554.
16. Brocchini S, James K, Tangpasuthadol V, Kohn J. Structure-property correlations in a combinatorial library of degradable biomaterials. *Journal of Biomedical Materials Research* 1998 Oct;42(1):66-75.
17. Meredith JC, Karim A, Amis EJ. High-throughput measurement of polymer blend phase behavior. *Macromolecules* 2000 Aug;33(16):5760-5762.
18. Washburn NR, Yamada KM, Simon CG, Kennedy SB, Amis EJ. High-throughput investigation of osteoblast response to polymer crystallinity: influence of nanometer-scale roughness on proliferation. *Biomaterials* 2004 Mar-Apr;25(7-8):1215-1224.
19. Zelzer M, Majani R, Bradley JW, Rose FRAJ, Davies MC, Alexander MR. Investigation of cell-surface interactions using chemical gradients formed from plasma polymers. *Biomaterials* 2008;29:172-184.
20. Kohn J. Implants: the biodegradable future. *Medical Device Development* 2006:35-36.
21. Tourniaire G, Collins J, Campbell S, Mizomoto H, Ogawa S, Thaburet JF, et al. Polymer microarrays for cellular adhesion. *Chemical Communications* 2006 May(20):2118-2120.
22. Urquhart AJ, Anderson, D.G., Taylor, M., Alexander, M.R., Langer, R., Davies, M.C. High Through-put Surface Characterisation of a Combinatorial Material Library. *Advanced Materials (In press)* 2007.
23. Lynn DM, Anderson DG, Putnam D, Langer R. Accelerated discovery of synthetic transfection vectors: Parallel synthesis and screening of degradable polymer library. *Journal of the American Chemical Society* 2001 Aug;123(33):8155-8156.
24. Anderson DG, Lynn DM, Langer R. Semi-automated synthesis and screening of a large library of degradable cationic polymers for gene delivery. *Angewandte Chemie-International Edition* 2003;42(27):3153-3158.
25. Morgenthaler S, Zink C, Spencer ND. Surface-chemical and morphological gradients. *Soft Matter* 2008;4:419-434.

26. Meredith JC, Sormana JL, Keselowsky BG, Garcia AJ, Tona A, Karim A, et al. Combinatorial characterization of cell interactions with polymer surfaces. *Journal of Biomedical Materials Research Part A* 2003 Sep;66A(3):483-490.
27. Simon CG, Eidelman N, Kennedy SB, Sehgal A, Khatri CA, Washburn NR. Combinatorial screening of cell proliferation on poly(D,L-lactic acid)/poly(D,L-lactic acid) blends. *Biomaterials* 2005 Dec;26(34):6906-6915.
28. Hubbell JA. Biomaterials science and high-throughput screening. *Nature Biotechnology* 2004 Jul;22(7):828-829.
29. Diaz-Mochon JJ, Tourniaire G, Bradley M. Microarray platforms for enzymatic and cell-based assays. *Chemical Society Reviews* 2007;36(3):449-457.
30. Takeuchi I, Lauterbach J, Faselka MJ. Combinatorial Materials Synthesis. *Materials Today* 2005:18-26.
31. de Gans BJ, Duineveld PC, Schubert US. Inkjet printing of polymers: State of the art and future developments. *Advanced Materials* 2004 Feb;16(3):203-213.
32. de Gans BJ, Schubert US. Inkjet printing of well-defined polymer dots and arrays. *Langmuir* 2004 Aug;20(18):7789-7793.
33. Zhang R, Liberski A, Khan F, Diaz-Mochon JJ, Bradley M. Inkjet fabrication of hydrogel microarrays using in situ nanolitre-scale polymerisation. *Chemical Communications* 2008 Mar(11):1317-1319.
34. Anderson DG, Levenberg S, Langer R. Nanoliter-scale synthesis of arrayed biomaterials and application to human embryonic stem cells. *Nature Biotechnology* 2004 Jul;22(7):863-866.
35. Folkman J, Moscona A. Role of Cell-Shape in Growth-Control. *Nature* 1978;273(5661):345-349.
36. Anderson DG, Putnam D, Lavik EB, Mahmood TA, Langer R. Biomaterial microarrays: rapid, microscale screening of polymer-cell interaction. *Biomaterials* 2005 Aug;26(23):4892-4897.
37. Hern DL, Hubbell JA. Incorporation of adhesion peptides into nonadhesive hydrogels useful for tissue resurfacing. *Journal of Biomedical Materials Research* 1998 Feb;39(2):266-276.
38. Mant A, Tourniaire G, Diaz-Mochon JJ, Elliott TJ, Williams AP, Bradley M. Polymer microarrays: Identification of substrates for phagocytosis assays. *Biomaterials* 2006 Oct;27(30):5299-5306.

39. Liberski AR, Tizzard GJ, Diaz-Mochon JJ, Hursthouse MB, Milnes P, Bradley M. Screening for Polymorphs on Polymer Microarrays. *Journal of Combinatorial Chemistry* 2008;10:24-27.
40. Simon CG, Stephens JS, Dorsey SM, Becker ML. Fabrication of combinatorial polymer scaffold libraries. *Review of Scientific Instruments* 2007 Jul;78(7).
41. Yang Y, Bolikal D, Becker ML, Kohn J, Zeiger DN, Simon CG. Combinatorial polymer scaffold libraries for screening cell-biomaterial interactions in 3D. *Advanced Materials* 2008 Jun;20(11):2037-+.
42. Garbassi F, Morra, M., Occhiello, E. *Polymer Surfaces: from physics to technology*. Chichester: John Wiley & Sons Ltd, 1998.
43. Thissen H, Johnson G, McFarland G, Verbiest BCH, Gengenbach T, Voelckera NH. Microarrays for the evaluation of cell-biomaterial surface interactions - art. no. 64130B. In: Voelcker NH, editor. *Smart Materials Iv*, 2007. p. B4130-B4130.
44. Meredith JC, Karim A, Amis EJ. Combinatorial methods for investigations in polymer materials science. *MRS Bull* 2002 Apr;27(4):330-335.
45. Tweedie CA, Anderson DG, Langer R, Van Vliet KJ. Combinatorial material mechanics: High-throughput polymer synthesis and nanomechanical screening. *Advanced Materials* 2005 Nov;17(21):2599-+.
46. Sormana JL, Meredith JC. High-throughput discovery of structure-mechanical property relationships for segmented poly(urethane-urea)s. *Macromolecules* 2004 Mar;37(6):2186-2195.
47. Thaburet JFO, Mizomoto H, Bradley M. High-throughput evaluation of the wettability of polymer libraries. *Macromolecular Rapid Communications* 2004 Jan;25(1):366-370.
48. Vickerman JC, Briggs D, editors. *ToF-SIMS - Surface Analysis by Mass Spectrometry*. Manchester: IM Publications and SurfaceSpectra Ltd, 2001.
49. Briggs D. *Surface Analysis of Polymers by XPS and Static SIMS*. Cambridge: Cambridge University Press, 1998.
50. Feldman LC, Mayer JW. *Fundamentals of Surface and Thin Film Analysis*. New York: Elsevier Science Publishing Co., 1986.
51. Briggs D, Seah MP. *Practical Surface Analysis: Auger and X-ray Photoelectron Spectroscopy*. Chichester: Wiley, 1990.

52. Binnig G, Quate CF, Gerber C. Atomic Force Microscope. *Physical Review Letters* 1986 Mar;56(9):930-933.
53. Morris VJ, Kirby AR, Gunning AP. *Atomic Force Microscopy for Biologists*. London: Imperial College Press, 1999.
54. Lal R, John SA. Biological Applications of Atomic-Force Microscopy. *Am J Physiol* 1994 Jan;266(1):C1-&.
55. Vansteenkiste SO, Davies MC, Roberts CJ, Tendler SJB. Scanning probe microscopy of biomedical interfaces. *Prog Surf Sci* 1998 Feb;57(2):95-136.
56. Vansteenkiste SO, Corneillie SI, Schacht EH, Chen X, Davies MC, Moens M, et al. Direct measurement of protein adhesion at biomaterial surfaces by scanning force microscopy. *Langmuir* 2000 Apr;16(7):3330-3336.
57. Bhushan B, Koinkar VN. Nanoindentation Hardness Measurements Using Atomic-Force Microscopy. *Appl Phys Lett* 1994 Mar;64(13):1653-1655.
58. Castner DG, Ratner BD. Biomedical surface science: Foundations to frontiers. *Surface Science* 2002 Mar;500(1-3):28-60.
59. Colbourn EA. Computer-Simulation of Defects and Reactions at Oxide Surfaces. *Surface Science Reports* 1992;15(8):281-319.
60. Lamberti C. The use of synchrotron radiation techniques in the characterization of strained semiconductor heterostructures and thin films. *Surface Science Reports* 2004;53(1-5):1-197.
61. Taylor M, Urquhart AJ, Anderson DG, Williams PM, Langer R, Alexander MR, et al. A Methodology for Investigating Protein Adhesion and Adsorption to Microarrayed Combinatorial Polymers. *Macromolecular Rapid Communications* 2008;29(15):1298-1302.
62. Graham DJ, Wagner MS, Castner DG. Information from complexity: Challenges of TOF-SIMS data interpretation. *Applied Surface Science* 2006 Jul;252(19):6860-6868.
63. Tyler B. Interpretation of TOF-SIMS images: multivariate and univariate approaches to image de-noising, image segmentation and compound identification. *Applied Surface Science* 2003 Jan;203:825-831.
64. Biesinger MC, Paepegaey PY, McIntyre NS, Harbottle RR, Petersent NO. Principal component analysis of TOF-SIMS images of organic monolayers. *Analytical Chemistry* 2002 Nov;74(22):5711-5716.

65. Henry M, Dupont-Gillain C, Bertrand P. Characterization of insulin adsorption in the presence of albumin by time-of-flight secondary ion mass spectrometry and X-ray photoelectron spectroscopy. *Langmuir* 2008 Jan;24(2):458-464.
66. Wagner MS, Castner DG. Characterization of adsorbed protein films by time-of-flight secondary ion mass spectrometry with principal component analysis. *Langmuir* 2001 Jul;17(15):4649-4660.
67. Yang L, Lua YY, Jiang GL, Tyler BJ, Linford MR. Multivariate analysis of TOF-SIMS spectra of monolayers on scribed silicon. *Analytical Chemistry* 2005 Jul;77(14):4654-4661.
68. Baytekin HT, Wirth T, Gross T, Treu D, Sahre M, Theisen J, et al. Determination of wettability of surface-modified hot-embossed polycarbonate wafers used in microfluidic device fabrication via XPS and ToF-SIMS. *Surface and Interface Analysis* 2008 Mar-Apr;40(3-4):358-363.
69. Belu AM, Yang ZP, Aslami R, Chilkoti A. Enhanced TOF-SIMS imaging of a micropatterned protein by stable isotope protein labeling. *Analytical Chemistry* 2001 Jan;73(2):143-150.
70. Hashimoto H, Nakamura K, Takase H, Okamoto T, Yamamoto N. Quantitative TOF-SIMS imaging of DNA microarrays produced by bubble jet printing technique and the role of TOF-SIMS in life science industry. *Applied Surface Science* 2004 Jun;231-2:385-391.
71. Lee CY, Harbers GM, Grainger DW, Gamble LJ, Castner DG. Fluorescence, XPS, and TOF-SIMS surface chemical state image analysis of DNA microarrays. *Journal of the American Chemical Society* 2007 Aug;129(30):9429-9438.
72. Belu AM, Graham DJ, Castner DG. Time-of-flight secondary ion mass spectrometry: techniques and applications for the characterization of biomaterial surfaces. *Biomaterials* 2003 Sep;24(21):3635-3653.
73. Green FM, Gilmore IS, Seah MP. Mass accuracy- TOF-SIMS. *Applied Surface Science* 2006 Jul;252(19):6591-6593.
74. Briggs D, Fletcher IW, Goncalves NM. Positive secondary ion mass spectrum of poly(methyl methacrylate): a high mass resolution ToF-SIMS study. *Surface and Interface Analysis* 2000 May;29(5):303-309.

75. Ward RJ, Wood BJ. A Comparison of Experimental and Theoretically Derived Sensitivity Factors for Xps. *Surface and Interface Analysis* 1992 Sep;18(9):679-684.
76. Urquhart AJ, Taylor M, Anderson DG, Langer R, Davies MC, Alexander MR. TOF-SIMS analysis of a 576 micropatterned copolymer array to reveal surface moieties that control wettability. *Analytical Chemistry* 2008 Jan;80(1):135-142.
77. Barnes G. *Interfacial science: an introduction*. Oxford: Oxford University Press, 2005.
78. Whitesides GM, Laibinis PE. Wet Chemical Approaches to the Characterization of Organic-Surfaces - Self-Assembled Monolayers, Wetting, and the Physical Organic-Chemistry of the Solid Liquid Interface. *Langmuir* 1990 Jan;6(1):87-96.
79. Bain CD, Whitesides GM. A Study by Contact-Angle of the Acid-Base Behavior of Monolayers Containing Omega-Mercaptocarboxylic Acids Adsorbed on Gold - an Example of Reactive Spreading. *Langmuir* 1989 Nov-Dec;5(6):1370-1378.
80. Wenzel RN. Surface Roughness and Contact Angle. *Journal of Physical and Colloid Chemistry* 1949;53(9):1466-1467.
81. Herzberg WJ, Marian JE. Relationship between Contact Angle and Drop Size. *Journal of Colloid and Interface Science* 1970;33(1):161-&.
82. Pease DC. The Significance of the Contact Angle in Relation to the Solid Surface. *Journal of Physical Chemistry* 1945;49(2):107-110.
83. Urquhart AJ, Anderson DG, Taylor M, Alexander MR, Langer R, Davies MC. High throughput surface characterisation of a combinatorial material library. *Advanced Materials* 2007 Sep;19(18):2486-2490.
84. Gustavsson P, Johansson, F., Kanje, M., Wallman, L., Linsmeier, C.E. Neurite guidance on protein micropatterns generated by a piezoelectric microdispenser. *Biomaterials* 2007;28:1141-1151.
85. Barry JJA, Howard D, Shakesheff KM, Howdle SM, Alexander MR. Using a core-sheath distribution of surface chemistry through 3D tissue engineering scaffolds to control cell ingress. *Advanced Materials* 2006 Jun 6;18(11):1406-+.

86. Whittle JD, Barton D, Alexander MR, Short RD. A method for the deposition of controllable chemical gradients. *Chemical Communications* 2003(14):1766-1767.
87. Bourgesmonnier C, Shanahan MER. Influence of Evaporation on Contact-Angle. *Langmuir* 1995 Jul;11(7):2820-2829.
88. Kwok DY, Neumann AW. Contact angle measurement and contact angle interpretation. *Advances in Colloid and Interface Science* 1999 Aug;81(3):167-249.
89. Adamson AW. *Physical chemistry of surfaces*. 6th ed. New York: John Wiley & Sons, 1997.
90. Yu HZ, Soolaman DM, Rowe AW, Banks JT. Evaporation of water microdroplets on self-assembled monolayers: From pinning to shrinking. *Chemphyschem* 2004 Jul;5(7):1035-1038.
91. Rowan SM, Newton MI, McHale G. Evaporation of Microdroplets and the Wetting of Solid-Surfaces. *Journal of Physical Chemistry* 1995 Aug;99(35):13268-13271.
92. Holly FJ. Wettability of Hydrogels .1. Poly(2-Hydroxyethyl Methacrylate). *Journal of Biomedical Materials Research* 1975;9(3):315-326.
93. Ellison AH, Fox HW, Zisman WA. Wetting of Fluorinated Solids by Hydrogen-Bonding Liquids. *Journal of Physical Chemistry* 1953;57(7):622-627.
94. Amirfazli A, Kwok DY, Gaydos J, Neumann AW. Line tension measurements through drop size dependence of contact angle. *Journal of Colloid and Interface Science* 1998 Sep;205(1):1-11.
95. Kennedy SB, Washburn NR, Simon CG, Amis EJ. Combinatorial screen of the effect of surface energy on fibronectin-mediated osteoblast adhesion, spreading and proliferation. *Biomaterials* 2006 Jul;27(20):3817-3824.
96. Lee JH, Khang G, Lee JW, Lee HB. Interaction of different types of cells on polymer surfaces with wettability gradient. *Journal of Colloid and Interface Science* 1998 Sep;205(2):323-330.
97. Wijnans S, de Gans BJ, Wiesbrock F, Hoogenboom R, Schubert US. Characterization of a poly (2-oxazoline) library by high-throughput, automated contact-angle measurements and surface-energy calculations. *Macromolecular Rapid Communications* 2004 Dec;25(23):1958-1962.

98. Taylor M, Urquhart AJ, Zelzer M, Davies MC, Alexander MR. Picoliter Water Contact Angle Measurement on Polymers. *Langmuir* 2007;23(13):6875-6878.
99. Fowkes FM. Attractive Forces at Interfaces. *Industrial and Engineering Chemistry* 1964;56(12):40-&.
100. Lee LH. Roles of Molecular-Interactions in Adhesion, Adsorption, Contact-Angle and Wettability. *Journal of Adhesion Science and Technology* 1993;7(6):583-634.
101. Fowkes FM. Additivity of Intermolecular Forces at Interfaces .1. Determination of Contribution to Surface and Interfacial Tensions of Dispersion Forces in Various Liquids. *Journal of Physical Chemistry* 1963;67(12):2538-&.
102. Relini A, Sottini S, Zuccotti S, Bolognesi M, Gliozzi A, Rolandi R. Measurement of the surface free energy of streptavidin crystals by atomic force microscopy. *Langmuir* 2003 Apr;19(7):2908-2912.
103. Mangipudi V, Tirrell M, Pocius AV. Direct Measurement of Molecular-Level Adhesion between Poly(Ethylene-Terephthalate) and Polyethylene Films - Determination of Surface and Interfacial Energies. *Journal of Adhesion Science and Technology* 1994;8(11):1251-1270.
104. Ticehurst MD, Rowe RC, York P. Determination of the Surface-Properties of 2 Batches of Salbutamol Sulfate by Inverse Gas-Chromatography. *International Journal of Pharmaceutics* 1994 Oct;111(3):241-249.
105. Owens DK, Wendt, R.C. Estimation of the Surface Free Energy of Polymers. *Journal of Applied Polymer Science* 1969;13:1741-1747.
106. Shimizu RN, Demarquette NR. Evaluation of surface energy of solid polymers using different models. *Journal of Applied Polymer Science* 2000 Jun;76(12):1831-1845.
107. Bellonfontaine MN, Mozes N, Vandermei HC, Sjollema J, Cerf O, Rouxhet PG, et al. A Comparison of Thermodynamic Approaches to Predict the Adhesion of Dairy Microorganisms to Solid Substrata. *Cell Biophysics* 1990 Aug;17(1):93-106.
108. Busscher HJ, Vanpelt AWJ, Deboer P, Dejong HP, Arends J. The Effect of Surface Roughening of Polymers on Measured Contact Angles of Liquids. *Colloids and Surfaces* 1984;9(4):319-331.

109. Dejong S. Simpls - an Alternative Approach to Partial Least-Squares Regression. *Chemometrics and Intelligent Laboratory Systems* 1993 Mar;18(3):251-263.
110. Xu QS, de Jong S, Lewi P, Massart DL. Partial least squares regression with Curds and Whey. *Chemometrics and Intelligent Laboratory Systems* 2004 Apr;71(1):21-31.
111. Rawsterne RE, Todd SJ, Gough JE, Farrar D, Rutten FJM, Alexander MR, et al. Cell spreading correlates with calculated logP of amino acid-modified surfaces. *Acta Biomater* 2007 Sep;3(5):715-721.
112. Leo AJ, Hoekman D. Calculating log P(oct) with no missing fragments; The problem of estimating new interaction parameters. *Perspect Drug Discov Design* 2000;18:19-38.
113. Fisher JP, Dean D, Engel PS, Mikos AG. Photoinitiated polymerization of biomaterials. *Ann Rev Mater Res* 2001;31:171-181.
114. Liu FPP, Rials TG, Simonsen J. Relationship of wood surface energy to surface composition. *Langmuir* 1998 Jan;14(2):536-541.
115. Araujo YC, Toledo PG, Leon V, Gonzalez HY. Wettability of silane-treated glass slides as determined from X-ray photoelectron spectroscopy. *Journal of Colloid and Interface Science* 1995 Dec;176(2):485-490.
116. Priest C, Stevens N, Sedev R, Skinner W, Ralston J. Inferring wettability of heterogeneous surfaces by ToF-SIMS. *Journal of Colloid and Interface Science* 2008 Apr;320(2):563-568.
117. Faucheux N, Schweiss R, Lutzow K, Werner C, Groth T. Self-assembled monolayers with different terminating groups as model substrates for cell adhesion studies. *Biomaterials* 2004 Jun;25(14):2721-2730.
118. Shyue JJ, De Guire MR. Acid-base properties and zeta potentials of self-assembled monolayers obtained via in situ transformations. *Langmuir* 2004 Sep;20(20):8693-8698.
119. Drummond CJ, Georgaklis G, Chan DYC. Fluorocarbons: Surface free energies and van der Waals interaction. *Langmuir* 1996 May;12(11):2617-2621.
120. Otto M. *Chemometrics: statistics and computer application in analytical chemistry*. Weinheim: Wiley-VCH, 1999.
121. Chilkoti A, Schmierer AE, Perezluna V, Ratner BD. Investigating the Relationship between Surface-Chemistry and Endothelial-Cell Growth - Partial

- Least-Squares Regression of the Static Secondary-Ion Mass-Spectra of Oxygen-Containing Plasma-Deposited Films. *Analytical Chemistry* 1995 Sep;67(17):2883-2891.
122. Shen MC, Wagner MS, Castner DG, Ratner BD, Horbett TA. Multivariate surface analysis of plasma-deposited tetraglyme for reduction of protein adsorption and monocyte adhesion. *Langmuir* 2003 Mar;19(5):1692-1699.
123. Perezluna VH, Horbett TA, Ratner BD. Developing Correlations between Fibrinogen Adsorption and Surface-Properties Using Multivariate-Statistics. *Journal of Biomedical Materials Research* 1994 Oct;28(10):1111-1126.
124. Ferrari S, Ratner BD. ToF-SIMS quantification of albumin adsorbed on plasma-deposited fluoropolymers by partial least-squares regression. *Surface and Interface Analysis* 2000 Dec;29(12):837-844.
125. Manne R. Analysis of 2 Partial-Least-Squares Algorithms for Multivariate Calibration. *Chemometrics and Intelligent Laboratory Systems* 1987 Aug;2(1-3):187-197.
126. Geladi P, Kowalski BR. Partial Least-Squares Regression - a Tutorial. *Analytica Chimica Acta* 1986 Jul;185:1-17.
127. Haaland DM, Thomas EV. Partial Least-Squares Methods for Spectral Analyses .1. Relation to Other Quantitative Calibration Methods and the Extraction of Qualitative Information. *Analytical Chemistry* 1988 Jun;60(11):1193-1202.
128. Bro R, Rinnan A, Faber NM. Standard error of prediction for multilinear PLS - 2. Practical implementation in fluorescence spectroscopy. *Chemometrics and Intelligent Laboratory Systems* 2005 Jan;75(1):69-76.
129. Taylor M, Urquhart AJ, Anderson DG, langer R, Davies MC, Alexander MR. High-throughput Analysis of a Library of Micro-arrayed Materials Reveals Tuneable Surface Energies. In preparation 2008.
130. Brereton R. *Applied Chemometrics for Scientists*. Chichester: Wiley, 2007.
131. Lee JLS, Gilmore IS, Seah MP. Quantification and methodology issues in multivariate analysis of ToF-SIMS data for mixed organic systems. *Surface and Interface Analysis* 2008 Jan;40(1):1-14.

132. Wilson CJ, Clegg RE, Leavesley DI, Pearcy MJ. Mediation of biomaterial-cell interactions by adsorbed proteins: A review. *Tissue Engineering* 2005 Jan;11(1-2):1-18.
133. Vroman L. Effect of Adsorbed Proteins on Wettability of Hydrophilic and Hydrophobic Solids. *Nature* 1962;196(4853):476-&.
134. Horbett TA. Principles Underlying the Role of Adsorbed Plasma-Proteins in Blood Interactions with Foreign Materials. *Cardiovascular Pathology* 1993 Jul-Sep;2(3):S137-S148.
135. Koehler JA, Ulbricht M, Belfort G. Intermolecular forces between proteins and polymer films with relevance to filtration. *Langmuir* 1997 Jul;13(15):4162-4171.
136. Snellings G, Vansteenkiste SO, Corneillie SI, Davies MC, Schacht EH. Protein adhesion at poly(ethylene glycol) modified surface. *Advanced Materials* 2000 Dec;12(24):1959-+.
137. Wang MS, Palmer LB, Schwartz JD, Razatos A. Evaluating protein attraction and adhesion to biomaterials with the atomic force microscope. *Langmuir* 2004 Aug;20(18):7753-7759.
138. Eckert R, Jeney S, Horber JKH. Understanding intercellular interactions and cell adhesion: Lessons from studies on protein-metal interactions. *Cell Biology International* 1997 Nov;21(11):707-713.
139. Kidoaki S, Matsuda T. Adhesion forces of the blood plasma proteins on self-assembled monolayer surfaces of alkanethiolates with different functional groups measured by an atomic force microscope. *Langmuir* 1999 Oct;15(22):7639-7646.
140. Sethuraman A, Han M, Kane RS, Belfort G. Effect of surface wettability on the adhesion of proteins. *Langmuir* 2004 Aug;20(18):7779-7788.
141. Bremmell KE, Kingshott P, Ademovic Z, Winther-Jensen B, Griesser HJ. Colloid probe AFM investigation of interactions between fibrinogen and PEG-like plasma polymer surfaces. *Langmuir* 2006 Jan;22(1):313-318.
142. Weber N, Bolikal D, Bourke SL, Kohn J. Small changes in the polymer structure influence the adsorption behavior of fibrinogen on polymer surfaces: Validation of a new rapid screening technique. *Journal of Biomedical Materials Research Part A* 2004 Mar;68A(3):496-503.

143. McGurk SL, Green RJ, Sanders GHW, Davies MC, Roberts CJ, Tendler SJB, et al. Molecular interactions of biomolecules with surface-engineered interfaces using atomic force microscopy and surface plasmon resonance. *Langmuir* 1999 Jul;15(15):5136-5140.
144. Pasche S, Voros J, Griesser HJ, Spencer ND, Textor M. Effects of ionic strength and surface charge on protein adsorption at PEGylated surfaces. *Journal of Physical Chemistry B* 2005 Sep;109(37):17545-17552.
145. Tsapikouni TS, Allen S, Missirlis YF. Measurement of interaction forces between fibrinogen coated probes and mica surface with atomic force microscope: The pH and ionic strength effect. *Biointerphases* 2008;3(1):1-8.
146. Muller DJ, Engel A. The height of biomolecules measured with the atomic force microscope depends on electrostatic interactions. *Biophysical Journal* 1997 Sep;73(3):1633-1644.
147. Alexander MR, Duc TM. A study of the interaction of acrylic acid/1,7-octadiene plasma deposits with water and other solvents. *Polymer* 1999 Sep;40(20):5479-5488.
148. Du H, Chandaroy P, Hui SW. Grafted poly-(ethylene glycol) on lipid surfaces inhibits protein adsorption and cell adhesion. *Biochimica Et Biophysica Acta-Biomembranes* 1997 Jun;1326(2):236-248.
149. Ostuni E, Grzybowski BA, Mrksich M, Roberts CS, Whitesides GM. Adsorption of proteins to hydrophobic sites on mixed self-assembled monolayers. *Langmuir* 2003 Mar;19(5):1861-1872.
150. Sigal GB, Mrksich M, Whitesides GM. Effect of surface wettability on the adsorption of proteins and detergents. *Journal of the American Chemical Society* 1998 Apr;120(14):3464-3473.